THE DISTRIBUTION, MORPHOLOGY, AND TEMPORAL SIGNATURE OF ROCK GLACIERS IN THE TOBACCO ROOT MOUNTAINS, MONTANA

Andrew R. Gustin

Submitted to the faculty of the University Graduate School
in partial fulfillment of the requirements for the degree
Master of Sciences
in the Department of Geological Sciences,
Indiana University
September, 2013

Accepted by the Graduate Faculty, Indiana University, in partial fulfillment of the requirements for the degree of Master of Sciences

---

Greg A. Olyphant, Ph. D.

Sally L. Letsinger, Ph. D.

Bruce J. Douglas, Ph. D.

This work is not a solo act; the souls are many to include.
I'll do my best to credit those who influenced what soon you'll view.
Instead of giving formal thanks, it's up to you (the roles you played).
And with acceptance now received, I have concerns that I'll convey.
In part it's honoring the past, in part it's for the boding doom.
Yet here, entwined, amongst the words, a central theme can be exhumed.
And if you dare to take the task, to "realize what *lies* within,"
You just might be adept enough to understand where it begins.
To family, with support and love of unconditional resolve.
And through the nurture nature gave, my heritage I proudly call.
To friends whose backs have never turned, to those whose attitudes evolved.
It's with the ever-passing time that qualifying bounds are solved.
To lovers who renew my faith that someday I might find 'the one'.
Along the way-with broken hearts, entangled and amongst the fun.
To friendly Field Station folk that made this research possible.
To Forest Service workers who 'permitted' me to dig a hole.
To academic strangers who so kindly sent litter-ature.
To secretarial support with funding (and some paperwork).
To mentors who instilled in me their wisdom and their best advice.
Especially advisors who believed in me (to be precise).
To colleagues who would listen when they knew I needed them to hear.
To anyone who challenged me, or was a challenge to be near.
To bosses, both the good and bad; for both are most (by choice or fault).
The cowards don't admit their errors; they are not leaders…hardly scouts!
To Antler-style brotherhood of knowing when to dominate.
We rocked the cores with rocky roars, remembering that life's a game.
And far away from judgment, only howling Swamp Dogs can be heard.
Therein my words and music veer and stir, adjacent to the herd.
And in this way (and day by day) the sacred truths begin to show.
The phonies and the fakers won't identify their deeper goals.
And those who care what others think, they cannot ponder for themselves -
(The droning beat of cultish drums does not permit the mind to delve.)
The selfish and the selfless really are two sides of the same coin.

Degrees to which we give and take adjusted like ‘relates’ and ‘joins’.
Everything’s dynamic less the static of our inner peace. ~~A~~
We always choose which wolf to feed; requests from both shall never cease.
But consciously we can control what ultimately is our “fate”.
And poignantly I hope the world will change (before it is too late).
Take action for the common good and hold the earth above all else.
Economies have never been a measure of the planet’s wealth.
There is a bigger picture often muddled by society -
(How easy to forget you’re in a forest when it’s “trees” you see.)
And so they cut the forests down, and leave a couple trees for looks.
Burn coal and oil while they can, and fudge the numbers for the books.
Alternatives are waiting, but the ‘men’ in charge would lose *too much*.
So they suppress advances whilst their pocketbooks are *full-to-touch*.
And holding so much power, well, they use it to acquire more.
Abuse their best intentions, and extend their rights to trample ours.
A sad but true reality with hardly any warning signs ->
The copper statue in New York: ~~Iconic~~ Ironic (liberty declines).
And with a guise of terror, in-secure homeland, justice for all.
We ride upon another wave and watch our civil rights dissolve.
A growing revolution as the planet starts to counter back.
An age of ice is coming; not a speculation, but a fact.
I see these matters only as an artifact of time…
The end of which is coming up (collective consciousness align).
I expect resistance, but I’m eager to persist.
If action isn’t taken now, our opportunity is missed.
The people have the power to enact the change we need.
With unity, we overcome corruption, hate, and greed.
I beg that we not gamble with our one and only home.
These thoughts I must acknowledge, written (roughly) in this poem.
If you should choose to doubt me, with my heart upon my sleeve,
At least always remember this: If God Is Time, Yes. You’ll believe.

Andrew R. Gustin

The Distribution, Morphology, and Temporal Signature of Rock Glaciers in the Tobacco Root Mountains, Montana

A detailed analysis of nearly 250 periglacial deposits (mostly rock glaciers) in the Tobacco Root Mountains of southwestern Montana was performed using geospatial analysis techniques on high-resolution digital orthophotographs to better understand controls on their distribution and morphology. The geographic information system terrain analysis included the determination of morphometric attributes for the deposits (bounding geometry, thickness, surface area), and the extraction of spatial and topographic parameters such as slope, aspect, elevation, and incident clear-sky radiation. A field campaign was also undertaken, aimed at determining the relative ages of periglacial deposits and the nature of their contributing headwalls. A multivariate analysis of relative age data from 21 deposits revealed groupings that are consistent with at least four periods of periglacial activity. Of these, the Early Neoglacial was by far the most common. A morphometric analysis indicated that tongue-shaped rock glaciers have statistically lower surface slopes and larger maximum elevations, areas, thicknesses, and lengths than either lobate rock glaciers or protalus ramparts. Lobate rock glaciers also have statistically lower surface slopes and larger areas, thicknesses, and lengths than protalus ramparts. Most rock glaciers and protalus ramparts in the Tobacco Root Mountains emanate from topoclimatic niches that minimize incident solar radiation. The greatest difference in radiation reduction between morphologies occurs on the winter solstice, with tongue-shaped deposits receiving the least radiation and protalus ramparts receiving the most. Fracture orientation in the contributing headwall appears to influence the size of a given deposit, with the largest deposits having contributing headwalls with fracture planes parallel to compositional banding and dip-slope. Headwall retreat associated with deposit development ranges from 1-35 m. Based on the inferred ages of deposits, headwall retreat rates in the Tobacco Root Mountains were calculated to range between 0.5 and 3.5 mm/yr during periods of active periglaciation.

Table of Contents

List of Figures

List of Tables

I. Introduction

Periglacial deposits are transitional landforms that often form in alpine environments when climatic conditions support permafrost but are not sufficient to promote active glaciers. Three morphological types of gravity-driven rubble deposits are the focus of this research - protalus ramparts, lobate rock glaciers, and tongue-shaped rock glaciers. Talus deposits were only mapped as part of a larger periglacial deposits and were not outlined otherwise. All of the deposits are comprised of coarse boulder debris that derives from adjacent cliffs and therefore can be considered to be alpine lithofacies (Madole, 1972). Each lithofacies is associated with a particular depositional environment and no two morphologies form simultaneously in the same place. Talus is the least mobile because the voids are filled mostly with air. Protalus ramparts extend outward from talus slopes but differ from rock glaciers in that their boulders do not appear to have moved since deposition. Rock glaciers are the most mobile of the alpine lithofacies owing to interstitial ice that allows for creep to occur as a result of shearing in the ice-filled rock rubble. In some cases, rock glaciers can form when rock debris covers and reactivates a receding or stagnated glacier. The insulating effects of the debris cover and additional weight produce increased shear stress that can cause the ice-cored rock glacier to move down-slope at a high rate relative to other rock glaciers.

The importance of periglacial deposits with respect to recording past periods of climate change has long been recognized. Having a better understanding of prior periods of change can assist with recognizing modern-day climate shifts. Several studies including those of Humlum (1998), Konrad et. al (1999), and Refsnider and Brugger (2007) have attempted to use periglacial advances as a proxy for reconstructing paleoclimates. This practice works well for localized studies, but variability in microclimatic conditions such as elevation and deposit orientation (relative to prevailing winds and insolation) makes correlation within and between mountain ranges difficult. For this reason, the need for continuing periglacial studies in a variety of different topoclimates and geographic locations is still pertinent.

The primary purpose of this study is to quantify the distribution and morphology of selected periglacial deposits in the Tobacco Root Mountains. Through remote sensing and field work, a database consisting of geospatial, temporal, geologic, and topoclimatic information was gathered and subjected to statistical analyses. This was done in an effort to objectively describe the unique periglacial signature of the Tobacco Root Mountains and contribute to the growing database of geomorphic evidence concerning late glacial and early Holocene climate change.

Previous Studies of Rock Glaciers and Related Deposits

Rock glaciers have been recognized and described for over a century. The first detailed publication discussing these deposits was written by Capps (1910), who coined the term “rock glacier” in his study of rock rubble deposits in Alaska. Nearly 50 years later, a more quantitative study was conducted by Wahrhaftig and Cox (1959), who identified around 200 rock-glacier deposits in Alaska and examined their distribution, morphology, and evolution. This paper seems to have ushered in an era of similar studies that has persisted to the present day. During the 1960s and 70s, studies were conducted by Benedict (1965, 1973), Birkeland (1973) Birkeland et al., (1979), Madole (1972), and White (1971) on rock glaciers in the Colorado Front Range. In addition to developing a standard model for rock-glacier development, these studies established a chronology to describe the recognized periods of development.

Periglacial deposits likely form in alpine regions at the cessation of every glacial period, but the evidence for older deposits is often erased by subsequent glacial advances (Gibbons et al., 1984). For this reason, the majority of high-altitude periglacial features observable today were formed since the end of the last glacial period. There are four recognized periods of periglacial activity represented by rock glaciers around the world. Following the nomenclature suggested by Benedict (1973) for the middle Rocky Mountains, these stades (with their approximated ages) are known as the Late Pinedale (10,000 – 8,500 YBP), the Early Neoglacial (5,000 – 3,000 YBP), the

Audubon (1,850 - 900 YBP), and the Gannett Peak (300 - 100 YBP). The two most recent glacial periods in the Rocky Mountains are designated as the Pinedale (~30,000 - 20,000 YBP) and the Bull Lake (~150,000 YBP). Other stades of rock-glacier deposition likely occurred between the Bull Lake and the Pinedale; but if so, the extensive Pinedale glaciation has erased most evidence of this in the Rocky Mountains (Madole, 1972).

Madole (1972) views rock glaciers as being intermediate between talus lobes which are not periglacial and occur at the lowest elevations of alpine regions and glacial moraines which occur at the highest elevations and most shaded aspects. Periglacial deposits can be subdivided into three main sub-categories: protalus ramparts, lobate rock glaciers, and tongue-shaped rock glaciers. Protalus ramparts form at the base of semi-permanent snow fields as arcuate ridges of fallen debris. They are differentiated from true rock glaciers in that there is no evidence of post-depositional flowing of debris. In contrast, the debris comprising rock glaciers has flowed down-slope, and the motion is promoted by the existence of interstitial ice or an ice core that has been buried by the overlying rubble. The mass-movement by internal deformation produces diagnostic furrows and ridges along the surface of the flowing deposit.

The two main classes of rock glaciers are further differentiated by the rate at which they accumulate debris and creep downhill. Lobate rock glaciers generally form in less optimal topoclimatic settings, and as a result they tend to accumulate ice and debris at a less rapid rate. This results in a width that is larger than the length. Tongue-shaped rock glaciers often originate from cirques developed in optimal niches for debris production and ice preservation. Increased headwall erosion contributing debris more rapidly and the presence of interstitial ice or underlying ice cores produces a high flow-rate that causes the deposit to be longer than wide. Because multiple types of deposits cannot form at the same location simultaneously, and because the elevations and settings at which different facies develop shifts with changes in the climate, the spatial distribution of neoglacial deposits changes over time, and the observed pattern can be used to infer information about the local paleoclimate.

Morris (1981) expanded on the facies concept for rock-glacier deposits, concluding that the relative size of a deposit is controlled by the preservation of an ice-core and/or interstitial ice-matrix as well as by the intensity of debris contribution. He argued that ice preservation is mostly controlled by topoclimatic factors including elevation, the amount of solar radiation reduction resulting from slope-aspect and shadowing by surrounding topography. Morris also noted that jointing in the contributing bedrock headwalls influences the rate of rockfall, which in turn affects the size of rock glaciers. Morris and Olyphant (1990) took these factors and applied them toward a more general model of lithofacies distribution.

Geospatial Analysis of Rock-glacier Distribution

With continual exponential improvements in computing technology (Moore's Law) and the advent of powerful geoprocessing software such as ESRI ArcGIS, the tasks of creating an inventory and analyzing the topographic and morphometric characteristics of periglacial deposits are more approachable now than ever before. Several recent studies have utilized this technology in order to better understand the underlying causes for the observed spatial patterns of periglacial deposits in alpine regions. Janke (2007) digitized the locations of many of the rock glaciers that had been previously identified in the Colorado Front Range and calculated spatial statistics of different deposit morphologies. He concluded that active tongue-shaped deposits have a similar spatial distribution to that of remnant glaciers, preferring north-facing aspects and with relatively gentle slopes compared to those of lobate deposits which are much more variable in their topographic distribution. He concluded that such a pattern supports the hypothesis that tongue-shaped deposits develop as debris-covered glaciers (glaciogenically) while lobate deposits form as a result of interstitial ice accumulation in rock rubble that originated as talus. Janke and Frauenfelder (2008) also examined the statistical significance of various contributing-headwall variables as they relate to rock-glacier development. The strongest correlation observed was

between rock glacier width and the contributing-headwall area, but a statistically significant correlation between contributing-headwall area and rock glacier area was also noted.

Brenning et al. (2007) evaluated the distribution of rock glaciers in the San Juan Mountains of Colorado and developed an additive model to predict occurrence based on topographic controls. The model was able to predict rock glacier occurrence with 91% accuracy as a function of elevation, regional trends, solar radiation in relation to slope, aspect, and slope curvature, as well as contributing-headwall properties such as contributing area. Their findings were similar to those of Brenning (2005) for the Andes of central Chile, but the relative importance of variables were different, highlighting the need for continued investigations in a variety of alpine settings.

Study Area

Although the Tobacco Root Mountains (**Figure 1**) are a well-studied range, there have been few investigations conducted on periglacial deposits, with the majority of these performed over three decades ago. The mountains are isolated from other ranges by basin fill, allowing the study area to be clearly defined. The presence of the Indiana University Geologic Field Station (IUGFS) as a base station in the northern part of the range was a wonderful asset and was ultimately what made this study logistically feasible. 4WD-road accessibility deep into many of the valleys enabled excursions to be planned in all parts of the range. Field campaigns were conducted during both the summer of 2009 and 2010, although the majority of data was collected in 2009. The following sections describe the geology and Quaternary history that is the context for this study.

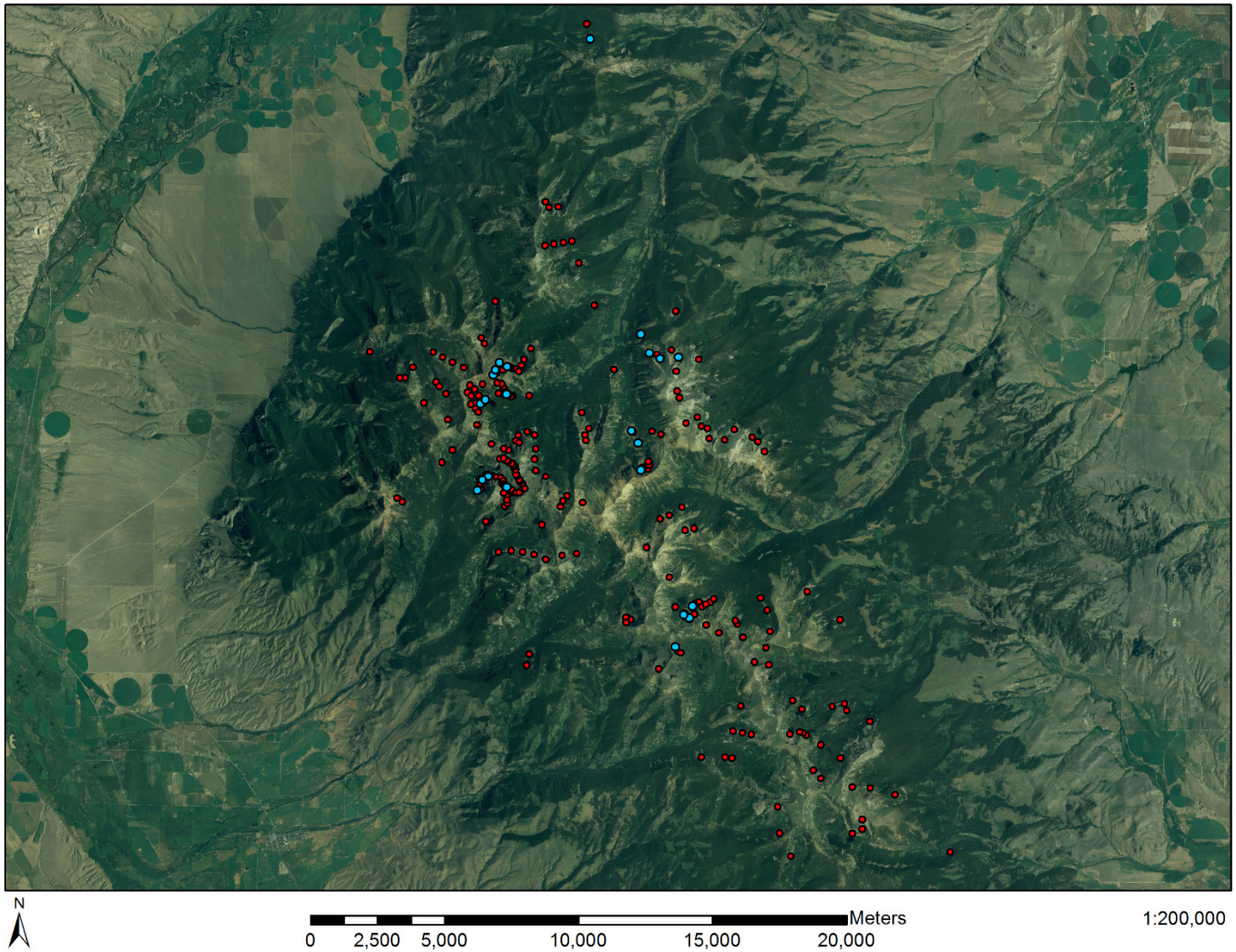

Figure 1: Aerial photograph of the study area and the Tobacco Root Mountains showing visited priority deposits (blue) and all identified deposits (red).

Geology of the Tobacco Root Mountains

The Tobacco Root Mountains formed as a domal block uplift during the Laramide Orogeny and appears roughly diamond-shaped in aerial view. The core of the range is composed of regionally metamorphosed Archean gneisses and schists which have been intruded by both Precambrian dikes and late-Mesozoic intermediate to felsic igneous rocks (Vitaliano and Cordura, 1979). The igneous core, known as the Tobacco Root Batholith, exists in the northeastern part of the range and is suspected to be a satellite of the regional Boulder Batholith (Schmidt et al., 1990). The flanks of the range are comprised of a sequence of folded and faulted sedimentary rocks dating from the Cambrian through the Cretaceous. The sedimentary rocks are mostly limestones, shales, sandstones, and dolostones, whereas some sedi-igneous rocks also exist. The block uplift is bounded by normal faults on both the east and west sides of the range, creating an abrupt transition from exposed bedrock to a pediment surface formed over the surrounding basin fill (Tansley et al., 1933). Although there are a wide range of lithologies throughout the study area, the majority of the bedrock that exists at higher elevations (where periglacial deposits occur) is metamorphic rock of Archean age; primarily quartzofeldspathic gneiss and hornblende gneiss, but schists, quartzites, marbles, and other metamorphic rocks can also be found. The two main metamorphic events these rocks were exposed to have been dated to around 2,700 Ma and 1,600 Ma (Mueller and Cordura, 1976). The composition of the Tobacco Root Batholith ranges from diorite to granite. The intrusion has been dated to between 74 and 76 Ma (Sarkar et al., 2009). Vitaliano and Cordura (1979) report that the long diabase dikes present in the south and northwest of the range have been dated to ~1,450 Ma and ~1,120 Ma.

Quaternary History of the Tobacco Root Mountains

Several people have examined the geomorphology of the Tobacco Root Mountains in varying degrees of detail. In a survey of the mining districts of the area, Winchell (1914) identified many of the glaciated valleys of the range, noting an abundance of moraines but an apparent

absence of deposits in the surrounding sedimentary basins. A more detailed examination of the geomorphology was performed by Tansley et al. (1933). They described the rise of the range as abrupt on the west side, corresponding to a normal fault and gradational on the east side owing to an erosional surface. Tansley et al. (1933) also identified the presence of a number of glacial features, and presented evidence for at least two different periods of glaciation. He postulated that during the earlier glaciation, valley ice capped many of the ridges and extended out of the main range and into the surrounding basins (in contrast with Winchell's observations). Tansley noted that many glacial lakes are present at high elevations, and that there are abundant accumulations of talus throughout the range. Additional evidence in support of an older glaciation that extended into the bounding structural basins was presented by Alden (1953). He identified till deposits and attempted to assign them ages, calling them "Wisconsin" (equivalent to Pinedale) and "pre-Wisconsin" (equivalent to Bull Lake) (see **Table 1** for nomenclature correlations). In his examination of the geomorphic history of the Jefferson Basin, Reshkin (1963) concluded that there is "scanty" evidence for a glaciation predating "Wisconsin" (Pinedale) in age, but stated that earlier Pleistocene ("Buffalo" or pre-Bull Lake) glaciers likely reached out into the Jefferson Basin. He said that Bull Lake deposits were overridden by the more extensive Pinedale deposits. Reshkin (1963, p.126) identified a lateral moraine that extends from the west side of the range onto the pediment of the Jefferson Basin at the mouth of Indian Creek Valley. He stated that this valley "displays evidence of the most extensive advance of any Pinedale glacier on the west flank of the Tobacco Root Mountains." He also indicated that no terminal moraine was found, suggesting the glacier did not advance far onto the pediment after leaving the valley. Reshkin refuted some of the evidence that Alden cited for "pre-Wisconsin" till in the South Boulder Valley by suggesting instead that there are discontinuous outwash terraces for several miles beyond the terminal moraine.

Jacobs (1967) produced the first detailed study of the glacial and periglacial deposits in the Tobacco Root Mountains. His study focused primarily on deposits found at low elevations

Table 1: Summary of Neoglacial nomenclature and associated attributes from referenced studies.

Name	Study	Period (YBP)	Type	Evidence
Gannett Peak	Benedict (1968), Richmond (1962, 1965), Hall	~300-100	Periglacial Advance	Relative Age
Arapaho Peak	Benedict (1973)			Relative Age
Audubon	Miller (1973), Birkeland, Dowdeswell, Hall	~950-1,900	Periglacial Advance	
Mid Neoglacial	Hall (1990)	~1500	Periglacial Advance	Relative Age
Arikaree	Benedict (1968), Madole (1972),	1,000-1,900	Periglacial Advance	Lichen
Neoglacial	Hall and Michaud (1988)	~2500	Protalus Advance	Radiocarbon & Relative Age
Triple Lakes	Benedict (1968, 1973)	~3000-5000		
Temple Lake	Madole (1972)	?	Periglacial Advance	Relative Age, Soils
Temple Lake II	Miller (1973)	2,500-3750		
Temple Lake I	Miller (1973)	>4,000-?		
Early post-Altithermal	Hall (1984)	~3600	Periglacial Advance	Radiocarbon
Early Neoglacial	Birkeland (1973), Dowdeswell, Hall (1986)	~3000-5000	Glacial Maximum	Benedict (1973), Radiocarbon
Late Holocene	Hall (1990)	<5000	Periglacial Activity	Relative Age?
Altithermal	Hall (1984)	~5300	Interglacial	Radiocarbon
Pinedale	Richmond (1960)	~8500		
post-Pleistocene	Jacobs (1967)	?		Soils
Early Holocene	Hall	~8600	Glacial Retreat	Radiocarbon
Santana Peak	Benedict (1968) (1973),	~8400-9950	Glacial Maximum	Radiocarbon
Late Pinedale	Madole (1972), Hall	~9850	Glacial Retreat	Radiocarbon
Late Pleistocene	Hall (1990)	~12,000		
Pinedale II	Hall and Michaud (1988)	~12,000	Glacial Maximum	Hornblende & Soils
Pinedale I	Hall and Michaud (1988)	20,000-25,000	Glacial Maximum	Hornblende & Soils
Middle Pinedale	Hall and Martin (1986)	~22,000 - 28,000	Glacial Maximum	Madole (1980a,b), Pierce (1979)
Pinedale	Birkeland (1973)	~15,000-18,000	Glacial Maximum	
Upper Wisconsin	Reshkin (1963)	?	Glacial Maximum	Observations
Early Wisconsin	Hall (1990), Hall and Shroba (1995)	~70,000-60,000	Glacial Advance	
Lower Wisconsin	Reshkin (1963)	?	Glacial Maximum	Observations
Bull Lake	Reshkin (1963), Birkeland (1973), (1986)	~135,000-160,000	Glacial Maximum	Pierce et al. (1976), Hornblende
Bull Lake	Hall and Michaud (1988)	~140,000		Hornblende & Soils
pre-Wisconsin	Alden (1954)	?	Glacial Maximum	
pre-Bull Lake	Hall and Martin (1986), Hall and Michaud (1988)	~260,000-300,000	Glacial Maximum	Hornblende & Soils

(below 2,375 m) and out of the main glaciated trunk valleys, but he did identify at least fourteen end-moraines. He also evaluated the elevations and aspects of 68 different well-formed cirques throughout the range. He found that northeast slopes tended to favor cirque development and attempted to assign relative ages to some of the moraine deposits based on correlations to type-locality deposits in the Wind River Range. He favored the hypothesis that glaciers had never left the main valleys of the Tobacco Root Mountains or entered the surrounding basins. In his investigation, Jacobs (1967) photographed a well-developed active rock glacier near Upper Mason Lake (**Figure 2**) and speculated its age to be "post-Pleistocene," with at least two periods of advancement. He also speculated that some of the other cirque deposits in the area could be rock glaciers, but acknowledged that some might actually be late-glacial moraines. With regard to the proto-cirque deposits that were the focus of his thesis, Jacobs concluded that "niche" or "slab" glaciers were the source of deposition. His argument for the assignment of the deposits as moraines was based on an analysis of soil, boulder lithology, and apparent scouring at the base of the deposit. Jacobs (1967) speculated that the proto-cirque deposits formed at such atypically low elevations owing to a unique micro-climate and increased precipitation.

In a subsequent paper adapted from his dissertation, Jacobs (1969) added discussion of the calculated orographic snow line (ELA) for the Tobacco Root Mountains. By calculating the median elevation of the lowest moraine and highest point on the cirque headwall for each valley, he found that the ELA was at approximately 8,500 feet during the last glacial period. He determined that the mean elevation of 68 well-developed cirques is about 9,000 feet. Jacobs stated that he found no other similar proto-cirque deposits in the Tobacco Root Mountains, and again cited a favorable micro-climate enhanced by nearby valley glaciers as the cause for the low-elevation periglacial activity.

Figure 2: A photo collage showing a mosaicked panorama of deposit 001 from 2010 (background) and the same deposit as photographed by Jacobs (1967; center top).

A considerable amount of work on the Quaternary history of the Tobacco Root Mountains was done by Robert Hall and his students and collaborators (Hall, 1977; Hall et al., 1980; Roy, 1980; Roy and Hall, 1980; Ward and Hall, 1982; Hall and Heiny, 1983; Hall, 1984; Hall and Martin, 1986; Hall and Michaud, 1988; Hall, 1990; Hall and Horn, 1993), who undertook field mapping and collected soil samples of glacial deposits in several of the main valleys including South Boulder, Cataract Creek, North and South Willow Creek, and Bear Gulch. Dating techniques including lichenometry, differential weathering, and hornblende etching were employed to determine the relative ages of several glacial and periglacial deposits. Hall (1984) and Hall and Martin (1986) published ages for the cessation of different glacial maximums based on more than 20 radiocarbon dates from charcoal and organic sediment collected in glacial bogs and lakes.

Hall (1984), Hall and Martin (1986), Hall and Michaud (1988), and Hall (1990) discussed geomorphic evidence of major glacial advances both prior to and during the “Bull Lake” stade (see **Table 1**), but that most of the deposits in the Tobacco Root Mountains are “Pinedale” in age. Radiocarbon dates from Bear Gulch Valley measured on charcoal found in a kettle on top of a lateral moraine suggests a minimum date of 9,870 ± 680 YBP for “late-Pinedale” moraine deposition. The advance and retreat of “early-Holocene” glaciers is recorded by moraines approximately 2km from most major cirque headwalls (Hall, 1984), and organic sediment that accumulated behind the Cataract Creek moraine has been dated to 8,690 ± 380 YBP (Hall and Martin, 1986). Hall and Martin (1986) were unable to use hornblende etching to differentiate between Late Pinedale (10,500-9,900 YBP) and Early Holocene (earlier than 8,800 YBP) deposits, and suggested lumping them together as a single event (10,500-8,000 YBP). Hall (1990) noted the possibility of a small amount of “late Holocene” glacial deposition, but argued that the majority of recent deposits were periglacial in origin, consisting of rock glaciers and protalus ramparts. Hall (1990) stated that the majority of observable periglacial deposits were active in the Early Neoglacial on the basis of both radiocarbon and relative-age data, with a minimum radiocarbon age of ~3,600 YBP for the initialization of periglacial activity and a pronounced period

of periglacial advance around 2,500 YBP. Hall (1990) described a secondary pulse of periglacial activity on some Early Neoglacial deposits and described a relative-age difference of about 1,000 years between the older Early Neoglacial deposits and the superimposed “Mid Neoglacial” deposits (**Table 1**). Hall did not examine any deposits corresponding to the most recent neoglacial period (Gannett Peak).

Some additional work was done specifically on the rock glaciers of the Tobacco Root Mountains by Ward and Hall (1982). They established that some localities display two lobes of flow, with one atop the other representing multiple advances, whereas other sites only show evidence of one advance. They also suggested that the slope of a rock glacier may be linked to the source material available, which they speculated could be related to the orientation of foliation planes in the supplying headwalls. Ward and Hall (1982), like Jacobs (1967), indicated the presence of at least one rock glacier that appeared to still be active by way of interstitial ice; however, the location of this deposit was not clearly noted.

II. Methods

Remote Sensing and Feature Identification

An inventory of periglacial deposits focusing on protalus ramparts, lobate rock glaciers, and tongue-shaped rock glaciers was conducted for the Tobacco Root Mountains using high resolution (1 m) digital imagery (USDA-FSA, 2009) as the primary source of deposit identification (**Figure 1**). More than 250 deposits were identified using this method. Google Earth software was used to visualize the aerial imagery draped over a 10-m digital elevation model (DEM; Gesch et al., 2002). When a deposit was identified, its position was correlated in Google Earth and ArcGIS and the extent of the deposit was carefully mapped by digitizing a polygon boundary (**Figure 3**). The polygons, referred to as “deposit area,” include the bulge of the deposit and all talus chutes

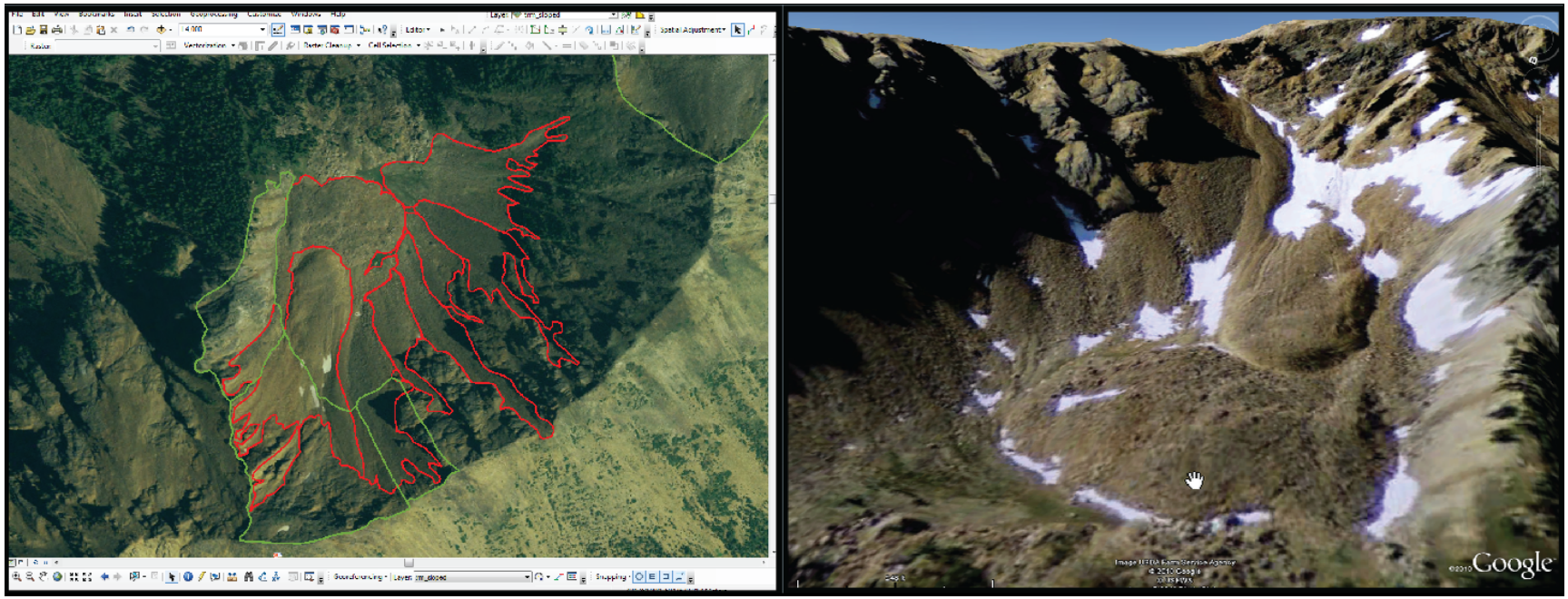

Figure 3: Screen capture from ArcGIS and Google Earth showing the process of identifying and outlining periglacial deposits at Little Granite Peak Cirque. In the image on the left, deposits are outlined in red and contributing rocksheds are outlined in green.

that contribute debris to the deposit. All major valleys in the mountain range were analyzed, and all notable deposits were outlined. Identified deposits were classified as protalus ramparts, lobate rock glaciers, or tongue-shaped rock glaciers based on the following criteria outlined in Madole (1972): **(1)** Protalus ramparts are arcuate ridges of debris that accumulate at the downslope edge of a snow bank, which itself is at the base of a talus slope. The debris shows no sign of movement post-deposition. **(2)** Lobate rock glaciers are lobes of debris having a larger width than length, which appear to have flowed post-deposition and have surface slopes less than the angle of repose. **(3)** Tongue-shaped rock glaciers are further differentiated from lobate rock glaciers as having a larger length than width. The presence of furrows along a rock-glacier surface was used as an indication that the deposit has moved since deposition.

The polygons representing deposit area were used to constrain the region of analysis for each deposit on the 10-m DEM and several DEM-derived raster datasets of equal resolution including slope and aspect. Data was extracted from the datasets using a tool called “Zonal Statistics” in the “Spatial Analyst” toolbar in Arc Toolbox. This dataset, referred to as “deposit data,” includes measurements of slope, aspect, area, and elevation. The DEM was also used in conjunction with information about Earth-Sun geometry to compute potential incoming solar radiation (insolation). The process of generating the derivative grids will be discussed in detail the “Potential Insolation” section. The types of zonal statistics derived for the extracted variables include minimum, maximum, average, sum, range, standard deviation, area, and count.

A subset of the deposit inventory (“priority deposits”) was selected for additional analysis. This dataset contains the 19 deposits that were visited in the field (not including secondary lobes) as well as 15 other prominently observable deposits. The additional analysis included more detailed measurements of deposit morphometry, an alternative method of volume estimation, and the generation of polygons encompassing the contributing headwalls above each deposit.

Morphometry

Areas

The planimetric rectangular area representing the deposit bulge (referred to as “block area”) was generated by estimating the length and average width of priority deposits. A polygon encompassing the contributing headwalls above the deposit bulge was also defined for priority sites. The headwall polygon outlines the debris rockshed of the deposit and includes both intact headwall outcrops and talus. The lower limit of a rockshed is defined as the point where the steeper talus slope (>35°) transitions into a more gently sloped bulge (<35°), as shown in **Figure 3**. As deposit polygons include both the bulge of the deposit and the contributing talus, a polygon representing only the exposed headwall outcrops (referred to as “headwall area”) was generated by clipping deposit polygons (and their talus slopes) out of rockshed polygons. Likewise, a polygon representing only the bulging lobe of a deposit (referred to as “bulge area”) was generated by clipping rockshed polygons and their talus slopes out of deposit polygons. Finally, a polygon representing only talus (referred to as “talus area”) was generated by finding the intersection of the rockshed and the deposit area polygon.

The deposit area was correlated to the bulge area (**Figure 4**) and headwall area (**Figure 5**), and best-fit equations were derived using the method of least-squares in order to facilitate the estimation of bulge area and headwall area for non-priority deposits. When this equation was applied to the deposit areas for the full dataset, the results are referred to as the “Interpolated Bulge Area” and the “Interpolated Headwall Area”, respectively.

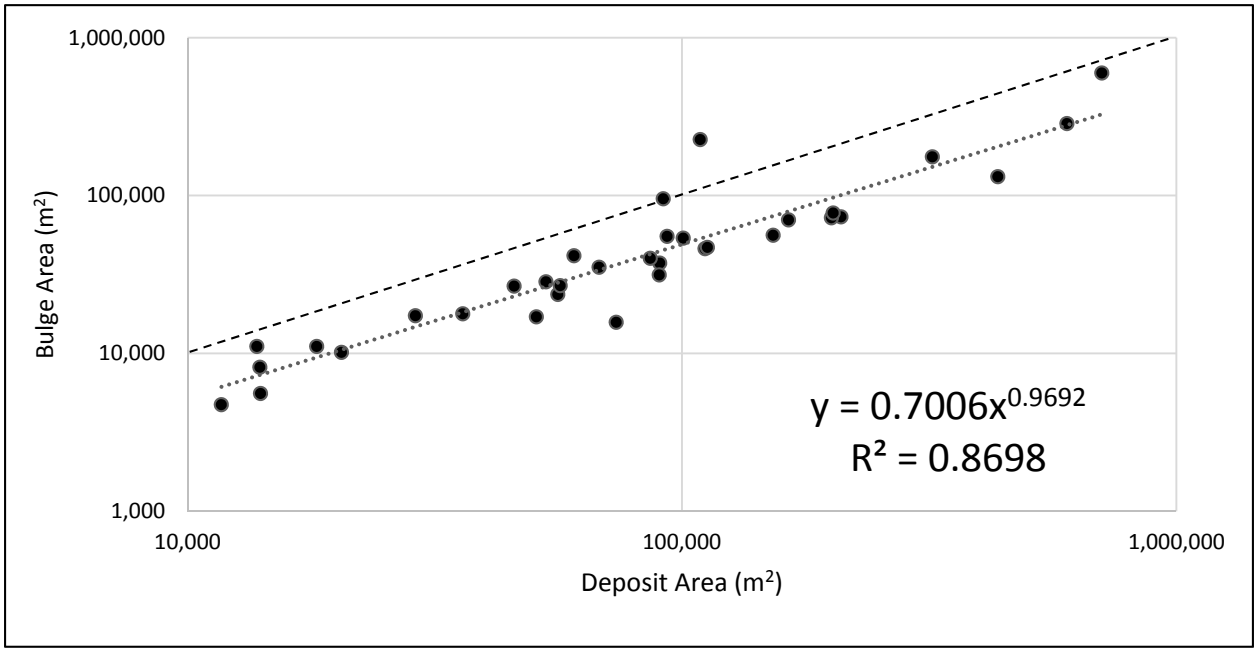

Figure 4: Relationship between deposit area and bulge area for priority deposits.

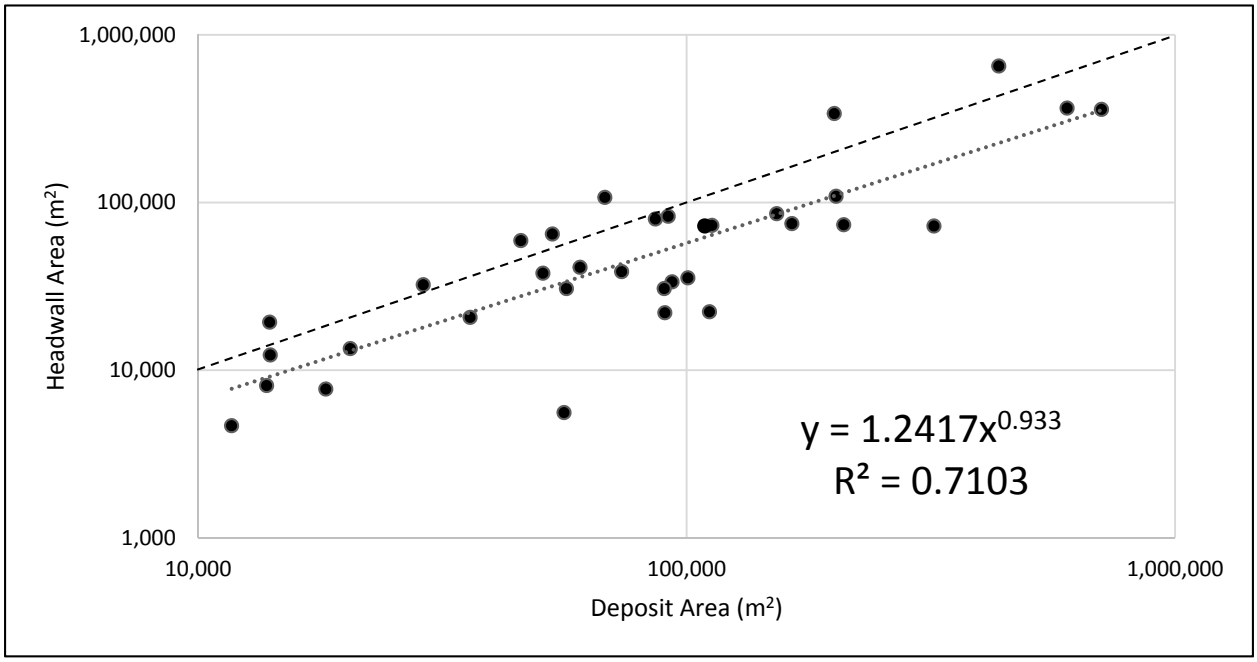

Figure 5: Relationship between deposit area and headwall area for priority deposits.

Length and Width

Length and width estimations were generated with the block area for priority deposits, but it was not possible to make an automated estimation of length and width directly for all deposits. However, a tool in ArcGIS called Minimum Bounding Geometry was used to circumscribe each deposit polygon with a Minimum Bounding Rectangle (MBR) (see **Figure 6**). The attributes generated with this tool for each MBR include short axis, long axis, and long axis orientation. For tongue-shaped deposits, the long axis length extends from the highest elevation talus to the lowest elevation reach of the deposit. For lobate rock glaciers and protalus ramparts, which are wider than they are long, the short axis of the MBR represents maximum length in the direction of flow. The long axis of the MBR represents the width of protalus ramparts and lobate rock glaciers, whereas the short axis of the MBR represents the width of tongue-shaped rock glaciers. The opposite of this is true for MBR length.

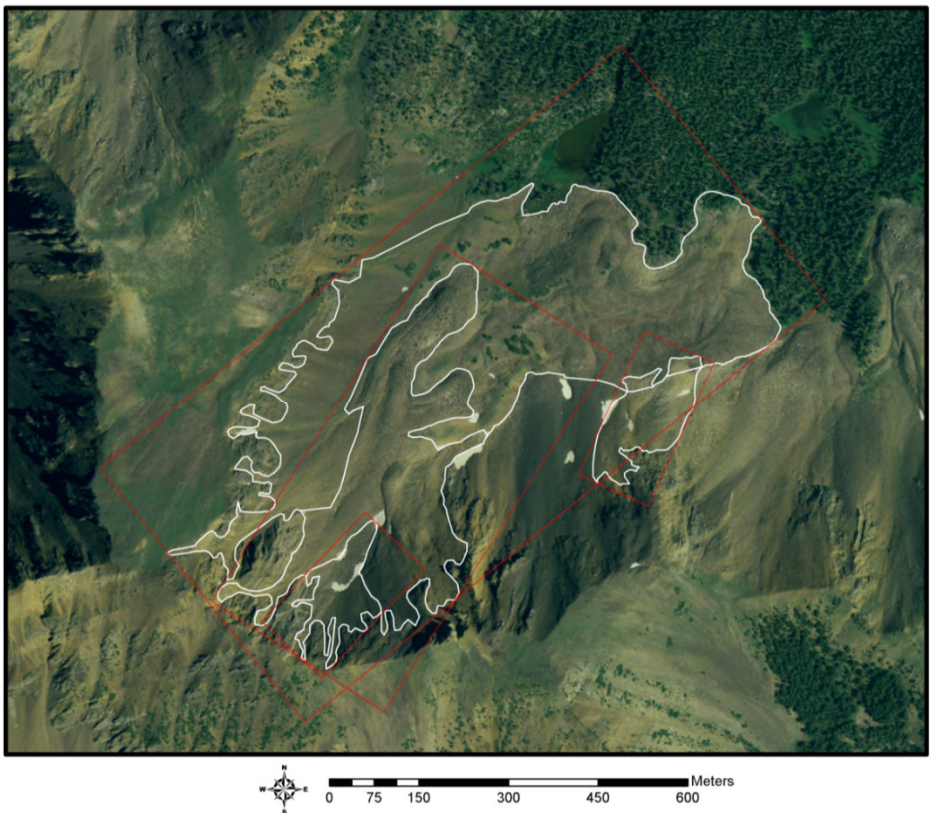

Figure 6: Aerial view of Curly Lake Cirque showing deposits (white) and MBR (red)

Deposit Thickness

Two methods were employed to estimate the thickness of deposits. One was an automated interpolation method for all deposits that was computationally efficient, and that produced results similar to the more time-consuming but more accurate slope-curve (SC) method used on priority deposits (see **Figures 7** and **8**). The interpolation method was applied to all deposits in the mountain range in an effort to determine the average thickness of deposits without the need for manual estimations.

SC Method: To calculate deposit thicknesses using the SC method, a longitudinal line was drawn along the center axis of the flow from below the lowest extent of the deposit to the intact headwall above the deposit. A series of points were evenly generated along the line, and at each point the elevation of the surface was extracted from a 10 meter DEM. The points were assigned X-Y coordinates so that the horizontal distance between points could be calculated. This information was exported to a spreadsheet where a longitudinal profile of the deposit was plotted. All points that were considered part of the bulge were removed, leaving the normal grade of the valley below and talus above. A second-order polynomial curve (quadratic) was then fit to the portion of data without the bulge included. The curve was intended to represent the original slope of the valley floor before it was covered by the deposit. Such a method is justified by the findings of Graf (1970), who showed that cirque and glacial valleys can be represented mathematically by a parabola. Using the equation of the generated curve, a series of data points corresponding to the original surface were created beneath the observed surface. By subtracting the elevation of these points from the elevation of the observed surface, the thickness (depth) along the center axis of the deposit was calculated and averaged (referred to as “SC thickness”).

Interpolation Method: In this method, the polygon representing the bulge of each deposit was used as a mask to remove data from a contour elevation layer comprised of polylines, and

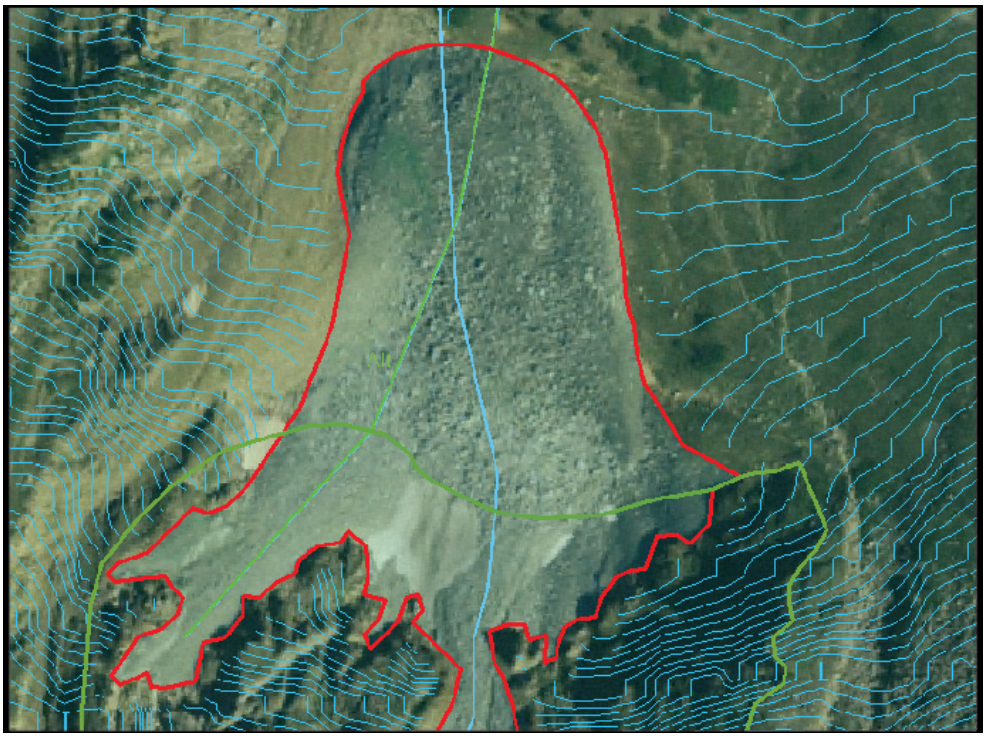

Figure 7: Screen capture of deposit 001 showing interpolation contour lines (blue), deposit outline (red), rockshed outline (green), and two slope-curve topographic profile lines running the length of the deposit (green and blue).

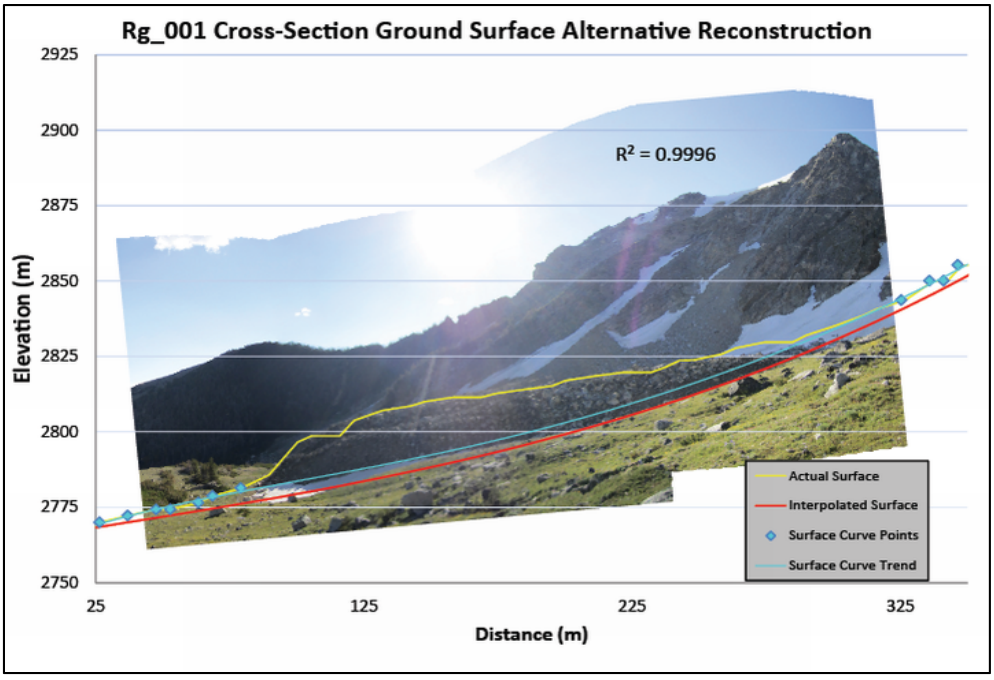

Figure 8: A composite image of deposit 001 showing the results of the two methods of volume estimation superimposed on a mosaicked profile photograph of the deposit.

the “interpolation” tool in Arc Toolbox was run on the resultant file to fill in the gaps caused by clipping out the bulge. This newly-interpolated polyline shapefile was then converted back into a DEM raster file representing the surface underneath the deposits. The interpolated DEM was subtracted from the original DEM using ArcMap 10.1 in order to generate an elevation difference grid (thickness). Zonal statistics were calculated on the difference grid to determine the average thickness of the bulge area. This method relies on the bulge being exposed on all sides in order to accurately capture the depth of the deposit. However, in many cases, the sides of the bulge were obscured or covered by surrounding talus deposits, resulting in a negative thickness estimate for some cells on the deposit. In order to compensate for this, the absolute value of the minimum thickness for each deposit was added to every cell of the deposit, ensuring that all cell values were positive.

When the interpolation method was compared to the SC method (priority deposits only; **Figure 9**), the interpolation method tended to generate greater thicknesses, especially at the upper end of the thickness range. However, for lower thicknesses the data tended to straddle the line of 1:1 correspondence.

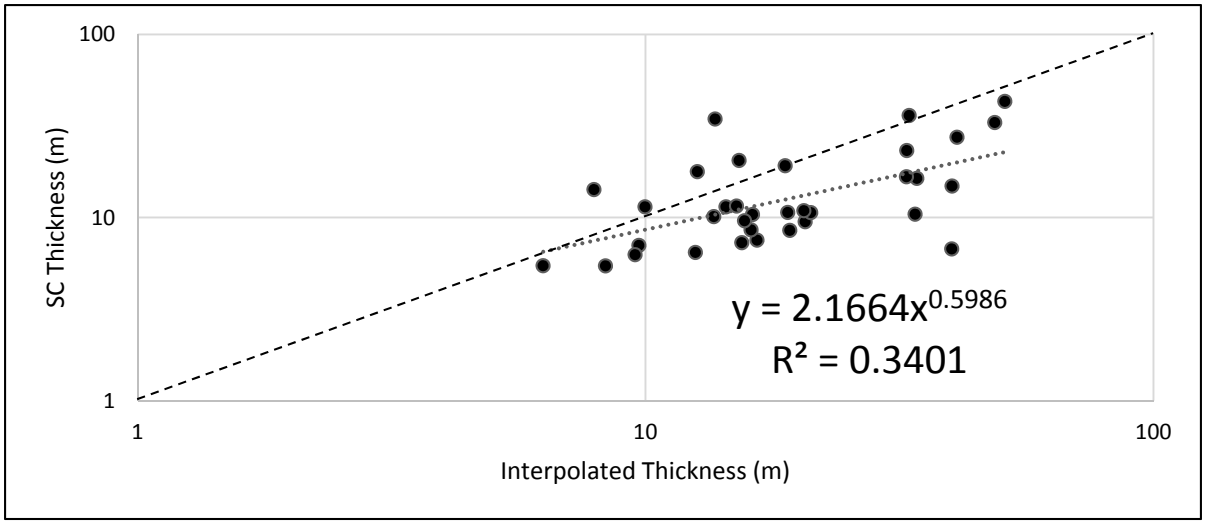

Figure 9: Relationship between interpolated thickness and SC thickness for priority sites.

Deposit Volume

Because there is a footwall slope of approximately 30° that exists between the block area and the bulge area of a rock glacier, the area used in the volume calculations of priority deposits was the sum of the block area and half of the difference in areas (block area – bulge area). This area is known as the "footprint" area (FP). The block length and width values were adjusted to reflect the footprint area while maintaining their original length-to-width ratio. The length, width, and thickness were then multiplied together to produce an estimate of deposit volume.

Potential Insolation

Four solar-radiation models were produced for the Tobacco Root Mountains in an attempt to isolate any relationships between radiation reduction due to topographic shading and rock-glacier occurrence and development. Potential insolation was determined by modifying the product of a tool in ArcGIS (Spatial Analyst Tools>Solar Radiation>Area Solar Radiation) that produces solar-radiation models considering Earth-Sun geometry and topography including slope, angle, and aspect, as well as shadowing by neighboring ridges (Fu and Rich, 1999). The models were generated using a 10-m DEM (Gesch et al., 2002) for the summer and winter solstices (Julian day 172 and 355, respectively), the vernal equinox (Julian day 79), and for the summer season (Julian days 79-265). The input parameters used for these models include a latitude of 45°, a sky size of 200x200 m, and both 14-day and 0.5-hour intervals. The model only considers the position of the sun and topographic shadowing, and does not account for differences in vegetation and surface albedo. The fractional (or percent) radiation reduction ($IR_{i,j}$) is defined as:

$$IR_{i,j} = 1 - \frac{I_{i,j}}{I_{max}}$$

where $I_{i,j}$ represents the potential radiation modeled for a given cell and I_{max} is the maximum modeled radiation value considering all cells. Potential insolation statistics were developed for the

deposit surface and contributing headwalls, as well as the areas receiving the lowest amount of solar radiation in the cirque of each deposit. In the case of the latter, descriptive statistics were calculated for circle-shaped polygons with a 20 meter radius centered on the areas of lowest solar radiation in the contributing headwall. This is referred to as the “cirque” dataset.

Relative-Age Criteria

Over the course of two field seasons (2009-2010), several attributes that are known to represent relative ages since deposition were measured at 24 sites. The deposits represented by the sites included tongue-shaped and lobate rock glaciers, protalus ramparts, and one of unknown origin. At five of these sites, relative-age measurements were made on a stratigraphic succession of flows originating from the same headwall. Each of the sites that were studied in the field were initially identified on aerial photographs. Accessibility, morphology, apparent age, elevation, aspect, and location were all considered in the process of selecting which sites to visit.

At each of the studied deposits, an appropriate area was selected prior to measuring relative-age variables. The measurement site was typically on the relatively flat debris mantle above the footwall or *snout* of the rock glacier. The site was chosen as close to the footwall as possible while making sure to select locations where boulders appeared undisturbed. This was done to increase the probability of finding boulders that have been exposed for the longest amount of time. In two cases (sites 014 and 080), the relative-age assessment was performed on the collapsed footwall of the deposit rather than the upper surface**.** This was done only when a deposit had developed a thick soil on its top and was covered by vegetation. In these cases, the collapsed footwalls provided the only suitable place to measure a sufficient number of exposed boulders. Footwall collapse only occurs after a rock glacier is inactive and the internal ice has melted, so relative-age data collected at these sites reflects the age of *deactivation* of the rock glacier rather than the age of *activation* that is reflected by data collected on the edge of debris mantles.

Once a suitable site was chosen, the center of the site was marked using a handheld GPS receiver. An effort was made to only mark the locations when the receiver displayed an uncertainty of less than 25 feet. In most cases, the uncertainty was less than 20 feet. The chosen site was also marked on an aerial photograph for cross-reference.

Birkeland (1973) was the first to argue for the use of multiple parameters in determining the relative ages of rock-glacier deposits. He noted that different parameters (measurable variables) have their own time span of effectiveness, outside of which it becomes difficult to accurately gauge relative age. He argued that only by combining and correlating apparent relative ages using multiple variables can an accurate assessment be performed.

As Dowdeswell (1982) states regarding relative-age dating, “To facilitate comparability between studies, and the replicability of any single study, it is … necessary to state explicitly the precise nature of the techniques used.” In this thesis nine different measures of relative age were made. These included boulder diameter, maximum lichen diameter, percent lichen cover, oxidation-rind depth, percent oxidation cover, boulder angularity, maximum pit depth, maximum crystal height, and the overall degree of boulder weathering (percent weathered). At each deposit visited in the field, measurements were made on 25 randomly selected boulders within an area roughly 10 m^2. The long axis of each boulder was measured to ensure that all boulders were larger than 0.5 meters in diameter. Large boulders were chosen because they have likely been exposed to weathering longer than smaller boulders due to the muesli effect (granular convection), a type of sorting that is observed in some rock-glacier debris mantles (Birkeland, 1973; Haeberli et al., 1998).

For each parameter evaluated at every site, the mean value was calculated. This generalized the values for a given site by finding the numerical average and reducing the effect of extreme values from individual boulders, which often do not represent the relative age of deposit accurately. In the case of lichen diameter, the maximum value for each site was also considered as it is likely to represent the most extreme age of the deposit.

Lichenometry

Birkeland (1973), among others, had success using the diameter of the largest lichen as an indicator of relative age for Holocene deposits. Accordingly, both the long and the short axis of the single largest lichen thallus on each boulder were measured using a mm scale. The apparent species of the measured lichen and a list of the most common species present were also recorded. Birkeland (1973) commented on the different species of lichen used in his study, stating that ideally *Rhizocarpon geographicum* (mapping lichen) would be the only species measured because of a published dating curve (Benedict, 1967), but that success is also possible using *Lecidea atrobrunnea* and *Lecanora thomsonii*. In this study *Rhizocarpon* was often used, but *Lecidea* or another genus was used when *Rhizocarpon* was not observed.

The percentage of lichen cover on a boulder has also been shown to be a good indicator of relative age (Birkeland, 1973; Dowdeswell, 1982). On most deposits, a visual comparison chart was used to estimate the percentage of the boulder surface covered with lichen, regardless of species composition.

Boulder Weathering

As a boulder containing mafic minerals weathers with time, the depth of oxidation rinds on the boulder increases (Porter, 1975); therefore, the amount of surface oxidation was also recorded as a relative-age indicator. The same visual comparison chart used to determine percentage lichen cover was used to estimate the percentage of surface oxidation. Oxidation-rind depths were measured by using a rock hammer to break away a fresh piece of each boulder. Care was taken to ensure that measurements were made perpendicular to the surface of the boulder and away from pre-existing fractures where apparent rind depth may not reflect exposure time to surface weathering. Boulder angularity was estimated using a different visual comparison chart that showed four degrees of boulder angularity. Birkeland (1973) showed that boulder angularity tends to decrease with time due to chemical and physical weathering.

When an area of minerals on the surface of a boulder disintegrates, a closed depression referred to as a pit develops (Birkeland, 1973), thus larger and more frequent pitting is proportional to duration of exposure to weathering. At each study site, each boulder was examined to determine whether or not pitting existed. On boulders with pits, the original surface of the boulder was visually reconstructed in order to measure the pit depth. The maximum pit depth for each examined boulder was measured. The maximum relief of an individual mineral grain above the surface of the boulder was also measured, following Dowdeswell (1982). According to Birkeland (1973), the presence and abundance of individual mineral grains is a good indicator of the degree of weathering of the boulder. If more than 10% of the boulder surface was covered with individual minerals standing in relief, the boulder was noted as being weathered.

Soil

The presence, composition, and horizon development of soil can be a critical variable in distinguishing between younger and older deposits (Birkeland, 1973). The majority of the deposits examined in this study showed at least some evidence of soil development. In most cases, the soil was weakly developed and could only be found along drainage furrows or in depressions. For the oldest deposits, significant soil development was present allowing vegetation to take hold. Whenever soil was present, a small soil pit was dug, the profile was described, and a sample of the soil representing each horizon was collected and its depth noted. For two of the sites that were covered in trees and had developed a thicker soil profile, a more extensive soil pit was dug and more samples were collected. Following the methods of Birkeland (1973), each soil profile was examined for the presence of loess because the thickness of loess and the development of soil horizons can be used as an indicator of relative age. In addition, if the deposits are below timberline, the thickness and maturity of vegetation covering them can help to differentiate relative ages.

Headwall Fracturing

Measurements of fracture density and orientation were made on the cliffs directly above 15 of the deposits that were visited in the field. Sites were chosen based on degree of exposure of the bedrock and fractures, ease and safety of accessibility, and apparent representativeness of the outcrop compared to the contributing region. At one site (029, **Figure 10**), photographs were taken from a known location in order to determine the degree of fracturing. For other sites, headwall measurements were made in multiple locations. This was done whenever there appeared to be a significant change either in lithology or nature of fracturing between two outcrops that were both contributing debris to the deposit below. At the majority of the sites visited, one location of headwall measurement was sufficient to capture the dominant nature of fracturing.

At each headwall measurement site, the geology of the bedrock was described for lithology, structural features, grain size, and estimated percent mineral content. In many cases, a representative hand-sample was collected for comparison. Each site was marked on a high-resolution aerial photograph and its location was also determined using a handheld GPS receiver, for which the accuracy of the measurement was noted. Physical conditions regarding the stability of the outcrop, the prevailing weather, and other factors which might affect the consistency of the measurements were recorded. The outcrops were examined to determine the dominant orientations of different fracture planes. Fracture planes were defined as a continuous separation in bedrock that is traceable for at least several feet. Whenever a plane was recognized, the strike and dip of the plane was measured and recorded. A tape measure was positioned perpendicular to the fracture plane and stretched across the exposed outcrop. The length of exposure varied depending on the outcrop and orientation being measured. The occurrence of notable fractures along the measured reach was counted and recorded. The width of the fractures was also noted.

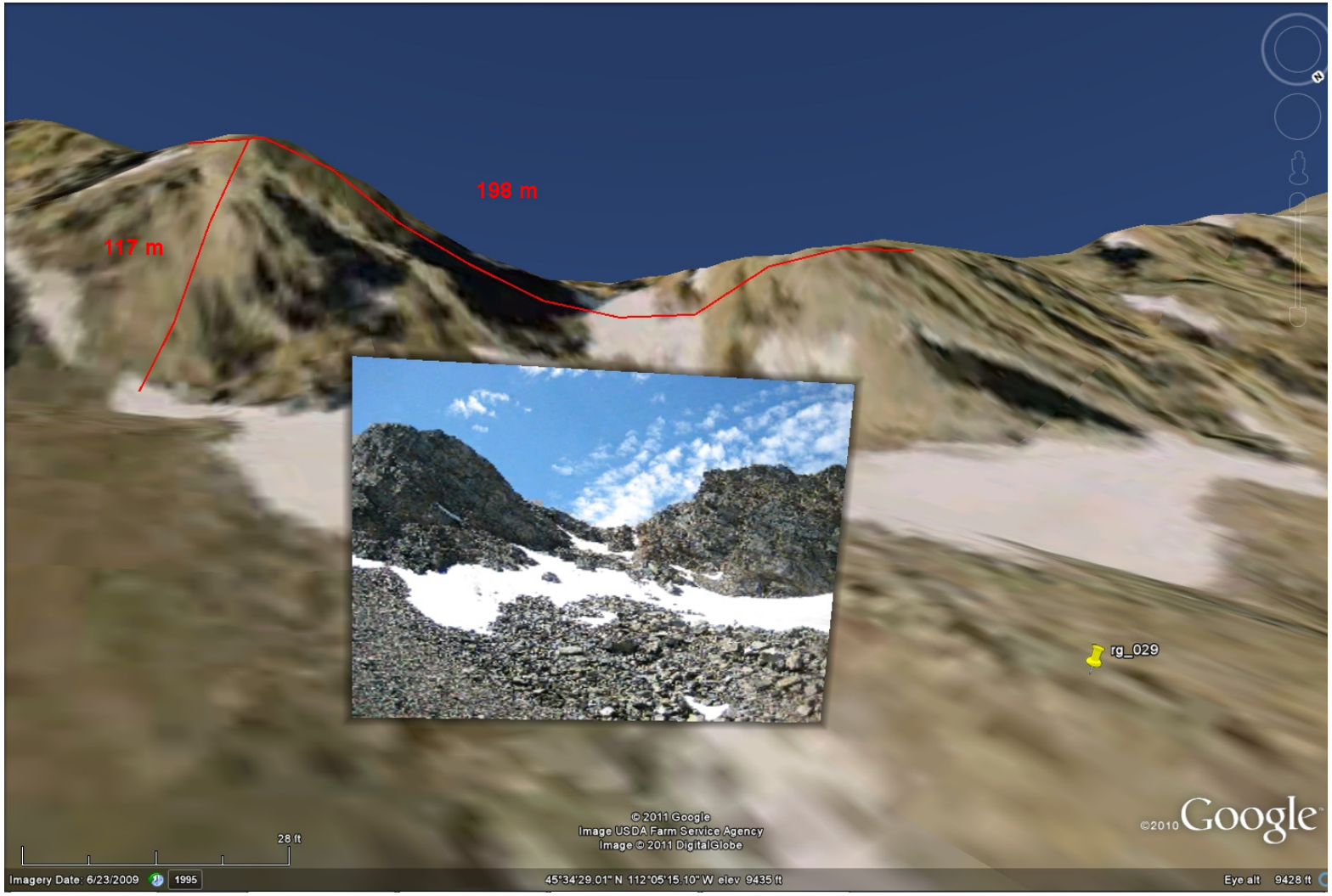

Figure 10: Screenshot from Google Earth showing the process of aligning the headwall photograph from deposit 029 geospatially in order to extract distance measurements and (ultimately) fracture density.

This process was repeated for the other dominant fracture planes (typically a total of 3-4 directions for each site). When the orientation of the fracture plane was the same as the dip slope or when the fracture plane was parallel to compositional banding/foliation, this information was noted. These conditions are thought to enhance the rate of rockfall and headwall erosion.

Statistical Methods

A variety of statistical methods were employed in this thesis for purposes of hypothesis generation and testing. The main focus of statistical analysis was determining (1) whether samples of data represent different underlying populations (difference of means testing), and (2) the statistical significance and functional nature of correlations between measured characteristics of periglacial deposit morphometry and related variables such as headwall fracturing and radiation reduction using least-squares regression and correlation analysis.

Comparison of Means

Variables for the three different morphologies examined in this study were compared using a Student's T-test to test the null-hypothesis that the samples come from the same population:

$$t = \frac{\overline{x_1} - \overline{x_2}}{\hat{S}_{\overline{x_1} - \overline{x_2}}}$$

where $\overline{x_1}$ and $\overline{x_2}$ represent the two sample means and $\hat{S}_{\overline{x_1} - \overline{x_2}}$ is an estimate of the standard deviation of the sampling distribution of the means. Preceding the t-test, an f-test was conducted to test the validity of the null-hypothesis of equal variance. In cases where the null-hypothesis of equal variance was accepted, a pooled standard deviation was used in the related t-test. Values of t represent the probability that the samples have the same mean and are from the same population.

Regression and Correlation Analysis

Correlation and regression analyses were conducted to identify and compare functional relationships between the different variables examined. Although Janke and Frauenfelder (2008) used simple linear regression to examine correlations among variables, a log-log plot with a power curve fit was chosen for most variables in this study due to the extreme range of values encountered (up to 5 orders of magnitude). Additionally, since both axes of these plots are logarithmic, the power trend is in linear form. The equation of the regression curve is:

$$\boldsymbol{y = \hat{a}x^{\hat{b}}}$$

which can be written in log-log analog as:

$$\boldsymbol{\log y = \log \hat{a} + \hat{b} \log x}$$

where $\hat{b}$ represents the estimated slope or gradient of the trend and $\log \hat{a}$ is an estimate of the log-*y* intercept, or value of y when *x=1*. Regression slopes and intercepts can also be tested for significance using a Student's t-test analogous to that presented above; the difference being that the parameter is tested versus a value of zero (null-hypothesis of no correlation) or against another known value such as $\hat{b}$=0.33 (isometry) in the case of comparing a regression slope relating length, width, or thickness to deposit volume.

Isometry and Allometry

The rate at which the dimensions of an area or a volume change determines whether the growth is isometric or allometric. Because periglacial deposits can develop from protalus ramparts to lobate and tongue-shaped rock glaciers (following the neoglacial facies model), an analysis of the proportional dimensions for each morphological class can give insight into this process and justify the classification scheme. Isometry describes relative growth that is equal in each dimension, whereas allometry describes asymmetrical growth. The number of dimensions for the variable being examined determines what the isometric growth value should be. The growth value is also referred to as "b," and is defined as the exponent of a power trend fit to a plot of the variable

and its comprising dimensions. For example, both the length and width of an area will have a b-value of 0.5 if growth is isometric. Accordingly, the length, width, and thickness of a volume will all have a b-value of 0.33 in cases of isometric growth. Finally, if two variables of equal dimension are compared, the isometric b-value will be 1.

Principal Components Analysis

Some of the relative-age variables are highly correlated to one another so a Principal Components Analysis (PCA) was performed in an attempt to reduce the original 13 variables into fewer numbers of underlying "factors" that still represent the majority of variance in the original data. PCA is a well-studied method for statistically analyzing the relationship between variables in large data sets, and has been used for over a century beginning with Pearson (1901). PCA can be applied to many different types of data (Wold et al., 1987), including relative-age data (Dowdeswell, 1982). The method seems particularly useful in relative-age-dating applications as the variables commonly used to assess relative age tend to have environmental and temporal limits to their effectiveness (Madole, 1972; Birkeland, 1973; **Figure 11**).

In PCA, a data matrix **(D_{nxm})** composed of **m** variables measured at **n** sites is manipulated to create a correlation matrix **(R_{mxm})** relating the m variables to one another. The characteristic roots or "eigenvalues" (λ) of the underlying principle components of the correlation matrix can be calculated using the following determinantal equation:

$$\boldsymbol{det(R - \lambda I) = 0}$$

where **I** is the identity matrix. There are an equal number of principle components as original variables in **R,** and the sum of the eigenvalues associated with all components is exactly equal to **m**.

Data reduction using PCA produces as many principle components as original variables **m**, but the first two or three components are typically sufficient to represent the majority of variance in the data. The first component often accounts for over half of the variance and each

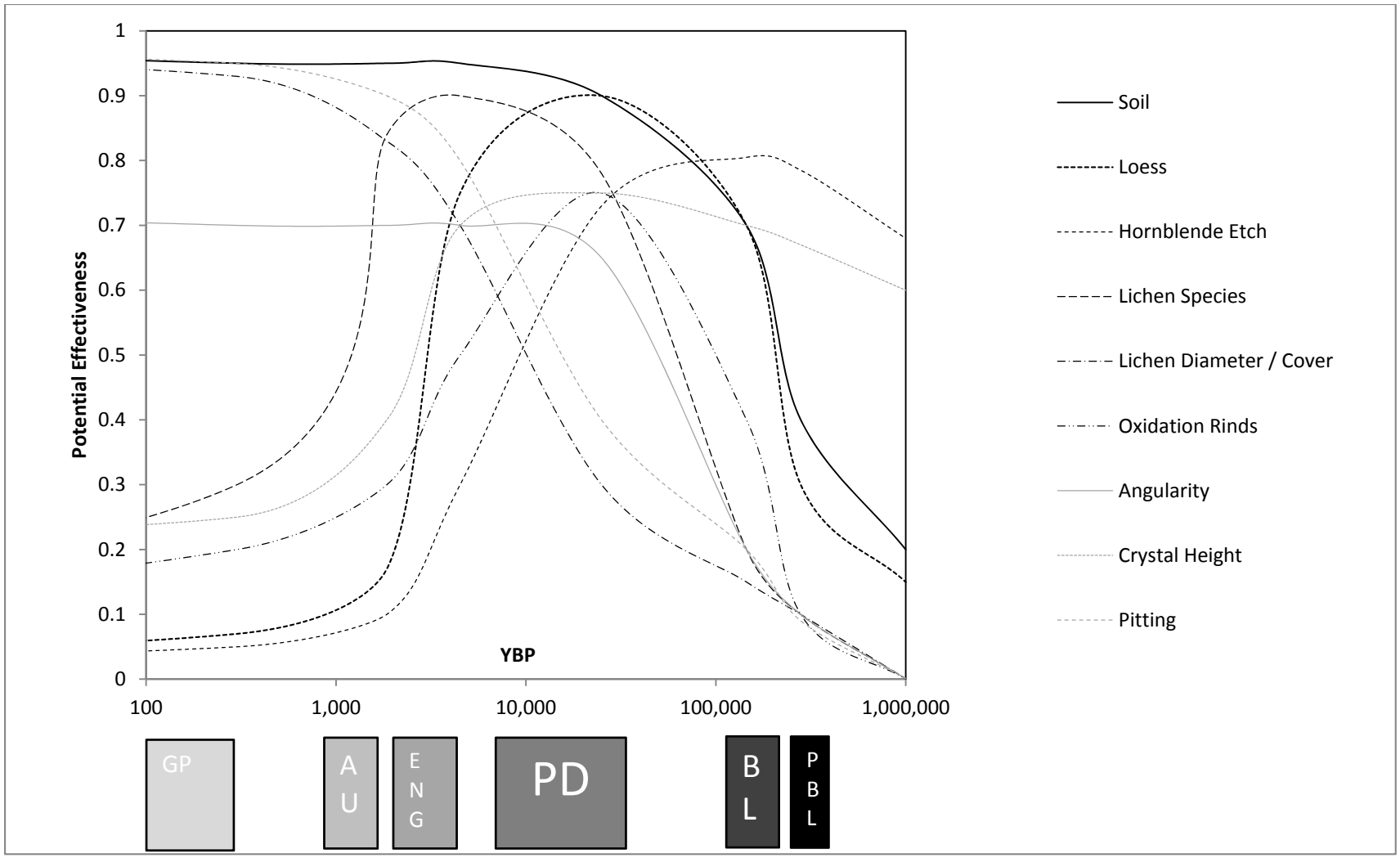

Figure 11: Schematic diagram showing the potential effectiveness of several relative age variables. The periods of periglacial development are labeled: GP=Gannett Peak, AU=Audubon, ENG=Early Neoglacial, PD=Pinedale, BL=Bull Lake, PBL=Pre-Bull Lake

successive component is less comprehensive than the former (Dowdeswell, 1982). The "residual," or statistically unaccounted variance, increases with each successive component. A component that fails to represent more variance than one of the original variables is deemed insignificant as it fails to reduce the data from its original form.

The original variables are related to the principle components through their eigenvectors ***x*** that can be calculated with the following equation:

$$(\boldsymbol{R} - \boldsymbol{\lambda}\, \boldsymbol{I})\, \boldsymbol{x} = \boldsymbol{0}$$

The elements of the vector **x** are known as "loadings" and can be interpreted as the weights relating the original variables to a particular principle component. Once the loadings and eigenvalues of the principle components have been calculated, the original data can be projected along the principle component axes by calculating their component scores $S_{j,k}$:

$$\boldsymbol{S_{j,k}} = \sum_{\boldsymbol{j=1}}^{\boldsymbol{m}} \boldsymbol{x_{j,i} y_{i,k}}$$

where $x_{j,i}$ represents the *ith* component loading for eigenvector *j* and $y_{i,k}$ represents the standardized magnitude of variable *i* for observation *k.* Each principle component is orthogonal to the preceding component so that there is no correlation between principle components. The component scores can be plotted in multi-dimensional space in order to identify potential groupings of the original measured sites.

III. Reconnaissance Investigations

A reconnaissance investigation was undertaken to validate the accuracy of remotely sensed boundaries and make measurements of relative age and headwall fracturing for selected deposits. Periglacial deposits ranging in morphological development from protalus ramparts to tongue-shaped rock glaciers were examined at 24 sites throughout the Tobacco Root Mountains. The deposits were visited over the course of 10 field campaigns on all sides of the range, but especially in the East and West Fork South Boulder River Valleys. An effort was made to get

representative sites from all parts of the study area while examining deposits with a wide range of topoclimatic characteristics, magnitudes, and morphologies. Factors such as ease of accessibility and proximity to other deposits also influenced the selection of field sites.

Bell Lake Cirque

Bell Lake Cirque is on the eastern side of the Tobacco Root Mountains in the headwaters of South Willow Creek (see **Appendix R and S; Figures R-1 and S-1**) and was the first cirque visited in the field. For the three sites in this cirque, a visual comparison chart was not referenced during the relative-age measurements. Accordingly, data recorded for visual variables such as percent lichen cover, percent oxidation, and angularity should be considered cautiously. The other relative-age variables that rely on physical measurements rather than visual estimation are more reproducible for these sites.

Deposits 058 and 059 (**Figure R-1**) appear as flows emanating from the same headwall with an azimuth of ~340˚. Deposit 058 is a moderately sized (~67,995 m^2) tongue-shaped rock glacier that ultimately extends to the shore of Bell Lake, and 059 is a small (~12,353 m^2) lobate rock glacier atop 058 and closer to the contributing headwall. The contributing headwalls for these deposits contain a talus chute that is nearly 400 meters tall. Fracture measurements were made at the base of this chute on an accessible headwall.

The surface of the basal deposit (058) has extensive soil development that fills the voids between the boulders and supports a sparse pine tree forest. However, no soil pit was excavated here to determine the thickness or development of the soil. Relative-age measurements were made in an area that was moderately open and sloped, above the collapsed footwall of the flow; however, the measured boulders were mostly buried in soil and only the upper exposed surface could be examined. Deposit 059 is superimposed on 058 just above the treeline in an area with a gentle (<20˚) slope. This superposition dictates that the deposit is younger than 058. The lack of vegetation and soil development on the much smaller boulders of 059 support this conclusion.

The final deposit examined in Bell Lake Cirque (060) appears to be a small (~11,709 m^2) protalus rampart at an elevation lower than Bell Lake. It emanates from a tall headwall that shades the deposit from the southern sky and has an azimuth of ~0˚. Headwall-fracture measurements were made about 50 meters above the deposit due to a lack of exposure at the base of the headwall cliff. Deposit 060 appears to be relatively thin and does not extend very far from its source headwall. It has coarse boulders with large interstitial voids, and shows minimal soil development. Relative-age measurements were made in an area that was exposed and with very little slope.

Sailor Lake Area

Three deposits were examined near the Sailor Lake area in the headwaters of the South Boulder Valley (see **Appendix R and S; Figures R-2 and S-2**). The first deposit examined in this area (008) is located southwest of Sailor Lake in a cirque containing Upper Sailor Lake. The cirque faces east with an azimuth of ~100˚. Deposit 008 is a relatively small (~14,047 m^2) lobate rock glacier, but it is one of the largest south-facing deposits in the Tobacco Root Mountains with an azimuth of ~170˚. Morphologically, it appears as a lobate rock glacier with a very steep slope (~40˚) extending to a large, gently-sloped (<10˚) collapsed footwall. The contributing headwalls are part of a prominent ridge that runs east-west and reaches an elevation of over 3,000 m. Fracture measurements were made on the cliff-face above the deposit, and relative-age measurements were made on a stable portion of the debris mantle above the collapsed footwall (**Figure R-2**).

The second deposit examined (116) extends over an area of ~28,894 m^2 and has an azimuth of ~110˚. It appears to be a protalus rampart that is encroaching towards the west side of Sailor Lake. The surface of the deposit is steep (<25˚) with a slight decrease in slope (>20˚) near the lake. The deposit seems to be fed debris primarily from a single chute that originates in a >2,900 m high, densely fractured headwall. Fracture measurements were made at two locations

and relative-age measurements were made at the base of the deposit near Sailor Lake (**Figure R-2**).

The final deposit (117), which occurs in Globe Lake Cirque to the northeast of Sailor Lake, covers an area of ~13,808 m^2 and has an azimuth of ~210˚. It appears to be one of a series of lobate rock glaciers that originate in a large rockshed north of Globe Lake. There are many bulges surrounding Globe Lake, but deposit 117 was chosen because of accessible outcrops and its large size relative to the other lobes. Fracture measurements were made at two locations on the intact headwall above the deposit, and relative-age measurements were made on a stable part of the debris mantle towards the base of the deposit (**Figure R-2**). Deposits 008, 116, and 117 are also referred to as SL-1, SL-2, and SL-3, respectively. A key correlating the numerical database name of each fully dated priority deposit with its locational name is listed in **Table 2** for reference.

Table 2: Correlations between database name and location name for 21 fully dated priority deposits.

Study Area	DB Name	Loc Name	Deposit Description
Sailor Lake	008	SL-1	South-facing deposit west of Sailor Lake
	116	SL-2	Deposit terminating in Sailor Lake
	117	SL-3	South-facing deposit near Globe Lake
Little Granite Peak	004	LGP-1.1	Basal lobe in Little Granite Peak Cirque
	003	LGP-1.2	Secondary lobe in Little Granite Peak Cirque
Sunrise Peak	025_1	SP-1.1	Basal lobe north of Sunrise Peak
	025_2	SP-1.2	Secondary lobe north of Sunrise Peak
	025_3	SP-1.3	Third lobe north of Sunrise Peak
	026_1	SP-2.1	Basal lobe northwest of Sunrise Peak
	026_2	SP-2.2	Secondary lobe northwest of Sunrise Peak
	028	SP-3	Deposit west of Sunrise Peak
	029	SP-4	Deposit east of Sunrise Peak near Sunrise Lake
Curly Lake	040	CL-1.1	Basal lobe in Curly Lake Cirque
	041	CL-1.2	Secondary lobe in Curly Lake Cirque
	036	CL-1.3	Third lobe in Curly Lake Cirque
	172	CL-2	Deposit near Curly Lake Cirque complex
Hollowtop	044	HM	Deposit west of Hollowtop Mountain
Branham	094	BR	Deposit in Branham Lakes Cirque
South Boulder	080	SBE	Basal lobe in East Fork South Boulder Valley
	115	SBC	Deposit near the South Boulder Confluence
Brownback	014	BB	Secondary lobe north of Brownback Mountain

Little Granite Peak Cirque

Two deposits were examined in Little Granite Peak Cirque on the northeast side of the peak (see **Appendix R and S; Figures R-3 and S-3**). The cirque is in a small hanging valley perched in the side of the trough that constitutes the eastern South Boulder River trunk valley. It is shaded by ridges that exceed 3,100 m to the east and south. One of the reasons that this site was chosen is because of a distinct superimposing relationship displayed by the two main deposits in the cirque. The deposits have an azimuth of ~15˚. The larger (~112,655 m^2) basal deposit (004) is spatulate in morphology (tongue-shaped with a widened front) and with very little slope on its down-valley half. The superimposed deposit (003) is tongue-shaped and covers an area of ~47,187 m^2.

There was still a significant amount of snow present on the upper parts of the talus feeding the flows when the site was visited on July 17th, 2009. The snow was several meters thick in places. Deposit 004 has a large collapsed footwall and a fairly steep (~45˚) front, whereas the footwall of 003 shows no evidence of collapse. Observations of the footwall of 003 indicate that it is comprised of boulders surrounded by a wet fine-grained matrix of sediment. The moisture in the matrix was at least partially from the melting snow, but the steep angle and lack of footwall collapse suggests that the deposit may still be actively deforming. Relative-age measurements for both deposits were collected on top of the flows, close to their fronts. Fractures were measured on a headwall above these deposits. Deposits 004 and 003 are also referred to as LGP-1.1 and LGP-1.2, respectively (**Table 2**).

Sunrise Peak Area

On the western side of the range, there are several short trunk valleys whose waters flow westward into the Jefferson Basin. Some of the most pronounced and morphologically complex rock glaciers in the Tobacco Root Mountains are found near Sunrise Peak (3,108 m). Several flows emanate from the massive headwalls on the north, east, and west sides of Sunrise Peak

(see **Appendix R and S; Figures R-4 and S-4**). Three of these flows were examined in part because of their distinctiveness with furrows, ridges, and multiple flows. Heading from east to west, these flows are labeled 025, 026, and 028.

Deposit 025 is a moderately sized (~60,493 m^2) tongue-shaped deposit with an azimuth of ~335˚ and several successively smaller flows atop the basal deposit. Relative-age variables were measured on each of the three lobes of 025 labeled (in increasing stratigraphic order), 025_1, 025_2, and 025_3 (see **Figure R-4**). Multiple fracture measurements were made above the deposits as several different types of geology and varied fracture patterns were present in the contributing headwalls.

Deposit 026, on the northwest side of Sunrise Peak, is a massive (~90,223 m^2) deposit with an azimuth of ~285˚ that is described by Hall (1990) as being “a rock slide that turned into a rock glacier.” The deposit is wider than it is long, but only barely, with a length to width ratio of 0.857. It is bounded on both sides by other deposits, but 026 is a distinctive lobe that obtained more mass and grew larger than the adjacent deposits. The west and east sides of the deposit are completely covered in soil and dense vegetation, while the center has barren boulders at the surface. There is a very distinct contact between the vegetated and unvegetated surfaces, making it seem probable that the vegetated part could be the remnants of Hall’s “massive rock slide,” the center of which continued to move down slope as a rock glacier. The thick basal deposit is labeled as 026_1, and a much thinner second flow that covers the upper part of 026_1 is labeled as 026_2 (**Figure R-4**). Relative-age measurements were made on a stable portion of the debris mantles of each flow in a non-vegetated area, and fracture measurements were made at two locations on the headwall above the deposit.

Deposit 028 is a tongue-shaped rock glacier that emerges from a cirque-like hollow on the west side of Sunrise Peak and covers an area of ~36,030 m^2 with an azimuth of ~340˚. The deposit is about 50 m higher in elevation than 025_1 or 026_1 and it has easily distinguished flow lines, furrows, and ridges on its surface. Part of the contributing headwall is comprised of an iron-

rich intrusion, giving the deposit stripes of rusty orange color. Deposit 028 merges into another deposit to the east, but it is significantly thicker than the other deposit and is easily differentiable. Fracture measurements were made at three locations along the contributing headwalls; twice on more massive quartzofeldspathic gneisses and once on the intrusion that lies between them. Relative-age measurements were made on a stable part of the debris mantle near the collapsed footwall.

To the east of Sunrise Peak on the south side of the lake below a steep headwall there is a tongue-shaped deposit (029) with an azimuth of ~20˚ that covers an area of ~18,255 m^2 and terminates in Sunrise Lake (**Figure R-4**). The debris mantle of the deposit has an average slope of 27°, but an acceptably flat area was chosen for the relative-age measurements. Fracture density in the contributing headwalls was extracted from high-resolution photographs taken at a known location. The “Image Overlay” tool in Google Earth was used to visualize the photograph spatially in the position and orientation that it was originally photographed. Once the outcrops in the photo were correlated with the stretched topography in Google Earth, the height and width of the photographed outcrops were measured (**Figure 6**). Fracture-orientation measurements were made directly. Deposits 025_1, 025_2, 025_3, 026_1, 026_2, 028, and 029 are also referred to as SP-1.1, SP-1.2, SP-1.3, SP-2.1, SP-2.2, SP-3, and SP-4, respectively (**Table 2**).

Curly Lake Cirque

Curly Lake cirque (see **Appendix R and S; Figures R-5 and S-5**) is carved into the very highest reaches of a hanging valley of the South Boulder Valley, and its headwalls are the source of several deposits that flow towards Curly Lake with an azimuth of ~45˚. The deposits terminate at the edge of a smaller lake, known locally as “Spade Lake” because of its shape. Among the deposits are tongue-shaped lobes with smaller deposits superimposed on top. Relative-age measurements were made at sites labeled 040, 041, and 036. Site 040 is on a massive (~321,036 m^2) basal flow and site 041 is on a smaller (~104,739 m^2) flow superimposed upon deposit 040.

Both sites 040 and 041 were chosen close to the outer edge of the debris mantle. Site 036 is on a very small (~14,119 m^2) tongue-shaped deposit that is superimposed upon deposit 041 in the upper reaches of the cirque. A small (~20,493 m^2) protalus rampart (172) along the valley to the east of the cirque with an azimuth of ~15˚ was also examined. Fracture density and orientation were measured on the headwalls of deposits 036, 040, and 041 at two locations, on differing lithologies: a quartzofeldspathic gneiss and a quartzo-mafic gneiss. Fracture data was also collected on the headwalls of deposit 172 at two locations because of a change in foliation orientation. Deposits 040, 041, 036, and 172 are also referred to as CL-1.1, CL-1.2, CL-1.3, and CL-2, respectively (**Table 2**).

Hollowtop Mountain Area

Hollowtop Mountain is the tallest peak in the Tobacco Root Range, reaching 3,233 meters in elevation. There are several deposits in the immediate vicinity of the peak (see **Appendix R and S; Figures R-6 and S-6**). During the summer of 2009, deposit 044 on the west side of the peak was examined. During the following summer, deposit 001 on the east side of the peak was also examined.

Deposit 044 is a large (~200,634 m^2) tongue-shaped rock glacier that emanates from a northwest-facing cirque on the west side of Hollowtop and flows northward along a narrow valley. The valley and deposit make a 90° turn to the west near the outer edge of the deposit, with an azimuth of ~270˚. Valley sidewalls contribute talus along the upper half of the deposit. Although no headwall-fracture measurements were made above 044, measurements were made on a nearby deposit (189) which appears to be a moderately sized (~45,784 m^2) protalus rampart. Deposit 189 approaches 044, but there is no overlap of their debris mantles. Two headwalls were measured above 189. These headwalls appear to have the same orientation as the headwalls above deposit 044. Relative-age measurements were collected near the footwall of deposit 044 on a stable part of the debris mantle, but no such data was collected on deposit 189.

On the eastern side of Hollowtop, there is a tongue-shaped deposit (001) that covers an area of ~53,104 m^2 with an azimuth of ~355˚. Rather than being confined by a valley like deposit 044, this deposit flows freely down the wide floor of a north-facing cirque. The deposit is symmetrical, and has a very steep footwall (>45˚), with loose wet silty soil in the interstices between boulders. Similar to deposit 003 (Little Granite Peak Cirque), the angle and wetness of the footwall indicate that deposit 001 may still be active. This deposit was also studied by Jacobs (1967) who described it as a rock glacier. As shown in **Figure 7**, the deposit appears to have evolved since it was photographed by Jacobs (1967); the size and position of the footwall appears to have changed, and individual large boulders appear to have also moved. Relative-age measurements were made on a stable part of the debris mantle, and fracture density and orientation were measured on one of the contributing headwalls. Deposit 044 is also referred to as HM (**Table 2**).

Branham Lakes Cirque

One of the southernmost glacial valleys in the Tobacco Root Mountains is Branham Lakes Valley. At the northern end of this valley there are several deposits (see **Appendix R and S; Figures R-7 and S-7**). The largest of these is deposit 094 (~89,968 m^2), which has an azimuth of ~95˚ and emanates from a ridge that strikes roughly north-south and reaches over 3,000 m in elevation. Relative-age measurements were made on a stable part of the debris mantle near the footwall. This site had some of the largest boulders observed, with one over 10 meters long. It was also the final deposit visited in 2009, and it was overcast and raining during the analysis. Determinations of lithology and measurements of fracture density and orientation were made on two different contributing headwalls. Deposit 094 is also referred to as BR (**Table 2**).

East Fork South Boulder Valley

In the East Fork of the South Boulder River Valley there is a very large (~706,876 m^2) tongue-shaped deposit (080) that covers the entire width of the valley and has an azimuth of

~315˚ (see **Appendix R and S; Figures R-8 and S-8**). The deposit appears to originate from several sidewall cirques on the east side of the main trunk valley. Across the deposit there are ridges and furrows, indicating it once flowed. Parts of the deposit are covered by patches of trees, sometimes extensively, whereas others remain completely non-vegetated. Deposit 080 stands out as one of the largest by area in the Tobacco Roots and is topped by a smaller (~361,445 m^2) but still massive tongue-shaped rock glacier labeled 081.

Although the contributing headwalls for these deposits were not visited nor photographed in any detail, both deposits were examined in passing while hiking to Little Granite Peak Cirque and relative-age measurements were made on the collapsed footwall of the furthest down-valley reach of deposit 080. The measurements were collected in this area due to the upper surface of the deposit being thickly vegetated and most boulders being partially covered with soil. The boulders of the former footwall are more exposed than those in the upper surface of the deposit, making this the most reliable surface available for relative-age dating, though it indicates a minimum age for the deposit as it represents the cessation of the flow. Deposit 080 is also referred to as SBE (**Table 2**).

South Boulder River Confluence

Near the confluence of the East and West Fork South Boulder Rivers there is a large (~600,955 m^2) rubble deposit (115) along the east sidewall of the main trunk valley with an azimuth of ~280˚ (see **Appendix R and S; Figures R-9 and S-9**). The deposit extends into the main trunk valley but is tree-covered over most of the surface, obscuring its morphology. As a result, it is unclear whether this deposit is a lobate rock glacier or a landslide. Relative-age measurements were made on an exposed patch of boulders at 2,218 m elevation. The measurements were made a considerable distance up-slope from the terminus of the deposit in an area with a slope of ~30˚. A shallow soil pit was excavated in a patch of trees just up-slope and the presence of loess was noted. The soil was poorly developed with only a very thin (~3 cm)

A horizon over unweathered parent material. Furthermore, the maximum depth of loess was only 25 cm. The contributing headwalls of deposit 115 were not visited. Deposit 115 is also referred to as SBC (**Table 2**).

Brownback Cirque

Brownback Mountain is a prominent and isolated rubble-covered peak on the north end of the Tobacco Root Range near the Indiana University Geologic Field Station (see **Appendix R and S; Figures R-10 and S-10**). Although the peak only reaches 2,794 m, the nearly east-west orientation of Brownback Ridge shadows a large cirque with at least one massive (~435,586 m^2) tongue-shaped rock glacier (labeled as 014) on the north side of the peak with an azimuth of ~5˚. The deposit is mostly covered in dense vegetation; however, the collapsed footwall remains un-vegetated. This vegetation contrast caused by the distinctive arc of barren boulders defining the front-edge of the deposit is the primary reason that it was identifiable on aerial photographs. Although most of the deposit is tree-covered, ridges and furrows can be seen along the surface of the deposit; indications that it once flowed.

The area down-valley from the collapsed footwall of deposit 014 is vegetated by pine trees that all appear to be roughly the same age based on trunk diameter (see **Figure 12**), indicating that the deposit was initially vegetated over a relatively short period of time. A detailed examination of aerial photographs revealed the very rough outline of an extremely large (~1,171,393 m^2) deposit beneath 014, labeled 014a. However, its boundary is hard to determine, and field investigations were focused on the younger and more distinguishable deposit 014.

Relative-age measurements were made on part of the open, non-vegetated collapsed footwall at 2,134 m above sea level. The measurement site is bounded up-slope by a steep (~25˚) rise that abruptly intersects a relatively low-sloping and densely-vegetated debris mantle. A soil pit was excavated on the debris mantle, close to the footwall. The solum is mostly loess, with occasional angular clasts of the underlying coarse debris mixed in. Several hours of excavation

Figure 12: Photograph taken on deposit 014a showing trees with similar trunk diameters.

failed to reach the bottom of the loess; ultimately the presence of larger boulders limited the depth of the pit to about 1 m. The profile shows a gradual color change from 5YR 6/2 at 10 cm to 10YR 7/4 at 60 cm, signifying the transition into a weak B horizon.

The cirque and contributing headwall of deposit 014, located over a mile away from the collapsed footwall, was not visited in 2009. However, the site was revisited during the summer of 2010 and fracture measurements were made on the headwall. With an elevation of approximately 2,405 m, Brownback Cirque is possibly the lowest-elevation cirque in the Tobacco Root Mountains. The elevations of the proto-cirque hollows examined by Jacobs (1967) on the eastern side of Hollowtop Mountain are less than 2,375 m, but they do not meet the classic definition of a cirque. Brownback Cirque is well-developed, with coarse boulder rubble forming the floor. Since

the cirque is below treeline, much of the surrounding area is vegetated. The cirque floor, however, is mostly free of trees and vegetation (although some small trees have started to take hold). There are also a significant number of large, dead trees (**Figure 13**) that may have been killed by prolonged snow cover and/or ice movement during a recent glacial period, or potentially a fire (although charring was not observed). Deposit 014 is also referred to as BBF (**Table 2**).

Figure 13: Photograph taken from the headwall above Brownback Cirque showing part of deposit 014. A large accumulation of dead trees is visible in the lower right corner, and the Golden Sunlight Mine can be seen shining (like a beacon of hope) near the upper left corner.

IV. Results of Statistical Analyses

Remotely Sensed Data

Summary of Means

Priority Deposits

Because there are only 34 deposits in the priority dataset (**Appendix U, Table 1**), with tongue-shaped rock glaciers (n=24) favored over lobate rock glaciers (n=5) and protalus ramparts (n=5), averages are not considered for different morphological classifications; instead all priority deposits are averaged. A summary of these values is provided in **Table 3.** The average minimum bounding rectangle (MBR) length (489 m) is greater than MBR width (353 m), and the maximum length (1,730 m) is more than twice the maximum width (676 m). The average SC thickness (14.79 m ± 3.25) is more than 30% smaller than the interpolated thickness (21.6 m ± 4.1); however, the SC minimum and maximum values are only about 15% smaller than the associated interpolated values. The average slope of the deposit (bulge and talus; 26.8˚) is closer to the maximum value (34.8˚) than the minimum value (14.0˚). For deposit area, the average (132,296 m^2 ± 54,020) is larger than the average headwall area (90,731 m^2 ± 45,756), and the same trend holds true for the minimum and maximum values. This is likely caused by bulking in the deposit rubble and the formation of void space. The height of headwalls above deposits ranges from 56 m to 525 m with an average value of 265 m. Of the elevation variables, the largest range in values is found for minimum deposit elevation and the smallest range found for maximum elevation. The average values for the minimum, mean, and maximum elevations are 2,631 m, 2,731 m, and 2,898 m, respectively. Finally, the SC volume is (on average) slightly smaller than the interpolated volume ($1.55x10^6$ m^3 ± $1.26 x10^6$;$1.81x10^6$ m^3 ± $1.26 x10^6$).

Table 3: Summary of means and standard deviations for the priority dataset. FP=Footprint, SC=Slope Curve, MBR=Minimum Bounding Rectangle, RR=Radiation Reduction

Variable	Priority Deposits		
	n=34		
	Mean	StDev	SE Mean
Slope	26.83	5.15	0.88
Deposit Area	132,396	160,709	27,561
Headwall Area	90,732	136,122	23,345
FP Area	60,698	98,391	16,874
FP Length	271	214	37
FP Width	185	130	22
Min. Elevation	2631	192	33
Mean Elevation	2731	157	27
Max Elevation	2898	130	22
MBR Width	375	188	32
MBR Flow Length	555	444	76
SC Thickness	14.79	9.70	1.66
SC Volume	1,549,986	3,775,426	647,480
Interpolated Thickness	21.66	12.27	2.10
Interpolated Volume	1,811,847	3,748,497	642,862
Cirque Elevation	2845	128	22
Cirque Slope	47.07	5.55	0.95
Summer Solstice RR	0.228	0.050	0.009
Winter Solstice RR	0.783	0.131	0.022
Vernal Equinox RR	0.510	0.131	0.023
Summer Season RR	0.304	0.076	0.013

All Deposits

When the average dimensional variables for all deposits are compared with priority deposits (**Table 4**), it is apparent that the full dataset consists of features that are smaller than those of the priority dataset. A disproportionately high amount of well-developed, tongue-shaped rock glaciers in the priority dataset is the reason for the difference in average dimensions. The mean interpolated thickness for all deposits is 17.22 m ± 1.24 and the average deposit area is 76,476 m^2 ± 14,970. MBR length and width are 318 m ± 40 and 338 m ± 24, respectively, which indicates that the modal deposit morphology is more like a lobate rock glacier than a tongue-shaped rock glacier.

Table 4: Comparison of means between all data and priority data. MBR=Minimum Bounding Rectangle, Thick=Thickness, RR=Radiation Reduction

Variable	Priority Deposits n=34			All Deposits n=248			All Deposits vs. Priority Deposits	
	Mean	StDev	SE Mean	Mean	StDev	SE Mean	t-test	p-value
Slope	26.83	5.15	0.88	27	5.91	0.38	0.16	0.876
Area	132,396	160,709	27,561	76,476	117,880	7485	-1.96	0.058
Min. Elevation	2631	192	33	2688	160	10	1.88	0.061
Mean Elevation	2731	157	27	2762	151	9.6	1.1	0.271
Max Elevation	2898	130	22	2868	156	9.9	-1.04	0.298
MBR Width	375	188	32	338	184	12	-1.09	0.279
MBR Flow Length	555	444	76	318	310	20	-3.01	0.005
Interpolated Thick	21.66	12.27	2.10	17.22	9.80	0.62	2.02	0.050
Cirque Elevation	2845	128	22	2863	139	8.8	0.72	0.473
Cirque Slope	47.07	5.55	0.95	45.72	6.13	0.39	-1.21	0.225
Summer Solstice RR	0.228	0.050	0.009	0.209	0.060	0.004	-1.76	0.080
Winter Solstice RR	0.783	0.131	0.022	0.723	0.183	0.012	-2.36	0.022
Vernal Equinox RR	0.510	0.131	0.023	0.453	0.169	0.011	-1.9	0.059
Summer Season RR	0.304	0.076	0.013	0.272	0.095	0.006	-1.93	0.055

The dataset containing all deposits (n=248) is large enough to be separated by morphologic class (tongue=90, lobate=98, protalus=60) and facilitate statistical comparisons. These values are listed in **Table 5**. Beginning with morphometric variables, the ratio of MBR length-to-width decreases moving from the glacier end to the talus end of the neoglacial facies model of Madole (1972). Tongue-shaped deposits are nearly twice as long as they are wide (1.93), whereas the inverse is true for lobate rock glaciers (0.64) and protalus ramparts (0.47). Accordingly, tongue-shaped rock glaciers have the longest average length at 538 m ± 81.8, whereas lobate rock glaciers and protalus ramparts have progressively shorter averages (220 m ± 34.9 and 148 m ± 20, respectively). Tongue-shaped deposits also have the greatest average thickness (20.5 m ± 2.2), and the thickness of lobate deposits (15.6 m ± 1.8) is essentially equivalent to that of protalus ramparts (15.0 m ± 2.1). For the variable of MBR width, lobate rock

Table 5: Morphometric comparison of variables for all deposits. MBR=Minimum Bounding Rectangle, RR=Radiation Reduction

Variable	Morph.	n	Mean	StDev	SE Mean	Min.	Max.
Deposit Aspect	Tongue	90	5.76	-	-	-	-
	Lobate	98	351.92	-	-	-	-
	Protalus	60	48.99	-	-	-	-
Slope	Tongue	90	25.024	5.889	0.621	10.973	38.766
	Lobate	98	26.842	5.475	0.553	10.475	38.115
	Protalus	60	30.202	5.292	0.683	15.26	40.698
Area	Tongue	90	125,978	169,997	17,919	4032	1,171,393
	Lobate	98	56,851	67,196	6788	3164	531,191
	Protalus	60	34,276	31,108	4016	2537	111,394
Interpolated Volume	Tongue	90	1,382,454	2,750,663	289,945	23,520	21,313,915
	Lobate	98	532,497	1498,666	151,388	4956	14,507,292
	Protalus	60	280,911	394,281	50,901	3795	1,882,995
Min. Elevation	Tongue	90	2672.4	174.1	18.3	1944.9	2917.8
	Lobate	98	2684.6	135.6	13.7	2299.2	2967.9
	Protalus	60	2715.3	173.9	22.4	2109.6	3053.7
Mean Elevation	Tongue	90	2770.2	155.4	16.4	2092.6	3024.6
	Lobate	98	2748	131.8	13.3	2364	3039
	Protalus	60	2771.5	172	22.2	2154.5	3127.9
Max Elevation	Tongue	90	2907.3	142.5	15	2459.8	3147.1
	Lobate	98	2842.8	149.8	15.1	2432.7	3103.6
	Protalus	60	2851.6	175.9	22.7	2206.7	3209.4
MBR Width	Tongue	90	295.6	180.1	19	46.6	997.5
	Lobate	98	381.7	191.2	19.3	90.5	918.6
	Protalus	60	331.3	164.9	21.3	84.7	684
MBR Length	Tongue	90	538.2	388.2	40.9	95.3	2668.5
	Lobate	98	220.3	175.8	17.8	42.4	1356.2
	Protalus	60	148.3	77.5	10	32	329
Thickness	Tongue	90	20.46	10.48	1.1	6.15	50.99
	Lobate	98	15.583	9.247	0.934	2.968	70.075
	Protalus	60	15.03	8.4	1.08	2.93	40.09
MBR L/W	Tongue	90	1.934	0.767	0.081	0.390	3.925
	Lobate	98	0.636	0.458	0.046	0.195	2.712
	Protalus	60	0.468	0.155	0.02	0.207	0.840
Cirque Elevation	Tongue	90	2894.5	129.9	13.7	2522.6	3102.2
	Lobate	98	2840.5	133.9	13.5	2509.4	3104.2
	Protalus	60	2854.1	152.0	19.6	2294.7	3164.3

Variable	Morph.	n	Mean	StDev	SE Mean	Min.	Max.
	Tongue	90	2.19	-	-	-	-
Cirque	Lobate	98	345.95	-	-	-	-
Aspect	Protalus	60	13.67	-	-	-	-
	Tongue	90	45.381	6.727	0.709	24.561	61.361
Cirque Slope	Lobate	98	46.116	4.958	0.501	35.679	59.63
	Protalus	60	45.589	6.947	0.897	26.69	57.524
	Tongue	90	0.211	0.055	0.006	0.085	0.344
Summer	Lobate	98	0.208	0.055	0.006	0.083	0.343
Solstice RR	Protalus	60	0.206	0.075	0.010	0.092	0.378
	Tongue	90	0.775	0.121	0.013	0.212	0.862
Winter	Lobate	98	0.727	0.178	0.018	0.156	0.851
Solstice RR	Protalus	60	0.638	0.234	0.030	0.231	0.862
	Tongue	90	0.487	0.128	0.014	0.073	0.683
Vernal	Lobate	98	0.455	0.166	0.017	0.049	0.752
Equinox RR	Protalus	60	0.399	0.213	0.028	0.081	0.787
	Tongue	90	0.285	0.080	0.008	0.078	0.448
Summer	Lobate	98	0.270	0.089	0.009	0.088	0.463
Season RR	Protalus	60	0.254	0.120	0.016	0.074	0.510

glaciers have the largest average width at 382 m ± 38.6 followed by protalus ramparts at 331 m ± 42.6 and tongue-shaped deposits at 296 m ± 38.

The slope of tongue-shaped rock glaciers (~25° ± 1.2) is slightly less than that of lobate rock glaciers (~26.8° ± 1.1), whereas protalus ramparts (~30° ± 1.4) have the steepest slope. There is little difference between the average slopes of different morphologies in the cirque dataset, although the average slope of lobate rock glaciers (~46.1° ± 1.0) is slightly larger than protalus ramparts (~45.6° ± 1.8) and tongue-shaped rock glaciers (~45.4° ± 1.4).

The average aspect for tongue-shaped rock glaciers is just east of north at 5.8°, whereas the corresponding average cirque aspect is 2.2°. Lobate rock glaciers have an average aspect just west of north at 351.9°, and the cirque values have a slightly more westerly aspect, with an average of 346.0°. The aspects of protalus ramparts show the highest deviation from north; deposits average at 49.0°, and their cirques average at 13.7°.

For deposit area, there is a progressive decrease in values moving from the glacier end to the talus end of the neoglacial facies continuum. Tongue-shaped deposits (125,978 m^2 ± 35,838) cover more than twice the area of lobate deposits (56,851 m^2 ± 13,576), and protalus ramparts cover the smallest area (34,276 m^2 ± 8,032).

Tongue-shaped deposits receive less radiation than lobate deposits, which are less insolated than protalus ramparts. This is true for each of the four solar-radiation models examined; however, radiation-reduction values and their range among different morphologic types are most accentuated for the winter solstice (0.64-0.78) and the vernal equinox (0.40-0.49). The summer season (0.25-0.28) and the summer solstice (0.207-0.211) models show much smaller differences for the average insolation values of different morphologies. The standard error of the mean for these values is always smaller than the differences between morphologic classes with the exception of protalus ramparts in the summer season model.

Comparison of Datasets

Student's t-tests were used to compare the estimated mean morphometric attributes of priority and non-priority deposits within the Tobacco Root Mountains (**Table 4**). Based on the computed t-statistics, there is no statistically significant difference at the 95% confidence level between the average values of slope, area, elevation (minimum, mean, and maximum), MBR width, cirque elevation, cirque slope, summer solstice radiation reduction (RR), vernal equinox RR, and summer season RR. Although the null hypothesis that the samples come from the same poulation could not be rejected in the cases of area (p=0.058), minimum elevation (p=0.061), and the radiation-reduction models (SSol p=0.08; SE p=0.059; SSea p=0.055), the computed t-values are close to the specified confidence level. The t-values for MBR flow length (t=-3.01; p=0.005) and winter solstice RR (t=-2.36; p=0.022) for the priority dataset are statistically higher than those of the full dataset, as are the interpolated thicknesses (t=2.02, p=0.05).

In cases where the null-hypothesis is rejected, the underlying reason for the significant difference in means is likely the disproportionate amount of massive and well-developed tongue-

shaped deposits in the priority dataset. These deposits tend to be in more ideal topoclimatic settings with higher radiation reduction than the non-priority average, and they tend to have larger areas, lower minimum elevations, and longer flow lengths (**Table 4**).

Morphological Statistics

Morphometry

The results of t-tests among different morphological classes for all deposits are summarized in **Table 6**. For the comparison between tongue-shaped and lobate rock glaciers, the morphometric variables (area, MBR length, MBR width, interpolated thickness) all have p-values less than 0.05, which justify rejecting the null hypothesis and indicate that the populations have statistically different means.

The comparison between tongue-shaped rock glaciers and protalus ramparts yields fairly similar results to the comparison between tongue-shaped and lobate rock glaciers. The t-test results suggest that the null-hypothesis should be rejected for all morphometric variables except MBR width ($p=0.22$).

For lobate rock glaciers and protalus ramparts, the variables of area ($p=0.005$) and MBR length ($p=0.001$) are the only two that merit rejecting the null-hypothesis of equal means, although MBR width is close to the confidence interval ($p=0.092$).

The statistically significant differences of length and width between tongue-shaped rock glaciers and other deposits were expected, as the length-to-width ratio is used to define the different morphological classes of rock glaciers in the first place. Protalus ramparts and lobate rock glaciers are more similar in their morphology, but their magnitudes are different enough to cause statistically significant differences in their average values of length and area.

Topoclimate

The topoclimatic variables of slope and elevation (maximum, mean, minimum) were also compared among morphological classes (**Table 6**) to test the null hypothesis of equal means.

Table 6: Statistical results of morphometric mean comparisons for all deposits. MBR=Minimum Bounding Rectangle, RR=Radiation Reduction

All Deposits n=248	Tongue vs. Lobate		Lobate vs. Protalus		Tongue vs. Protalus	
	t-test	p-value	t-test	p-value	t-test	p-value
Deposit Area	3.61	0	2.86	0.005	3.61	0
MBR Width	-3.17	0.002	1.69	0.092	-1.23	0.22
MBR Length	7.13	0	3.53	0.001	9.25	0
Interpolated Thickness	3.39	0.001	0.37	0.709	3.36	0.001
Slope	-2.19	0.029	-3.79	0	-5.49	0
Min. Elevation	-0.53	0.595	-1.17	0.245	-1.48	0.141
Mean Elevation	1.06	0.291	-0.91	0.366	-0.05	0.961
Max Elevation	3.02	0.003	-0.34	0.737	2.13	0.034
Summer Solstice RR	0.41	0.681	0.1	0.918	0.4	0.694
Winter Solstice RR	2.2	0.029	2.51	0.014	4.18	0
Vernal Equinox RR	1.51	0.133	1.72	0.089	2.86	0.005
Summer Season RR	1.17	0.242	0.9	0.371	1.73	0.087

Beginning with tongue-shaped rock glaciers and lobate rock glaciers, the null hypothesis is only rejected for maximum elevation (p=0.003) and slope (p=0.029). For minimum and mean elevation, the p-values indicate that the populations are not significantly different (p=0.595; p=0.291).

The comparison of tongue-shaped rock glaciers and protalus ramparts again shows very similar results to the comparison of tongue-shaped and lobate rock glaciers. The null hypothesis could not be rejected in the cases of minimum and mean elevation (p=0.141; p=0.961), but slope (p=0) and maximum elevation (p=0.034) show statistically different averages. When comparing lobate rock glaciers to protalus ramparts, slope showed a distinct difference (p=0); however the three elevation variables did not.

In addition to the variables of elevation and slope, radiation reduction was evaluated using four solar-radiation models (summer solstice, winter solstice, vernal equinox, summer season) among the three morphological classes (**Table 6**). When testing for equal mean values, the null hypothesis could not be rejected for all cases in the summer solstice and summer season models (p=0.681-0.918; p =0.087-0.371, summer solstice and summer season, respectively). Failure to

reject the null hypothesis is seen in the vernal equinox model for tongue-shaped and lobate rock glaciers (p=0.133) and for lobate rock glaciers and protalus ramparts (p=0.089), whereas vernal equinox radiation reduction showed a significant effect on tongue-shaped rock glaciers and protalus ramparts (p=0.005). Finally, for the winter solstice model showed significant results in all three cases (p=0.000-0.029). This suggests that topoclimatic conditions during the winter months may have a greater influence on the development of periglaical deposits than during other times of the year.

A combined analysis of the interrelationships between both deposit and cirque aspect as well as radiation reduction among morphological classes is facilitated by the plots depicted in **Figures T-1 - T-8** (**Appendix T**). Fourth-order polynomials were fit to the trends relating radiation reduction to aspect, and are summarized in **Table 7.** In this table, '*a'* represents the multiplier of the x term and '*b'* represents the offset or y-value when x=0. Because aspect is displayed on the x-axis, the b-values signify radiation reduction for a north-facing aspect. Because the majority of rock glaciers tend to form with north-facing aspects, these values are practical for comparing the results. Beginning with deposit aspects on the winter solstice, tongue-shaped rock glaciers receive the most radiation reduction (b=0.7943) followed by lobate rock glaciers (b=0.7758) and finally protalus ramparts (b=0.7625). For the vernal equinox, this progression is inverted with tongue-shaped rock glaciers receiving the most insolation (b=0.605) followed by lobate rock glaciers (b=0.628) and protalus ramparts with the least insolation (b=0.6383). The same holds true for both the summer season and the summer solstice, with tongue-shaped rock glaciers receiving the most insolation (b=0.359; b=0.258, summer season and summer solstice, respectively) followed by lobate rock glaciers (b=0.372; b=0.272) and protalus ramparts (b=0.38; 0.281). Part of the reason for the inverse correlation between insolation and morphological class for most models is that the longer the deposit becomes, the more likely part of it will leave the shading of its surrounding headwalls and thus receive more solar radiation. This is most clearly

Table 7: Correlation tests for radiation reduction on all deposits. RadRed=Radiation Reduction, Poly=Polynomial, WS=Winter Solstice, VE=Vernal Equinox, Ssea=Summer Season, SS=Summer Solstice

	n	Correlation	a	b	R^2	Fig #
	248	Deposit Aspect vs. Deposit Mean RadRed WS	0.0054	0.7943	0.8815	T-1
	248	Deposit Aspect vs. Deposit Mean RadRed SE	-0.0008	0.6054	0.7894	T-2
	248	Deposit Aspect vs. Deposit Mean RadRed Ssea	-0.0009	0.3588	0.6592	T-3
Tongue	248	Deposit Aspect vs. Deposit Mean RadRed SS	-0.0006	0.2576	0.4929	T-4
4th Order Poly	248	Cirque Aspect vs. Cirque Mean RadRed WS	0.0067	0.7984	0.9584	T-5
	248	Cirque Aspect vs. Cirque Mean RadRed SE	-0.0016	0.5944	0.714	T-6
	248	Cirque Aspect vs. Cirque Mean RadRed Ssea	-0.0005	0.8201	0.9337	T-7
	248	Cirque Aspect vs. Cirque Mean RadRed SS	-0.0007	0.4737	0.5306	T-8
	248	Deposit Aspect vs. Deposit Mean RadRed WS	0.0068	0.7758	0.8904	T-1
	248	Deposit Aspect vs. Deposit Mean RadRed SE	0.0013	0.628	0.9483	T-2
	248	Deposit Aspect vs. Deposit Mean RadRed Ssea	-0.0014	0.3722	0.7788	T-3
Lobate	248	Deposit Aspect vs. Deposit Mean RadRed SS	-0.0013	0.2716	0.5772	T-4
4th Order Poly	248	Cirque Aspect vs. Cirque Mean RadRed WS	0.0077	0.8049	0.9682	T-5
	248	Cirque Aspect vs. Cirque Mean RadRed SE	-0.0021	0.6266	0.9192	T-6
	248	Cirque Aspect vs. Cirque Mean RadRed Ssea	-0.0008	0.8433	0.989	T-7
	248	Cirque Aspect vs. Cirque Mean RadRed SS	-0.0015	0.5073	0.8285	T-8
	248	Deposit Aspect vs. Deposit Mean RadRed WS	0.0081	0.7625	0.9578	T-1
	248	Deposit Aspect vs. Deposit Mean RadRed SE	-0.0013	0.6383	0.8965	T-2
	248	Deposit Aspect vs. Deposit Mean RadRed Ssea	0.0005	0.38	0.873	T-3
Protalus	248	Deposit Aspect vs. Deposit Mean RadRed SS	0.0001	0.2814	0.7721	T-4
4th Order Poly	248	Cirque Aspect vs. Cirque Mean RadRed WS	0.009	0.7742	0.9811	T-5
	248	Cirque Aspect vs. Cirque Mean RadRed SE	-0.004	0.6669	0.9161	T-6
	248	Cirque Aspect vs. Cirque Mean RadRed Ssea	-0.0012	0.8417	0.981	T-7
	248	Cirque Aspect vs. Cirque Mean RadRed SS	-0.0037	0.5529	0.8229	T-8

illustrated in **Figure 14**; when radiation reduction is averaged over the entire deposit, the trend of the data no longer follows the theoretical distribution seen when only the maximum value for each deposit is used (**Appendix T; Figures T-1 - T-8**). Because tongue-shaped rock glaciers are (on average) more likely to face north than lobate rock glaciers or protalus ramparts, the winter solstice model differs from the others, and tongue-shaped rock glaciers are the least insolated.

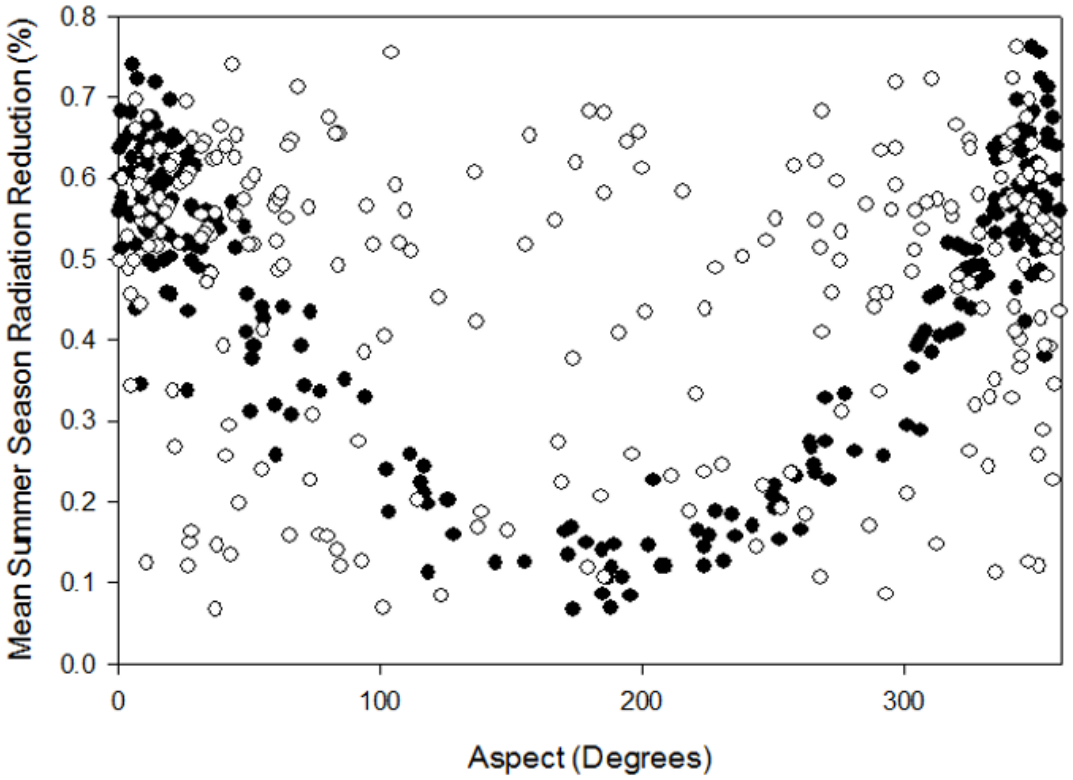

Figure 14: Cirque (black) and Deposit (white) Aspect vs Mean Summer Season Radiation Reduction.

In north-facing cirque aspects, the same trend of decreasing insolation is found moving from the glacial end to the talus end of the neoglacial facies spectrum for the vernal equinox and the summer solstice models. Tongue-shaped rock glaciers (b=0.594; b=0.474, vernal equinox and summer solstice, respectively) receive more insolation than lobate rock glaciers (b=0.627; b=0.507), with protalus ramparts receiving the least insolation (b=0.667; b=0.553). Although the vernal equinox results are very similar to the deposit results, the values for cirque radiation reduction on the summer solstice tend to be much larger (0.2-0.3) than equivalent values for the

deposits. The trends for the winter solstice and the summer season seem a little more random in terms of deposit morphology. Tongue-shaped rock glaciers (b=0.798; b=0.82, winter solstice and summer season, respectively) receive slightly more insolation than lobate rock glaciers (b=0.805; 0.843), whereas protalus ramparts receive the most insolation on the winter solstice (b=0.774) and nearly the same as lobate rock glaciers for the summer season (b=0.842). Although the deposit and cirque values are comparable for the winter solstice, summer season values are drastically different. Cirque points receive significantly less solar radiation (0.45-0.56) during the summer season than their associated deposits.

Regression Analysis

A correlation matrix for the different dimensional variables for priority deposits is provided in **Table 8**. The matrix exhibits fairly strong correlations, and the most correlated variables are SC volume, interpolated volume, deposit area, footprint area, MBR area, MBR length, and footprint length. Deposit area has the highest average correlation with other variables in the matrix ($\bar{r}$=0.817), and has particularly strong correlations with MBR area ($\bar{r}$=0.972), MBR length ($\bar{r}$=0.936), interpolated volume ($\bar{r}$=0.929), footprint area ($\bar{r}$=0.909), footprint length ($\bar{r}$=0.894), and SC volume ($\bar{r}$=0.89). Deposit area is well correlated with talus area ($\bar{r}$=0.816), MBR width ($\bar{r}$=0.813), headwall area ($\bar{r}$=0.793), and SC thickness ($\bar{r}$=0.784), but only moderately correlated with headwall height, footprint width, and interpolated thickness. The MBR variables are consistently more correlated with other morphometric attributes than the footprint variables, although the values for length are nearly the same ($\bar{r}_{MBR}$=0.774; $\bar{r}_{FP}$=0.760). Interpolated volume ($\bar{r}$=0.760) tends to be slightly more correlated with the dataset than SC volume ($\bar{r}$=0.724), but SC thickness ($\bar{r}$=0.673) is clearly more correlated than interpolated thickness ($\bar{r}$=0.486). The correlation between SC thickness and interpolated thickness is also moderate (r=0.609), highlighting the difficulty in reliably estimating thickness using a less refined interpolation method.

Table 8: Correlation matrix for priority deposits, shaded to represent nature of correlation. SC=Slope Curve, Int.=Interpolated, Vol=Volume, HW=Headwall, Dep.=Deposit, FP=Footprint, MBR=Minimum Bounding Rectangle, Thick=Thickness, Ht.=Height

	HW Ht.	Int. Thick	SC Thick	MBR Width	MBR Length	FP Width	FP Length	MBR Area	FP Area	Talus Area	HW Area	Dep. Area	SC Vol.
Int. Vol.	0.523	0.578	0.752	0.748	0.812	0.622	0.827	0.942	0.963	0.592	0.607	0.929	0.979
SC Vol.	0.478	0.44	0.731	0.737	0.763	0.647	0.792	0.931	0.986	0.485	0.548	0.89	
Dep. Area	0.685	0.568	0.784	0.813	0.936	0.626	0.894	0.972	0.909	0.816	0.793		
HW Area	0.724	0.404	0.513	0.579	0.858	0.365	0.766	0.774	0.599	0.828			
Talus Area	0.649	0.575	0.64	0.594	0.838	0.35	0.692	0.696	0.504				
FP Area	0.55	0.424	0.704	0.791	0.798	0.68	0.833	0.956					
MBR Area	0.673	0.51	0.735	0.811	0.921	0.58	0.927						
FP Length	0.736	0.597	0.757	0.724	0.942	0.395							
FP Width	0.49	0.207	0.566	0.726	0.44								
MBR	0.744	0.571	0.754	0.679									
MBR	0.731	0.452	0.646										
SC Thick	0.562	0.609											
Int. Thick	0.383												

Table 9: Correlation matrix for all deposits, shaded to represent nature of correlation. Dep.=Deposit, MBR=Minimum Bounding Rectangle, Int.=Interpolated, Ele.=Elevation

	Cirque Ele.	Dep. Mean Ele.	Dep. Max Ele.	Dep. Min Ele.	Int. Thickness	MBR Length	MBR Width	MBR Area
Dep. Area	-0.2	-0.393	-0.139	-0.526	0.513	0.769	0.527	0.832
MBR Area	-0.19	-0.357	-0.128	-0.481	0.533	0.892	0.582	
MBR Width	-0.201	-0.312	-0.108	-0.421	0.439	0.394		
MBR Length	-0.12	-0.31	-0.04	-0.47	0.558			
Int. Thick	0.072	-0.026	0.179	-0.196				
Dep. Min Ele.	0.812	0.956	0.756					
Dep. Max Ele.	0.892	0.893						
Dep. Mean Ele.	0.892							

When the full dataset (n=248) in **Table 9** is considered, there are strong correlations among the area variables and MBR length ($r_{deposit}$=0.77; r_{MBR}=0.89), with less of a correlation for interpolated thickness ($\bar{r}_{deposit}$=0.513; $\bar{r}_{MBR}$=0.533) and MBR width ($\bar{r}_{deposit}$=0.527; $\bar{r}_{MBR}$=0.582). The elevation variables are strongly correlated amongst themselves ($\bar{r}$=0.76-0.96), but are generally uncorrelated with the dimensional variables. For minimum deposit elevation, however, there is a moderate negative correlation with deposit area ($\bar{r}$=-0.53), MBR area ($\bar{r}$=-0.48), MBR width ($\bar{r}$=-0.42), and MBR length ($\bar{r}$=-0.47). A weak negative correlation is also seen between mean deposit elevation and the two area variables ($\bar{r}_{deposit}$=-0.393; $\bar{r}_{MBR}$=-0.357).

Isometry / Allometry

Isometric growth for two variables with the same dimensions is equivalent to a b-value of 1. Isometric growth of length, width, and thickness relative to deposit volume are all represented by an estimated b-value of 0.333. The relative changes in length, width, and thickness as deposit volumes increase were inferred by comparing the dimensional estimates in **Table 10** for priority deposits**.** Based on the tabled values, the growth of priority deposits is apparently allometric, with length having the largest exponent (b=0.382), followed by thickness (b=0.337), and finally width (b=0.281). The correlation is strongest between deposit volume and thickness ($\bar{\boldsymbol{r}}$=0.921) and progressively less for length ($\bar{\boldsymbol{r}}$=0.877) and width ($\bar{\boldsymbol{r}}$=0.763), yet all of the correlations are statistically significant at the 95% confidence level. Although the data seems to trend toward allometric growth, the t-tests of the null hypothesis that the b-values are equal to 0.33 indicate that there is no statistical difference at the 95% confidence level. The b-value for thickness is only slightly higher than isometric values (t=0.131; p=0.896), with width being lower (t=-1.239; p=0.224) and length higher (t=1.33; p=0.193). The limited number of data points for the priority deposits (n=34) makes it very difficult to reject the null hypothesis, but the trend in exponent values seems to suggest a divergence from isometry as deposits grow larger. This may be related to the shear strength of boulders with an ice matrix being overcome as deposits grow thicker,

Table 10: Isometry testing for the priority dataset. SC=Slope Curve, MBR=Minimum Bounding Rectangle, Int.=Interpolated, Dep.=Deposit

Test	a	b	Isometric 'b'	R^2	R	Result
Footprint Area vs. Footprint Length	0.636	0.559	0.5	0.757	0.870	
Footprint Area vs. Footprint Width	1.574	0.441	0.5	.659	0.812	
SC Deposit Volume vs. Footprint Length	1.525	0.382	0.33	0.769	0.877	t= 1.33 ; p=0.193
SC Deposit Volume vs. Footprint Width	4.083	0.281	0.33	0.582	0.763	t= -1.239 ; p=0.224
SC Deposit Volume vs. SC Thickness	0.161	0.337	0.33	0.848	0.921	t= 0.131 ; p=0.896
Int. Thickness vs. SC Thickness	2.166	0.599	1	0.340	0.583	Interpolated Thickness Transform
Int. Deposit Volume vs. SC Deposit Volume	0.467	1.027	1	0.892	0.945	Interpolated Dep. Volume Transform
Deposit Area vs. Footprint Area	0.757	0.950	1	0.919	0.959	Deposit Area Transform
MBR Area vs. Footprint Area	1.106	0.870	1	0.898	0.948	MBR Area Transform

forcing the deposits to extend down slope. The rate at which thickness increases seems to be isometric, but the growth of width may be limited by accommodation space. It may be that the slope of cirque floors encourages growth perpendicular to the headwalls (length) while limiting lateral growth (width).

The relative contributions of footprint length and width for footprint area are shown in **Figure 15** and summarized in **Table 10**. With isometry represented by a b-value of 0.5, the relationship is again allometric. Length (b=0.559; $\bar{r}$=0.87) has both a larger b-value and a stronger correlation with area than width (b=0.441; $\bar{r}$=0.812). However, the limited sample size again prevents the null hypothesis from being rejected in both cases (p_{length}=0.488; p_{width}=0.557).

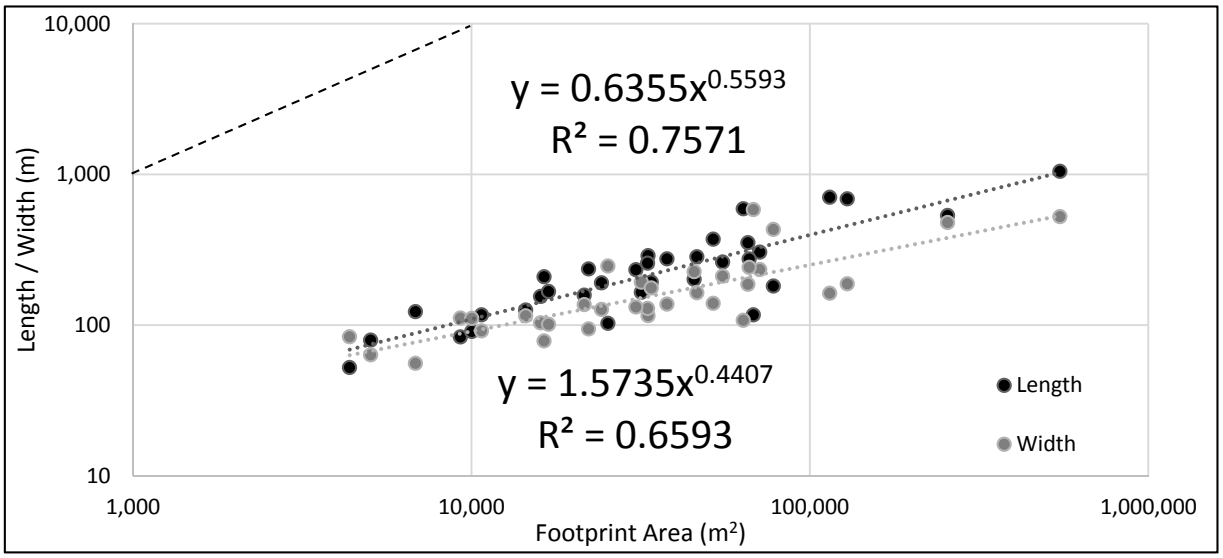

Figure 15: Comparison of footprint length and width relative to footprint area for priority deposits.

The relative rate of change of length and width for all deposits can only be considered for the MBR, as block length and width approximations were generated just for priority deposits. The MBR length and width are not directly analogous to the footprint length and width because the MBR encompasses the maximum extent of the deposit rather than representing the average dimensions of the bulge. Furthermore, the only thickness estimation for all deposits is the interpolation method, which likely overestimates the thickness of larger deposits relative to the

more refined SC method. For these reasons, MBR volume estimations were not generated, and the relative rate of growth for MBR length and width is only considered as it relates to MBR area.

To determine if the MBR exhibits a tendency for isometric growth, MBR length and width are plotted as dependent variables versus MBR area (**Figure 16**). The values from this figure are summarized in **Table 11**. As isometric growth is represented by a b-value of 0.5, the growth of the MBR is slightly allometric showing a preferential growth of MBR length (b=0.511) relative to MBR width (b=0.489). Although the sample size is much larger than the priority dataset, the mild degree of allometry indicated by the b-values is well within the 95% confidence level (p_{length}=0.556; p_{width}=0.576), and the null hypothesis cannot be rejected.

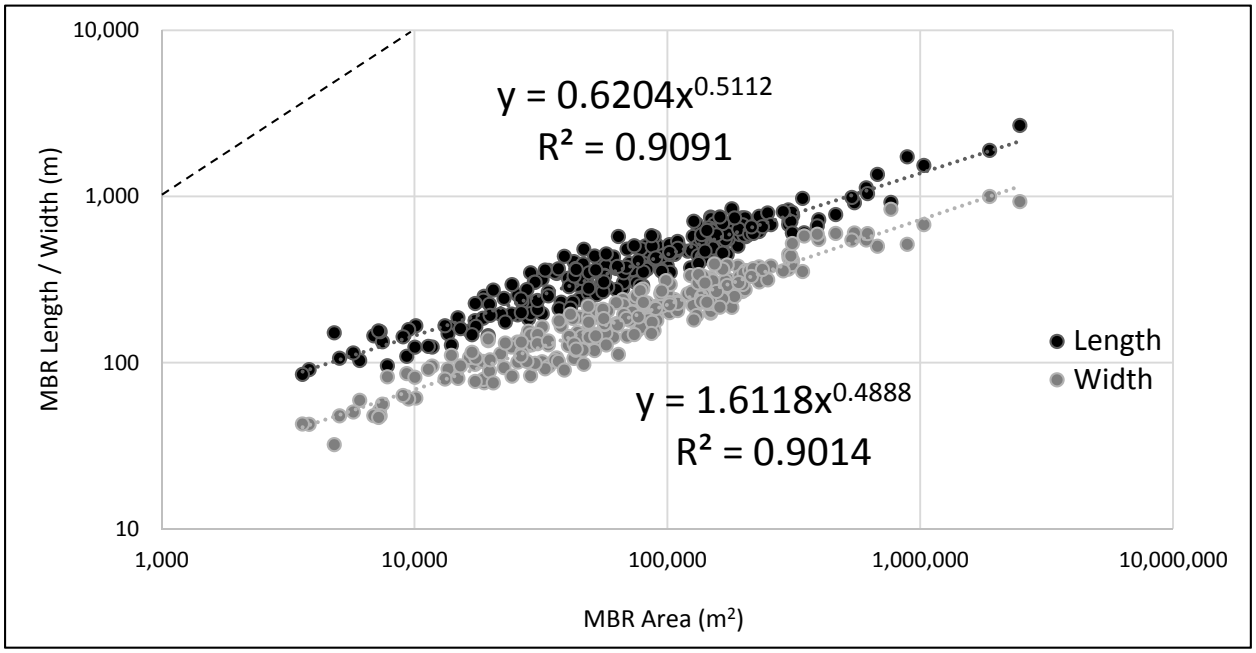

Figure 16: Comparison of MBR length and width relative to MBR area for all deposits

Table 11: Isometry testing for the minimum bounding rectangle (MBR) on all deposits

Test	a	b	Isometric 'b'	R^2	r
MBR Area vs. MBR Length	0.6204	0.5112	0.5	0.9091	0.9535
MBR Area vs. MBR Width	1.6118	0.4888	0.5	0.9014	0.9494

Headwall Area

Headwall area was plotted against deposit area (**Figure 17**) to identify whether the two variables have an isometric relationship (b=1). The deposit area shows allometric growth compared to headwall area (b=0.761; a=22.11). For larger deposits, the trend is close to being isometric. When the variables are tested for equal means, the null-hypothesis cannot be rejected (t=-1.15; p=0.253). This suggests that although deposit area appears to be growing at a faster rate than the area of its contributing headwall, the difference is not large enough to be statistically significant. One reason for the beginnings of allometric growth could be related to bulking in the boulders of the deposit and infilling with ice. The generation of voids between boulders allows rock that was tightly packed in the headwall to cover more area in the deposit and facilitate downslope expansion.

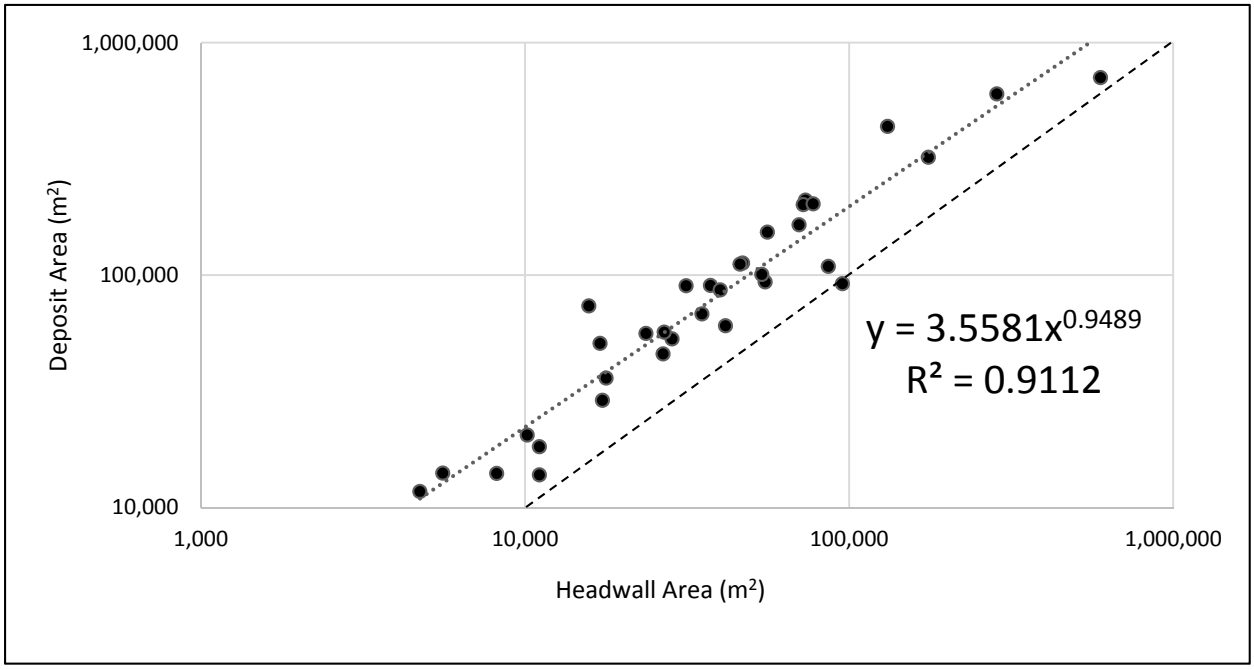

Figure 17: Relationship between headwall area and deposit area for priority deposits.

Headwall Data

Headwall Retreat

Headwall-retreat distance was calculated for priority deposits by dividing the estimated volume of rock in a deposit by the area of its contributing headwall. According to White (1971), the porosity of rock-glacier rubble is about 0.4, meaning that the volume of rock in a deposit is approximately 60% of the deposit volume once void space is accounted for. The calculated deposit volumes were reduced to this amount before reconstructing the distance of headwall retreat. The total headwall retreat associated with rock-glacier development is provided in **Table 12**. The priority deposits collectively account for more than 31 million cubic meters of rock debris that has accumulated from over 3 million square meters of headwall area. The mean headwall-retreat distance is 8.5 m, and the range of retreat distances for individual deposits ranges from 1.15 m-35.34 m.

A rough estimate of these values can be made for all deposits by using the best-fit equations in **Figures 5** and **18** to relate deposit area to headwall area ($y=1.2417x^{0.933}$, $R^2=0.7103$) and footprint area ($y=0.7574x^{0.9496}$, $R^2=0.9192$), respectively. Volume is approximated by multiplying the footprint area by the interpolated thickness. Although the calculations are not discussed in detail, they are provided in **Appendix U**, **Table 2** for reference. These calculations suggest that the Tobacco Root Mountains could have more than 116 million cubic meters of rock debris present in periglacial deposits accumulated from over 10.6 million square meters of headwall area. This implies that the volumes and headwall areas of priority deposits account for roughly 25% of the values for the whole range. The mean headwall-retreat distance for the range is 7.6 m with values ranging from 1.2 m-31.9 m.

Table 12: Calculations of headwall retreat distances for priority sites. Shaded deposits are priority sites that were not visited. HW=Headwall, Vol=Volume

Deposit #	HW Area (m^2)	Rock Vol (m^3)	HW Retreat (m)
001	64,867	152,351	2.35
002	37,820	81,778	2.16
004	73,042	371,931	5.09
006	22,310	184,072	8.25
008	12,301	28,661	2.33
009	73,577	760,302	10.33
014	650,657	1,146,377	1.76
016	85,649	636,576	7.43
018	33,618	853,209	25.38
025	41,029	212,267	5.17
026	22,004	198,098	9.00
028	20,629	74,001	3.59
029	7,717	46,861	6.07
032	5,577	134,885	24.18
040	72,355	2,557,409	35.35
044	339,387	886,126	2.61
048	74,723	1,360,447	18.21
057	38,660	61,096	1.58
058	107,118	227,974	2.13
060	4,661	14,263	3.06
061	19,330	22,397	1.16
062	79,613	222,570	2.80
066	131,033	2,423,626	18.50
072	35,528	321,479	9.05
080	358,946	11,873,797	33.08
086	30,638	124,555	4.07
089	82,746	666,335	8.05
094	30,638	272,994	8.91
114	108,799	381,824	3.51
115	365,211	6,604,670	18.08
116	32,319	108,330	3.35
117	8,099	34,903	4.31
172	13,447	60,905	4.53
189	59,290	97,994	1.65
Mean	92,451	976,619	8.74
St. Dev.	136,255	2,279,582	9.13
SE mean	23,368	390,945	1.57
Max	650,657	11,873,797	35.35
Min	4,661	14,263	1.16
Sum	3,143,337	33,205,061	297.09

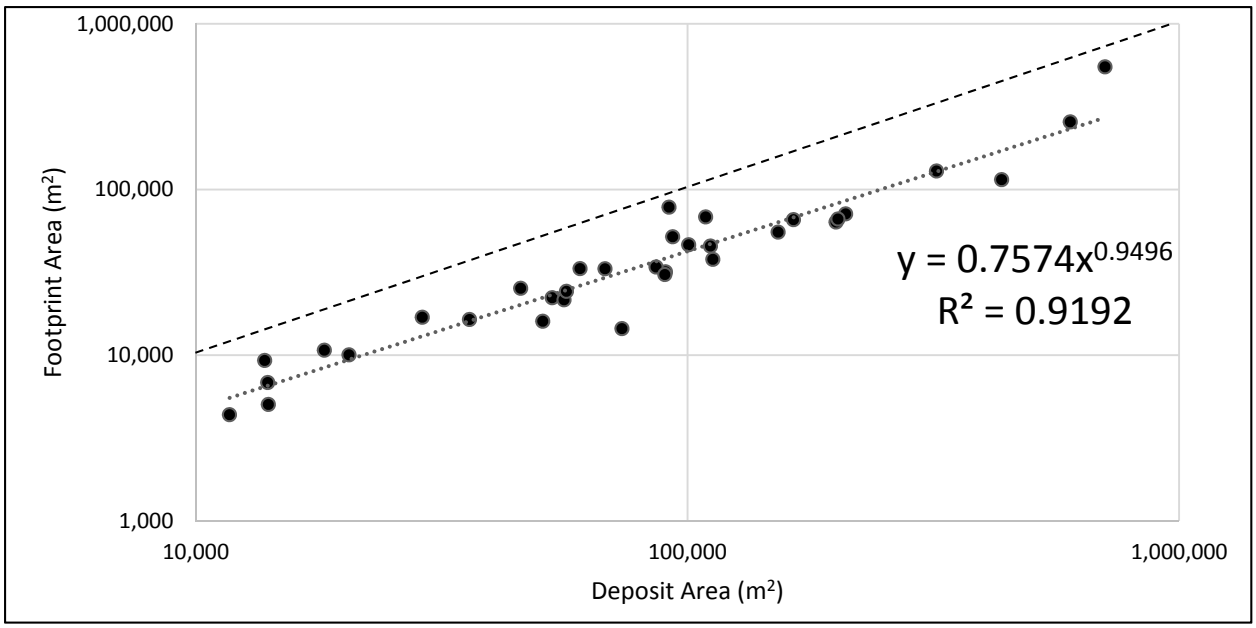

Figure 18: Relationship between deposit area and footprint area for priority deposits.

Headwall Fracturing

Data on lithology and headwall fracturing were collected above 15 of the study rock glaciers. A summary of this data is provided in **Table 13**. At every site examined, the dominant bedrock lithology in the contributing headwalls is of gneissic composition, varying from quartzo-feldspathic gneisses to mafic gneisses. There is a small degree of variability in lithology at some of the sites including a schistose headwall above deposit 094 and an igneous intrusion above deposit 028, but generally speaking the contributing headwalls are gneissic. The degree of foliation varies among sites, but compositional banding is steadily present, and there are often fractures that correspond with the foliation planes. All but five sites (014, 036, 058, 060, and 116) display compositional banding fractures (CBF). Additionally, fracture planes that are nearly parallel to the local dip slope (DSF) are present at several sites including 001, 004, 008, 014, 025, 028, 040, and 094. At least three directions of fracture plane orientation are present at each site, and approximately two-thirds of the sites display a fourth direction. The average dip of fracture planes from all sites is approximately 58˚, and average values for individual sites range from 43˚ to 69˚.

Table 13: Headwall fracture and other data for visited sites. Avg fr/m=Average Fractures/Meter, CBF=Compositional Banding Fractures, DSF=Dip Slope Fractures, Dia=Diameter, HW-headwall, Dep=Deposit, Ele.=Elevation

Deposit #	Avg fr/m	Geology	CBF?	DSF?	Boulder Dia (m)	Headwall Area (m^2)	Deposit Area (m^2)	HW Area / Dep Area	Min. Ele. (m)
001	1.92	QFG	Y	Y	1.65	64,867	53,104	1.2	2,777
004	1.53	QFG	Y	Y	0.93	73,042	112,655	0.6	2,778
008	1.46	QFG	Y	Y	0.86	12,301	14,048	0.9	2,791
014	1.54	QFG	N	Y	1.03	650,657	435,586	1.5	2,117
025	3.02	QFG	Y	Y	1.12	41,029	60,494	0.7	2,604
026	1.71	QMG	Y	N	1.36	22,004	90,223	0.2	2,549
028	3.07	QFG	Y	Y	1.25	20,629	36,030	0.6	2,646
029	1.53	QFG	Y	N	0.9	7,717	18,255	0.4	2,850
036	-	QFG	N	N	0.97	1,757	2,674	0.7	2,924
040	3.23	QFG	Y	Y	1.06	72,355	321,036	0.2	2,680
044	1.95	QFG	Y	N	1.25	339,387	200,634	1.7	2,496
058	2.56	QFG	N	N	0.93	107,118	67,995	1.6	2,670
060	1.48	QFG	N	N	1.14	4,661	11,709	0.4	2,644
080	-	-	-	-	0.86	358,946	706,876	0.5	2,398
094	1.36	QMG	Y	Y	1.4	30,638	89,968	0.3	2,791
115	-	-	-	-	0.95	365,211	600,955	0.6	2,125
116	7.41	QMG	N	N	0.85	32,319	28,894	1.1	2,702
117	3.35	QFG	Y	N	0.88	8,099	13,808	0.6	2,673
172	3.49	QFG	Y	N	0.96	13,447	20,493	0.7	2,775

Due to variable outcrop exposure and accessibility, a wide range of spans were used to determine fracture density (1.5-15 meters) with an average span length of approximately 5 meters. The average density of fracturing in the headwalls is fairly consistent, with all but one site falling within the range of 1.3-3.5 fractures per meter (**Table 14**). Fracture density appears to have an inverse correlation with boulder diameter at many of the sites (001, 026, 040, 044, 060, 094, 116, and 172). When the average fracture density and the average fracture plane dip are plotted against each other, there is a very slight and statistically insignificant positive correlation. There are two main groupings of headwalls with similar fracture-density values and one outlier site (**Figure 19).** One group ranges from about 1.5-2.5 fractures per meter and including sites 044, 014, 003, 001, 094, 060, 008, and 026. A slightly more fractured group ranges from 2.5–3.5 fractures per meter and includes sites 058, 172, 040, 117, 025, and 028. Finally, the headwall above deposit 116 is a highly fractured outlier with an average density of about 7.4 fractures per meter.

Table 14: Measured headwall fracture data with average fractures/meter and joint spacing.

Site	Avg fr/m	Joint Spacing (m)
001	1.92	0.52
003	1.53	0.65
008	1.46	0.69
014	1.54	0.65
025	3.02	0.33
026	1.71	0.59
028	3.07	0.33
029	1.53	0.65
040	3.23	0.31
044	1.95	0.51
058	2.56	0.39
060	1.48	0.67
094	1.36	0.74
116	7.41	0.13
117	3.35	0.30
172	3.49	0.29

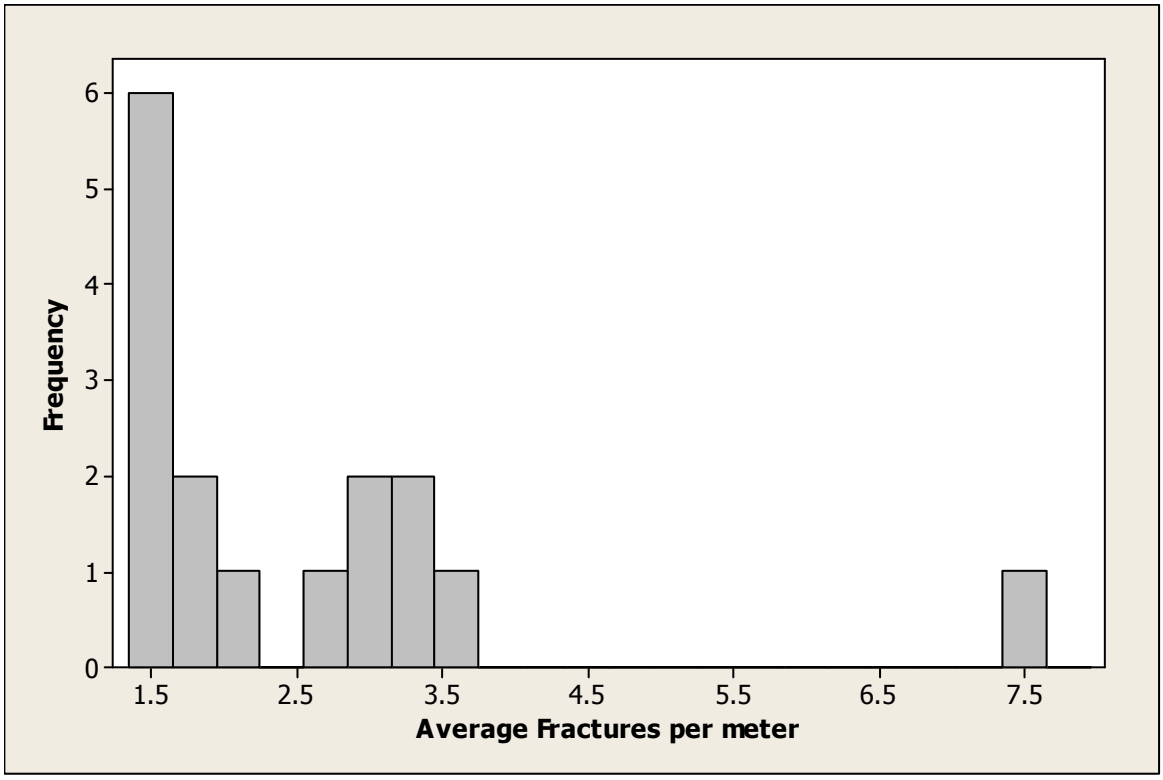

Figure 19: Histogram of fracture density for all measured sites.

Relative-age Data

Principle Component Loadings

Some of the variables measured at the first three sites examined (058-060) are not directly comparable with the rest of the dataset because of inconsistencies in operator methodology, and were therefore excluded from the PCA. Using data collected on the 21 remaining sites, a correlation matrix of the 13 variables used to calculate the eigenvalues and loadings of the principle components was generated (**Table 15**). Because of the small number of variables (n=13), only an r-value greater than 0.33 is considered statistically significant. There is a very strong positive correlation among the five lichen variables ($\bar{r}$=0.92-0.99), indicating a fair amount of redundancy in the measured characteristics. The lichen variables also exhibit strong to moderate correlations with boulder weathering variables; especially pitting cover ($\bar{r}$=0.91-0.95), maximum pit depth ($\bar{r}$=0.68-0.75), and crystal height ($\bar{r}$=0.62-0.71). Angularity has the strongest

Table 15: Correlation matrix for relative age data. From top to bottom, row labels stand for: Boulder Diameter, % Weathered, % Pitting Cover, Maximum Pit Depth, Oxidation Rind Depth, % Oxidized, Crystal Height, % Angularity, % Lichen Cover, Lichen Max Short Axis Dia., Lichen Average Short Axis Diameter, Lichen Maximum Long Axis Diameter, Lichen Average Long Axis Diameter.

	LLoAvg	LLoMax	LShAvg	LShMax	%Lichen	%Ang	XtalHt	%Ox	OxRind	PitMax	%Pitting	%Wea
BouDia	0.1	0.17	0.13	0.13	0.15	-0.25	0.51	0.01	0.1	0.5	0.04	0.52
%Wea	0.2	0.23	0.18	0.24	0.31	-0.38	0.6	-0.24	0.16	0.45	0.09	
%Pitting	0.91	0.92	0.95	0.91	0.93	-0.34	0.59	-0.24	-0.01	0.71		
PitMax	0.73	0.69	0.68	0.75	0.69	-0.58	0.85	-0.14	-0.02			
OxRind	-0.03	0.13	0.09	0.01	0.14	0.66	-0.18	-0.14				
%Ox	-0.39	-0.34	-0.3	-0.38	-0.39	0.24	-0.37					
XtalHt	0.69	0.64	0.62	0.71	0.65	-0.76						
%Ang	-0.42	-0.25	-0.27	-0.41	-0.3							
%Lichen	0.92	0.97	0.97	0.94								
LShMax	0.99	0.95	0.95									
LShAvg	0.94	0.99										
LLoMax	0.94											

correlations with crystal height ($\bar{r}$=-0.76), oxidation-rind depth ($\bar{r}$=0.66), and maximum pit depth ($\bar{r}$=-0.58); in contrast, angularity shows weak negative correlations with the maximum short axis lichen diameter ($\bar{r}$=-0.41) and the average long axis lichen diameter ($\bar{r}$=-0.42). Percent oxidation cover has weak negative correlations ($\bar{r}$=-0.34-0.39) with crystal height and all of the lichen variables except for the average short axis lichen diameter. There are no statistically significant correlations between oxidation cover and other variables. Likewise, oxidation-rind depth has no correlation with any of the variables other than angularity ($\bar{r}$=0.66). Boulder diameter and percent weathered have similar moderate positive correlations with each other ($\bar{r}$=0.52) and with maximum pit depth ($\bar{r}$=0.5; $\bar{r}$=0.45) and crystal height ($\bar{r}$=0.51; $\bar{r}$=0.6), but show no correlation with the remaining variables besides percent weathered and angularity ($\bar{r}$=-0.38).

A summary of the PCA analysis is provided in **Tables 16** and **17**. The first component has an eigenvalue of 7.59 which accounts for approximately 58% of the variance in the original data. Also, because of the strong inter-correlation among relative-age attributes, it only takes three components to collectively account for nearly 80% of the variance in the data matrix (**Table 16**). As shown in **Table 17**, Principle Component I (PC1) is dominated by positive loadings with the five lichen variables (0.29-0.33). PC1 also exhibits a positive loading with crystal height (0.29), maximum pit depth (0.28), pitting cover (0.24), and percent weathered (0.24). As pitting and crystal height are both related to mineral disintegration, it can be said that PC1 is primarily related to lichen growth and rock weathering which vary together in the study area.

Table 16: Eigenvector results for the relative age data statistical analysis.

Principle Component	Eigenvalue	Cumulative % of total variance
I	7.59	58.39
II	1.70	71.48
III	1.05	79.58

Table 17: The relative influence of variables on the first three principle components. Dia=Diameter

Variable	Component I	Component II	Component III
Boulder Diameter	0.155	0.547	0.386
% Weathered	0.242	0.35	-0.419
% Pitted	0.239	-0.317	0.183
Max Pit Depth	0.278	0.317	0.293
Oxidation Rind Depth	0.189	0.181	-0.548
% Oxidized	-0.228	0.149	0.203
Crystal Height	0.292	0.280	0.169
% Angular	-0.315	-0.068	0.053
% Lichen Cover	0.321	-0.011	-0.343
Max Short Lichen Dia	0.316	-0.285	0.058
Avg Short Lichen Dia	0.332	-0.122	0.179
Avg Long Lichen Dia	0.333	-0.156	0.170
Max Long Lichen Dia	0.296	-0.340	0.034

The vector representing Principle Component II (PC2) contains positive loadings with boulder diameter (0.55), percent weathered (0.35), maximum pit depth (0.32), and crystal height (0.28). The remaining variables are mostly not correlated with PC2, excluding maximum short lichen diameter (-0.29), maximum long lichen diameter (-0.34), and pitting cover (-0.32). These loadings indicate that PC2 is primarily a reflection of the degree of boulder weathering.

Principle Component III (PC3) has a strong to moderate negative association with oxidation-rind depth (-0.55), percent weathered (-0.42), and lichen cover (-0.34), but has moderate positive associations with boulder diameter (0.39), maximum pit depth (0.29), and oxidation cover (0.20). PC3 reflects an inverse correlation with rock weathering, especially for variables which are effective at representing longer time spans (Birkeland, 1973).

Although the pattern of correlation is complex, it appears that generally PC1 represents lichen growth and mineral weathering. PC2 seems to be more representative of boulder diameter and boulder weathering, and has a negative correlation with some lichen variables. Finally, PC3 inversely represents rock weathering based on variables that highlight older deposits (oxidation-rind depth and percent weathered).

Principle Component Scores

The component scores of 21 rock glaciers on each of the principle components are plotted in **Figure 20**. The most prominent feature of the plot is the cluster of sites representing deposits with similar component scores along PC1 and PC2.

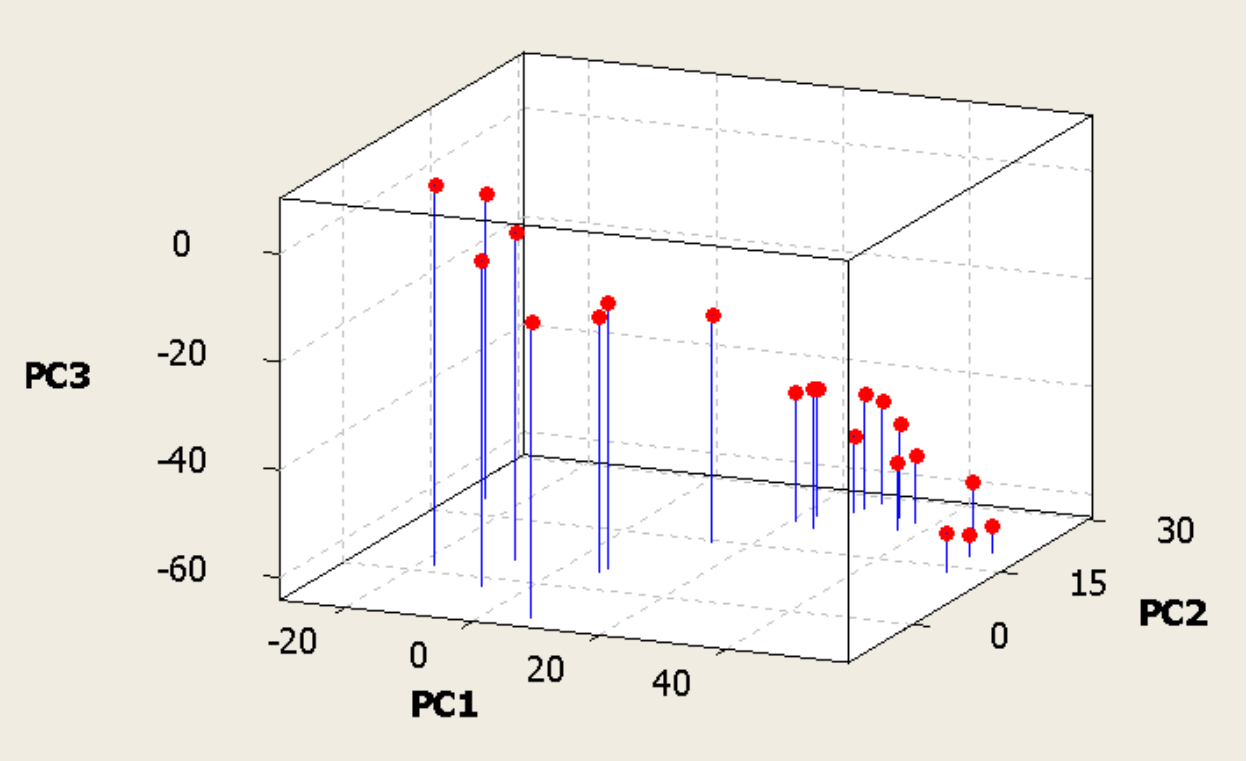

Figure 20: 3D scatterplot of the first three principle components showing older sites in the bottom right and younger sites in the top left.

Along PC1 there appear to be eight outlier sites; four with lower scores than the main cluster (116, 026_2, 003, and 036) and four with higher scores (044, 080, 014, and 115). The distribution of sites along PC2 reveals a slightly different trend than is seen along the first component**.** The main cluster of points is along the upper-end of the component, and as many as seven sites have component scores that appear to be outliers much lower than the main cluster (117, 025_3,116, 003, 026_2, 008, and 094). For PC3, two main groupings can be distinguished. The first group has low scores along PC3 and appears as a fairly tight cluster with high scores along both PC2 and PC1. The other group is comprised of 8 sites that have similarly high scores

along PC3 (094, 025_3, 117, 008, 026_2, 116, 003, and 036). In general, these sites are among the lowest scores for both PC2 and PC1.

Four distinct clusters have been identified and are outlined in **Figures 21a and 21b**. Cluster ‘a’ has low values along PC1 and PC2, but some of the highest values on PC3. Sites in this cluster include 003, 116, and 026_2. Cluster ‘b’ is an elongate cluster with high values on PC3 and moderate values on PC1 but somewhat variable values along PC2. Sites 8, 117, 025_3, and 094 are included in this group. Although sites in cluster ‘b’ were part of the “main cluster” discussed previously, the majority of sites in the “main cluster” are in cluster ‘c’. This cluster generally has high values on PC1 and PC2, but low values on PC3. Sites 025_2, 004, 172, 040, 041, 029, 026_1, 025_1, and 028 are all included in cluster ‘c’. Finally, cluster ‘d’ is comprised of four sites (080, 014, 044, 115) that have the highest values on PC1, moderate values on PC2, and the lowest values on PC3. The only site that does not fit within any of the labeled clusters is site 036. It has the lowest value on PC1 and one of the highest on PC3, with moderately high values on PC2. This unusual combination of component scores leaves site 036 in a group of its own. Based on the PCA analysis, site 036 is similar to sites in clusters ‘c’ and ‘d’ along PC2, but has very different values from these clusters along PC1 and PC3, indicating that it is likely more similar to cluster ‘a’.

Based on interpretations of the loadings of the three principle components, the four clusters may represent different periods of periglacial development. The PC1 scores suggest that cluster ‘a’ represents deposits with the least relative age, followed by clusters ‘b’ and ‘c’ of apparently similar age. Cluster ‘d’ most likely contains deposits with the most extreme relative age of any sites examined.

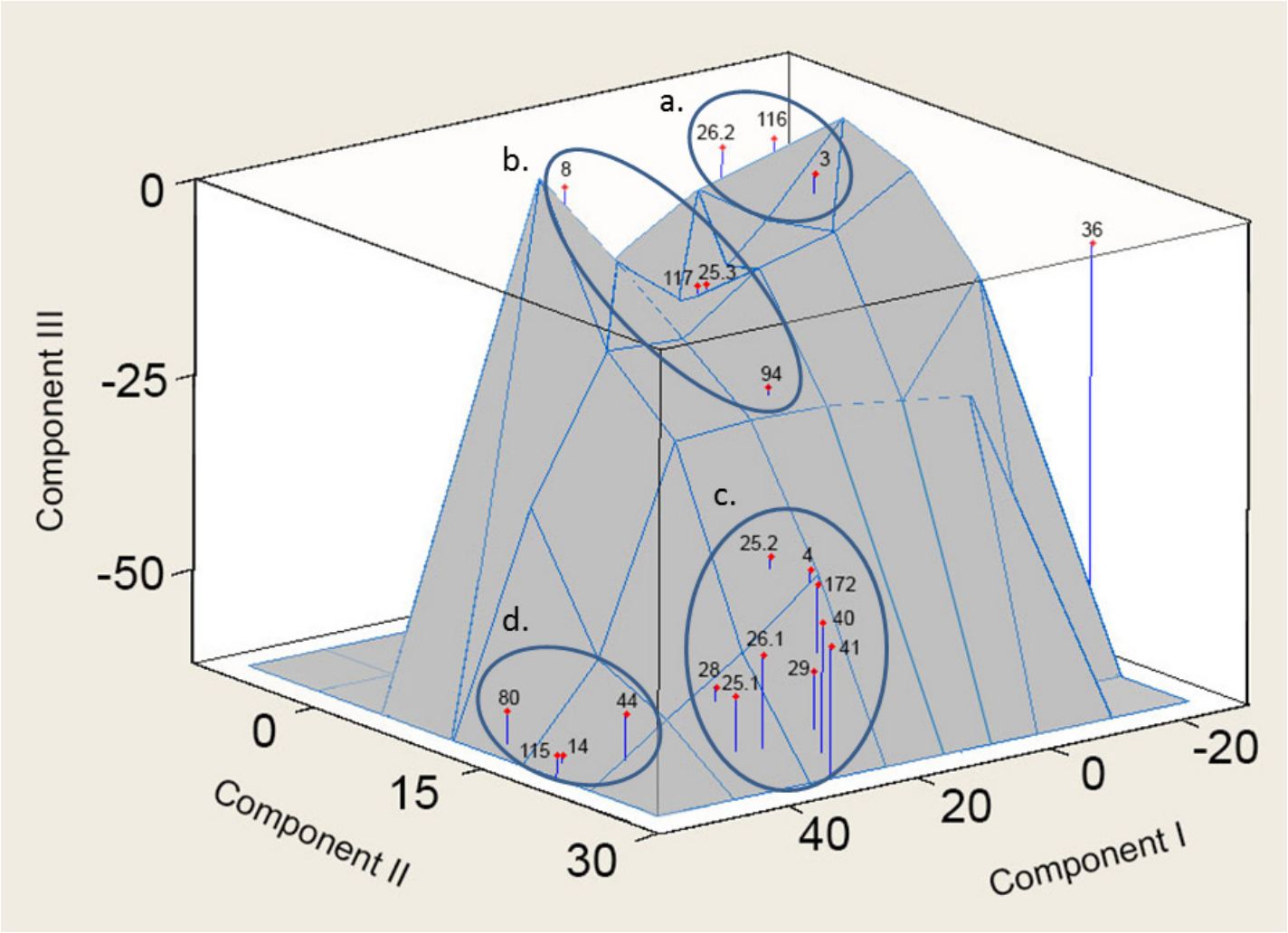

Figure 21a: Results from the first three principle components with database site and cluster labels. Computer generated mean surface is shown for visualization.

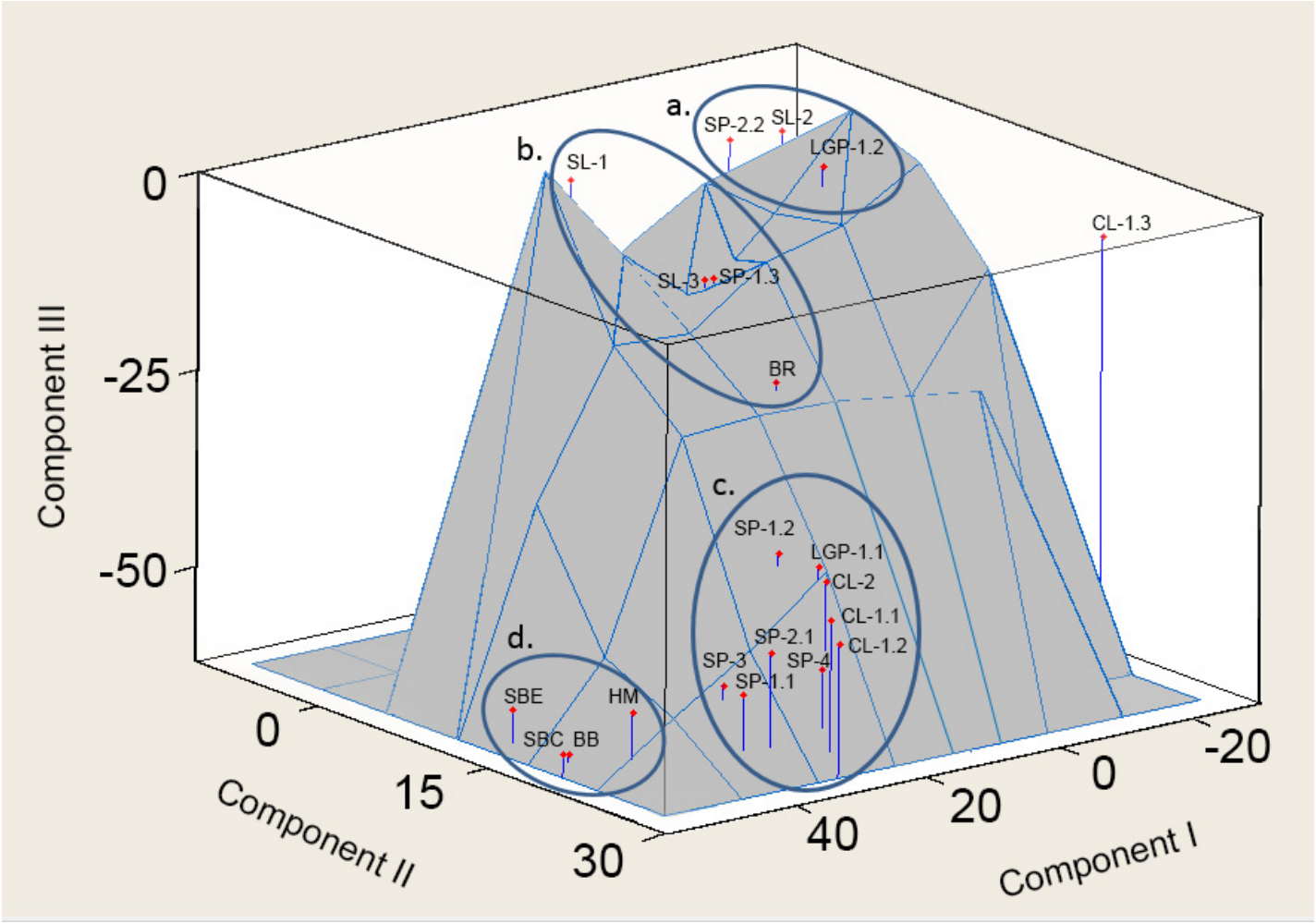

Figure 21b: Results from the first three principle components with locational site and cluster labels. Computer generated mean surface is shown for visualization. SBE=East Fork South Boulder River, SBC=South Boulder Confluence, BB=Brownback Cirque, HM=Hollowtop Mountain Area, SP=Sunrise Peak Area, CL=Curly Lake Area, LGP=Little Granite Peak Area, BR=Branham Lakes Cirque, SL=Sailor Lake Area

V. Discussion

Morphometry

Best-fit functions relating dimensional attributes to deposit volume indicate a slight tendency for length-favored allometric growth in the priority dataset of rock glaciers and protalus ramparts (**Table 10**). However, the small number of deposits subjected to the analysis precluded rejection of the null hypothesis of isometric growth. Though the dataset containing all deposits has a larger sample size than the priority dataset, the length and width estimations are generated using an MBR that encompasses both the deposit and the talus instead of just the footprint. Because the length-to-width ratios from the two datasets reflect different properties of the deposit, they could not be directly compared.

An analysis of all deposits identified in the Tobacco Root Mountains indicated that the proportion of MBR length to width for tongue-shaped rock glaciers is nearly 2:1, whereas the opposite is true for lobate rock glaciers and especially so for protalus ramparts. These results are slightly less pronounced than those found by Janke and Frauenfelder (2008), who reported a length-to-width ratio of about 2.3 for tongue-shaped rock glaciers, and a width-to-length ratio of nearly 3.0 for lobate rock glaciers in the Colorado Front Range. These morphometric findings are related to the definition of the different classes of periglacial deposits and they validate the accuracy of the morphological assignments.

Estimated mean values of deposit area and MBR length were also found to be statistically different between the three morphological classes (**Table 6**). Lobate rock glaciers and protalus ramparts in the Tobacco Root Mountains have mean values of MBR width and interpolated thickness that are not statistically different from each other, but inferences should be viewed with caution because measurements are not as accurate for the full dataset. A general result of this thesis is that lobate rock glaciers and protalus ramparts are more similar to each other than either of them are to tongue-shaped rock glaciers, although lobate rock glaciers tend to be larger.

Topoclimate

In the Tobacco Root Mountains, the average maximum elevation of tongue-shaped rock glaciers (2,907 m) is significantly greater than those of both lobate rock glaciers (2,843 m) and protalus ramparts (2,852 m). This suggests that development of tongue-shaped rock glaciers is optimized at higher elevations. One explanation is that accumulation of snow and preservation of interstitial ice (required for active flow) increases with elevation. Significantly different and decreasing deposit slopes were also observed when comparing protalus ramparts (~30˚) to lobate (~27˚) and tongue-shaped (~25˚) rock glaciers. This is, in part, related to the relatively flat cirque floor that rock glaciers extend across as they flow away from headwalls.

Ice accumulation and preservation is also related to slope and aspect, which, in turn, is related to prevailing wind direction and surrounding topography. Northern aspects promote radiation reduction in the Tobacco Root Mountains, and this thesis has shown that the largest tongue-shaped deposits exist at the least insolated aspects.

Regardless of whether cirque values or maximum deposit values are used for radiation reduction (**Appendix T: Figures T-1 – T-8**), the data fits fairly well to the theoretical distribution trend described, but not found, by Morris (1981). Morris attributed the disparity between the data and the theoretical distribution to the lack of control that orientation alone has on radiation shading. In the Tobacco Root Mountains, slope and orientation are indeed the primary influence on received solar radiation. This might be because they are more northerly and less elevated than the Sangre de Cristo Mountains studied by Morris (1981), and the headwalls and peaks do not exhibit as much relief. This influence of orientation, however, is strongest when small areas are considered and becomes less pronounced when data across an entire deposit are averaged.

One of the most apparent trends in the radiation-reduction models (**Appendix S; Figures S-1 – S-10**) is that deposits experience radically different amounts of radiation reduction on the summer solstice (0.207-0.211) and winter solstice (0.638-0.775). When mean values of morphological classes are compared (**Table 6**), the summer solstice and summer season models

show no statistically significant differences. However, tongue-shaped rock glaciers and protalus ramparts receive statistically different amounts of radiation reduction on the vernal equinox, and all three morphological classes have statistically different values for the winter solstice model. The low angle of the sun and limited hours of sunlight on the winter solstice accentuate the topoclimatic differences among deposits of the three morphological classes. These findings suggest that reduction of incident solar radiation facilitates snow accumulation and preservation during the winter. The increasing tendency of periglacial deposits to develop with north-facing aspects moving from the talus to the glacier end of the neoglacial facies spectrum coincides with the amount of radiation reduction received by these deposits.

The results of this thesis indicate a tendency for larger rock-glacier deposits to develop below north-facing cirque headwalls. This tendency is stronger for tongue-shaped deposits and progressively less so for lobate deposits and protalus ramparts. Whereas some tongue-shaped deposits have southerly aspects, the majority have aspects within 60˚ of north (azimuths from 300˚ - 60˚). Lobate deposits also dominantly favor northern aspects, but there is more variability to this trend. Even protalus ramparts are slightly more common with northerly aspects, but they appear at all aspects within the Tobacco Root Mountains. These findings agree with those of Janke (2007), who reported that tongue-shaped deposits, like glaciers, tend to occupy the topoclimatic niches most preferable for ice preservation, with higher elevations and northerly aspects. The predictive model of Brenning et al. (2007) also includes a correlation between rock-glacier occurrence and relative insolation, but indicates additional influences from elevation and contributing-headwall properties.

In the Tobacco Root Mountains, periglacial deposits with the largest areas sometimes exist at lower elevations with northerly cirque aspects. As discussed in Madole (1972), the intensity of a given glacial period determines which topoclimatic setting will be most favorable for periglacial activity. When a glacial period becomes intense enough, glaciers develop and are likely to destroy pre-existing periglacial deposits. It is therefore conceivable that older rock glaciers at

higher elevations were eroded by Pinedale glaciers. Only at low elevations in non-glaciated valleys would rock glaciers that are Pinedale or older be preserved. This provides one possible explanation for larger deposits having lower minimum elevations in the study area.

Headwalls

In the Tobacco Root Mountains, measurements of headwall fracturing above many of the best developed rock glaciers suggest that fracture orientation may influence the size of a deposit. This point was alluded to by Ward and Hall (1982), who indicated that the orientation of foliation planes may affect the amount of source material and possibly the slope of the deposit. Unfortunately, only an abstract is available for this paper, and no physical data has been published.

Fracture planes with orientations corresponding to foliation encourage headwall retreat by exploiting natural zones of weakness within the mineralogy of the bedrock and establishing an avenue for freeze-thaw erosion. Fractures of this nature were noted at most sites where headwalls were examined, and their influence on deposit area seems to be enhanced when dip-slope fracturing is present. Deposits with dip-slope fracturing include some of the largest identified for their respective aspects (001, 004, 008, 014, 025, 040, 094). The dip-slope orientation of the fracture plane encourages debris that is dislodged from the headwall through freeze-thaw weathering to slide with momentum down-slope and away from the headwall. This has the effect of accelerating the rate at which the deposit receives debris. When both foliation and fracture orientation happen to coincide with the dip slope, the conditions may be ideal for accelerated deposit growth.

Among the deposits studied in the field, the density of fracturing in the headwall does not seem to correlate with deposit area. One reason for this may be that the metamorphic gneisses that comprise most of the Tobacco Root Mountains tend to have a similar amount of fracturing throughout. Olyphant (1981) examined joint spacing for comparable bedrock in the Blanca Massif

and found average values from 0.8-2.5 meters, whereas in the Tobacco Root Mountains, average joint spacing is denser with values ranging from 0.13-0.74 meters. Because of the consistently high average fracture density in this study area, the relative fracture orientation may be a more critical factor controlling the degree to which periglacial deposits can develop.

There was a positive correlation between headwall-fracture density and average boulder diameter for many of the sites examined, but there was no apparent correlation between boulder diameter and deposit area. This trend does not appear to be frequently discussed in other studies, and it is only valid for approximately 60% of sites examined (n=9). One reason that this trend is not more consistent could be anisotropy between fracturing in the examined headwalls and the original headwalls that eroded to generate the deposits. Changes in both lithology and fracture density were recorded on different parts of the same contributing headwall for some deposits, so it is reasonable to assume that these changes could also occur with headwall erosion. In the current study, PC2 of the relative-age-indicator data is strongly related to boulder diameter. Because boulder diameter is often related to headwall-fracture density, PC2 may be more linked to fracturing than it is to relative age and calls to question whether boulder diameter is truly an indicator of relative age.

Headwall area and deposit area are positively correlated in the Tobacco Root Mountains, with deposit area consistently larger than headwall area. Previous studies have found similar results; Janke and Frauenfelder (2008) report a positive correlation (R^2=0.55) for these variables, with the residual attributed to “talus production factors.” The strength of the correlation for priority sites in the current study is even stronger (R^2=0.71), and the trend corresponds with non-significant allometric growth (b<1). The implied (by allometry) faster growth of deposit area relative to headwall extension is likely related to bulking and void space in the deposit, but is also potentially a function of the headwall height being consistently much larger than the deposit thickness. This would enable a relatively small headwall area to produce enough rock debris to form a deposit that covers a larger area.

The current study found no apparent correlation between degree of headwall fracturing and deposit area, which concurs with the findings of Morris (1981). He reported a significant correlation between the influence of fracturing and topoclimatic severity, suggesting that fracturing may only impact the development of a deposit after necessarily intense topoclimatic conditions have been satisfied (e.g., sufficient radiation reduction and ice preservation). Morris goes on to say that jointing may have its strongest control on rock-glacier development in mild topoclimatic settings and becomes less important in more severe settings. This implies that the largest rock glaciers will tend to originate from highly shaded topoclimatic niches with headwalls that have prevalent and ideally oriented fracture planes, but that either a severe topoclimate or intense jointing alone may be sufficient to produce rock glaciers.

Whereas the area of a headwall is limited by the availability of bedrock, the rate of headwall retreat may be directly related to fracture orientation. In the Tobacco Root Mountains, the most massive deposits develop in north-facing cirques surrounded by large areas of contributing headwall with fracture planes parallel to dip slope and/or compositional banding. This is hypothesized to have occurred at Brownback Cirque (014), Sunrise Peak (025), Curly Lake (040), and the East Fork South Boulder Valley (080), although no headwall measurements were made above 080.

Calculated headwall-retreat distances for priority deposits ranged from 1.15 m-35.34 m with an average value of 8.5 m. This corresponds with the erosion of over 3 million square meters of headwall area and the accumulation of over 31 million cubic meters of rock debris in periglacial deposits. Interpolated estimates for all deposits yield similar results, with headwall-retreat distances ranging from 1.2 m-31.9 m and an average value of 7.6 m. The Tobacco Root Mountains could have as much as 10.6 million square meters of headwall area contributing to over 116 million cubic meters of periglacial rock debris.

Although there are only 34 priority deposits, they contain the mass of roughly 25% of the 248 periglacial deposits identified in the range. This follows with the results from the statistical

comparison of datasets where the null hypothesis of equal means is rejected or nearly rejected for attributes such as length, thickness, and area. Because the priority dataset contains many of the most developed deposits identified and represents a quarter of the periglacial activity in the range, it is uniquely suited to reveal the most influential factors in rock-glacier success. Only after relative ages are assigned can the headwall-retreat rates be calculated and the deposits with the largest erosion rates be identified.

Relative-Age Dating

The Principle Components Analysis of relative-age measurements on 21 periglacial deposits in the Tobacco Root Mountains identified three principle components that collectively represent about 80% of the variance in the dataset. PC1 accounted for over half of the variation in the relative-age data and is primarily related to the lichen growth and mineral weathering, whereas PC2 and PC3 were progressively less representative of the total variance in the data and less straightforward to interpret. Both PC2 and PC3 are positively correlated to boulder diameter; however, as discussed previously, this variable seems to be more related to fracture density than relative age. “Percent weathered” has a strong correlation with both PC2 and PC3, although the correlation is positive for PC2 and negative for PC3. This same relationship holds true for oxidation-rind depth, and the inverse is true for percent pitting cover. Although these three variables are useful for highlighting the highly weathered sites, they are somewhat redundant. Also, it is difficult to estimate percent weathered for more recent deposits because all measures of relative age must be objectively and simultaneously considered. Because increasing lichen cover obscures and discourages the rate of development of surface-weathering features (Birkeland, 1973), older deposits can be assigned anomalously low values for these same variables. Another complication with the oxidation data is that the rate of oxidation that a boulder experiences is linked to the mineralogical content of the source headwalls. There is a moderate amount of lithological variation across the Tobacco Root Mountains from felsic to mafic

mineralogy, and as a consequence, percent oxidation cover and percent weathered may not always be reliable variables for gauging relative age. This knowledge adds some caution to the interpretation of PC2 and PC3 results, and justifies the reliability of PC1 results. This same technique was used by Dowdeswell (1982), who ultimately only considered the component I values in his study.

The lichen data (a dominant influence on PC1) has proven to be a reliable and popular indication of the relative age of a deposit (Birkeland, 1973; Dowdeswell, 1982), but it is not without its downfalls. Benedict (1990, 1991) has shown that lichen-growth rates can be affected by variations in solar radiation and precipitation. Because precipitation is strongly controlled by the local topography, two lichens of the same species at similar elevations in the same mountain range can have greatly different growth rates. In addition, lichens are susceptible to “snowkill” if they are buried under a snowpack and exposed to anoxic conditions for too long (Benedict, 1993). The older a lichen is, the more likely that it will be exposed to adverse growth conditions. For this reason, superposition and other observed data are considered when assessing the validity of the PCA and assigning ages.

Because of the inherent shortcomings in the original relative-age indicators, as well as the resulting principle components, data from each site should be considered in the context of absolute age limits for the Tobacco Root Mountains established by Hall (1984) and Hall and Martin (1986) with comparisons made to similar studies summarized in Dowdeswell (1982). Together, this data will be used to suggest the relative ages of deposits in the priority dataset. The ages presented in **Table 18** represent a detailed consideration of all available data. Starting with the most recent deposits, the age assignments of all dated deposits will be discussed. The ages are constrained to the main periods of periglacial development widely recognized in the Rocky

Table 18: Summarized results of the relative-age analysis showing all data parameters as well as elevation and final age assignments, sorted by lichen cover. From left to right, column headers stand for: Boulder Diameter, % Weathered, Maximum Pit Depth, Oxidation Rind Depth, % Oxidized, Crystal Height, % Angularity, % Lichen Cover, Lichen Max Short Axis Dia., Lichen Average Short Axis Diameter, Lichen Maximum Long Axis Diameter, Lichen Average Long Axis Diameter, and Average Elevation.

Site	BD (m)	% Wea	Pit Max (cm)	OxRind (cm)	%Ox	XtalHt (cm)	%Ang	%Lichen	LShMax (cm)	LShAvg (cm)	LLoMax (cm)	LLoAvg (cm)	Avg Ele. (m)	Cluster	Apparent Age
036	0.97	54	0.31	0.07	38	0.05	100	0.0	1.0	0.0	1.0	0.4	2939	n/a	GP
116	0.85	20	2.57	0.15	41	0.15	84	7.5	10.4	4.2	11.6	4.9	2745	A	AUD
026_2	0.87	20	0.55	0.01	12	0.14	77	17.6	9.0	5.2	10.0	5.8	2619	A	AUD
059	1.02	64	3.04	-	35	0.52	47	22.4	14.0	7.0	18.5	8.4	2740	-	ENG
003	0.91	36	1.68	0.20	49	0.16	91	26.0	13.1	7.6	14.3	8.4	2837	A	ENG
094	1.40	72	3.86	0.10	25	0.59	80	27.5	15.2	10.6	17.1	11.5	2839	B	ENG
025_3	0.85	48	1.52	0.07	24	0.20	79	28.6	13.2	8.4	15.7	9.2	2691	B	ENG
060	1.14	96	5.85	-	25	0.83	37	29.4	17.8	5.0	18.3	5.6	2749	-	ENG
058	0.93	84	3.19	-	21	0.68	42	35.8	15.0	6.8	17.0	7.7	2709	-	ENG
117	0.88	46	2.23	0.02	25	0.18	88	39.4	14.0	7.3	15.5	8.2	2725	B	ENG
025_2	0.98	90	2.54	0.19	29	0.30	76	50.4	16.0	8.6	16.5	9.1	2665	C	ENG
172	0.96	98	1.41	0.08	35	0.23	83	50.8	16.1	8.3	16.4	8.9	2874	C	ENG
040	1.06	100	2.43	0.23	34	0.53	71	53.4	13.5	8.2	14.8	8.8	2763	C	ENG
008	0.86	16	2.01	0.05	23	0.21	85	54.4	15.8	8.8	18.3	9.9	2828	B	ENG
041	1.05	100	3.60	0.20	30	0.38	68	56.8	11.7	7.9	11.9	8.4	2760	C	ENG
004	0.93	88	2.82	0.52	30	0.24	85	57.6	12.2	7.8	12.8	8.5	2808	C	ENG
029	0.90	100	1.62	0.17	17	0.33	81	61.2	10.0	6.8	10.5	7.4	2878	C	ENG
026_1	1.36	98	3.95	0.22	24	0.37	69	63.8	13.5	9.5	13.7	10.3	2602	C	ENG
025_1	1.12	100	2.71	0.22	20	0.38	68	71.0	13.5	8.7	14.5	9.2	2648	C	ENG
028	1.25	100	2.85	0.23	19	0.34	79	73.2	15.0	8.5	18.0	9.2	2684	C	ENG
044	1.25	100	6.14	0.21	14	1.03	60	77.6	19.5	9.8	20.1	10.6	2589	D	LPD
080	0.86	100	2.40	0.29	7	0.48	67	81.0	24.4	9.2	30.5	10.9	2378	D	LPD
115	0.95	100	3.93	0.37	9	0.67	60	89.9	18.6	12.0	20.7	13.1	2218	D	PD
014	1.03	100	2.54	0.22	7	0.36	67	90.6	19.8	10.3	21.1	11.0	2134	D	PD

Mountains. From most recent to oldest, these include the Gannett Peak, the Audubon, the Early Neoglacial, and the (late) Pinedale.

Gannett Peak

As defined by the studies in Dowdeswell (1982), Gannett Peak (300-100 YBP) deposits generally lack the weathering characteristics and lichen dimensions seen in older deposits. Because PC1 has a strong positive correlation with the lichen data and many of the mineral weathering variables examined, Gannett Peak deposits would likely have the lowest values of any deposit along this component. Three of the four sites that are low-end outliers along PC1 (116, 026_2, 003) constitute cluster 'a' in **Figure 21**. The remaining site (036) is an outlier along PC2 relative to cluster 'a' and has the most negative value of any site along PC1. When values for individual variables are considered, 036 appears to be the only site that matches the summary of Gannett Peak deposits in Dowdeswell (1982). Every boulder examined at this site had less than 10% lichen cover and a maximum lichen diameter of less than 3 cm.

Because PC2 and PC3 have a more complex relationship with the relative-age data and are difficult to interpret, individual variables were evaluated. For site 036, the boulder angularity is 100%, and boulder diameter, percentage of oxidation, and percent weathered are all moderate. Boulder diameter is primarily related to the degree of fracturing in the source headwall, but two processes can complicate this. As a rock-glacier deposit flows, the largest boulders will tend to rise to the surface due to the muesli effect (granular convection). However, the longer that a boulder is exposed to weathering, the smaller it becomes. This, along with the absence of lichen growth, influences the outlier PC2 value. Based on the component scores and values of individual variables, it is hypothesized that 036 is the only Gannett Peak deposit that was examined. Using this deposit as reference, this research found that Gannett Peak deposits have a minimum elevation of about 2,860 m, and a typical length of around 120 m.

Audubon

The study by Dowdeswell (1982) was performed in the Audubon Cirque in Colorado. Audubon Cirque deposits have maximum lichen diameters from 4-8 cm, with average lichen cover ranging from 10-50%. Based on these values, Audubon deposits should have slightly higher values along PC1 than the Gannett Peak deposit. In **Figure 21**, sites that fit this description are labeled 'a' (026_2, 116, 003). These sites have the lowest PC3 values of all examined sites. Along PC1, only the Gannett Peak deposit (036) has a lower value. Along PC2, only site 008 has a lower value; but its placement in cluster 'b' due to a moderate PC1 score suggests that 008 must be older than the Audubon.

The lichen cover of the three sites in cluster 'a' are within the range reported by Dowdeswell, but the maximum lichen diameters all exceed values seen in his study. Sites 026_2 and 116 have lichen diameter values somewhat close to the published range (10 cm and 11.6 cm, respectively). Site 003, however, has a maximum lichen diameter (14.3 cm) that is far greater than the reported Audubon values. Site 003 is a secondary / upper lobe overlying deposit 004. Deposits of this nature were specifically referenced by Hall (1990). He concluded based on radiocarbon dates that the primary Early Neoglacial advance was around 3,600 YBP. Hall also used relative-age dating to estimate approximately 1,000 years of age difference between lobes of these types of deposits. He concluded that both lobes are Early Neoglacial in age, suggesting that the Early Neoglacial period may have been active until 2,600 YBP. This, coupled with ambiguity in the lichen data, suggests that deposit 003 may have originated late in the Early Neoglacial rather than during the Audubon. For this reason, it will be considered in the next section.

The other two sites in cluster 'a' (026_2, 116) have lichen diameter values within 4 cm of the Audubon range outlined by Dowdeswell. Both sites have similarly extreme values along all three components, and are presumably the same age. Based on all of the available data, this age is most likely Audubon. Previous studies including Miller (1973) suggest that Audubon periglacial

activity occurred from 1,000-2,000 YBP. An average of the two Audubon deposits yields a minimum elevation of about 2,673 m and a typical length of about 140 m.

Early Neoglacial

As is common in the Rocky Mountains, a significant amount of periglacial activity took place in the Tobacco Root Mountains during the Early Neoglacial period (Hall, 1984). Dowdeswell summarizes Early Neoglacial deposits as having more than 50% lichen cover and maximum lichen diameters that are typically greater than 10 cm. Birkeland (1973) states that these variables, along with lichen species composition, offer the best clues as to whether a deposit is Early Neoglacial or older. In the current study these variables are most strongly represented by PC1, making it particularly useful in identifying Early Neoglacial deposits (**Figure 11**). Referring to **Figure 21**, cluster 'a' sites are followed on PC1 by a series of sites with similar values. Sites with the lowest PC1 values tend to have low values along PC2 and high values along PC3, forming cluster 'b' (008, 025_3, 117, 094). Alternatively, sites with moderate to high PC1 values tend to have similarly high PC2 and low PC3 values, forming cluster 'c' (025_2, 004, 172, 029, 040, 041, 026_1, 025_1, 028). On the upper end of PC1 there are four sites labeled as cluster 'd' (044, 080, 115, 014) that are outliers to cluster 'c'. Based on their deviation from the cluster 'c' sites and the extreme values of several relative-age variables, sites in cluster 'd' are presumably older than the Early Neoglacial and will be discussed in the next section.

Every site in cluster 'c' and cluster 'b' have maximum lichen diameters greater than or equal to the 10 cm lower-limit for Early Neoglacial deposits found in Dowdeswell (1982). For lichen cover, all of the sites in cluster 'c' have values exceeding the 50% lower limit set by Dowdeswell. For sites in cluster 'b', the lichen cover values are consistently smaller with only one site greater than 50% (008; 54%). Lichen cover is an important control for the variation seen along the principle components within Early Neoglacial sites. Based on the similarity of relative-age data for sites in cluster 'c', it is reasonable to assume that these deposits were all active at roughly the

same time. Hall (1984) dated the main periglacial advance of the Early Neoglacial to be about 3,600 YBP in the Tobacco Root Mountains.

For the deposits in cluster ‘b’ and site 003, the deviation from cluster ‘c’ along PC2 and PC3 merits a deeper investigation. Two sites (003, 025_3) are on the uppermost lobe of a deposit with multiple lobes. As discussed in the previous section, deposits of this sort were examined by Hall and the upper lobes were estimated to have formed approximately 2,600 YBP. This places the final period of Early Neoglacial activity just before the radiocarbon-dated cessation of Early Neoglacial advances (~2,500 YBP) taken from organic matter found at the base of a melt outwash deposit (Hall and Michaud, 1988). This time gap reduces the amount of exposure these deposits experienced to only 70% of the time that sites from cluster ‘c’ have hypothetically experienced. This causes notably unique values along all three principle components for sites 003 and 025_3 compared to sites on deposits formed during the primary Early Neoglacial advance (cluster ‘c’).

The other three sites in cluster ‘b’ (008, 117, and 094) are all on deposits which originate in south-facing cirques. Two of these deposits (008, 117) are located near Sailor Lake and have southern aspects. Deposit 094 is in a south-facing cirque near Branham Lakes but has an eastern aspect. Site 008 has the lowest value of any site along PC2 and the one of the highest values along PC3. Whereas sites 117 and 094 have slightly lower values along PC3 and a higher values along PC2, all the three sites have similar values for PC1. They all also have similarly high angularities and low oxidation depths, leading to low percentage weathered estimations and extreme PC2 and PC3 values. Despite these low scores, the PC1 and supplemental lichen data suggest that the deposits are at least Early Neoglacial in age. As the deposits all have increased southern exposure, accumulated snow packs should melt more rapidly than they do on deposits that face north. This decreases both the amount of time that liquid water is in contact with boulders and the likelihood of freeze-thaw weathering. Aspect seems to affect the rates of oxidation, lichen growth, and boulder rounding, causing south-facing deposits to have outlier values along PC2

and PC3 (cluster 'b', **Figure 21**) and to appear relatively less weathered than north-facing deposits of presumably similar absolute ages.

The Early Neoglacial deposits identified have an average minimum elevation of about 2,715 m and a typical length of about 225 m. A consideration of individual values yields a minimum elevation range from 2,600-2,850 m and a length range from about 80-690 m.

Pinedale

Although lichen data is very useful for differentiating Early Neoglacial deposits from younger deposits, it is increasingly difficult to interpret lichen data for older deposits. This point is best illustrated in **Figure 11**. According to this figure, only oxidation-rind depth, soil, and other subsurface data such as hornblende etching can consistently differentiate between Neoglacial deposits and Pleistocene-aged deposits. The figure also indicates that angularity and general surface weathering (percent weathered, pitting) could still potentially be useful. For this reason, these variables are given more weight when considering sites that are likely Pinedale or older. Dowdeswell does not include lichen values for Pinedale deposits in his report, but he does summarize other variables. Oxidation-rind thickness is variable across studies but seems to average at about 1.5 cm, boulder angularity tends to be less than 20%, and the maximum pit depth is generally at least 8 cm.

Lichen cover is not as definitive as other variables for identifying Pinedale deposits, but older deposits should have the largest lichens. Furthermore, angularity is still a reliable variable for older deposits. Because of this, PC1 is useful for identifying deposits that are potentially older than the Early Neoglacial. Sites that are upper outliers of cluster 'c' on PC1 can be seen as cluster 'd', a small group on the lower left side of **Figure 21** comprised of sites 044, 080, 115, and 014. PC2 is mostly related to boulder diameter and weakly related to oxidation and angularity. The inverse correlation with pitting cover and lichen diameter further complicate the interpretation of PC2, and in general it does not seem well suited for identifying the oldest deposits. As percent

weathered and oxidation-rind thicknesses are applicable variables for Pleistocene deposits, PC3 is useful. The four sites outlined by cluster ‘d’ have the lowest PC3 values of any site examined, with 014 and 115 clearly the most extreme.

Of the sites in cluster ‘d’, none of them have the lack of angularity (roundness) that Dowdeswell (1982) outlines. Degree of angularity was determined in this study using a visual comparison chart that was likely scaled differently than those used in previous studies. Although the percent of angularity is not near the outlined range, these four sites have the lowest angularity of any site examined (60-67%). They also have some of the deepest oxidation rinds and pits in the dataset, although the average value for these variables is less than the maximum value listed by Dowdeswell (1982). Even though lichen data are not always reliable for older sites, the sites in cluster ‘d’ are distinguished by having the highest lichen cover and largest lichen diameters observed.

For Pleistocene deposits, one of the most distinguishing characteristics is the soil that generally develops at the surface. In these soils, the thickness of loess and the depth of the B-horizon can be reliable indicators the relative age. In addition to this, some age constraints can be placed on deposits based on their position relative to glaciated valleys. Both deposits 080 and 115 partially exist in the East Fork South Boulder River Valley. As this valley is known to have been extensively glaciated in the Pinedale (Hall, 1990), these deposits must have developed since then, suggesting that they could be Late Pinedale in age. As no clear distinction was found between the Late Pinedale and Early Holocene advances, an absolute age range for these deposits as defined by Hall (1984) would be between 9,900 and 8,500 YBP.

The age assignment for deposit 115 may ultimately be inconsequential to this study, as it is speculated to be a landslide rather than a periglacial deposit. Assuming it is a landslide, the Late Pinedale is hypothesized to be the time when the deposit was no longer blocked by the main valley glacier and spilled out of its hanging valley. An initial, smaller landslide could have occurred

while the main valley was still entrenched with glacial ice during the Pinedale, but the final (and potentially only) movement of the deposit must have occurred in the Late Pinedale.

Because deposit 080 is located farther up valley than 115, it is interpreted as being younger. Due to its size and location, the deposit is hypothesized to have originated as an ice-cored rock glacier. As the Pinedale glaciers receded, two pulses of rock-glacier development were recorded in deposits 080 and 081. Across its surface, deposit 080 is covered in soil and trees in parts and has barren boulders in other parts. When soil was present, it appeared to be thin, although no soil pit was excavated to verify this. If it was formed at the end of the Pinedale, deposit 080 would have been exposed to only a minimal amount of loess deposition from the receding Pinedale glaciers. This explains why only some areas of the deposit have developed soil and vegetation.

Deposits 014 and 044 are both in minor valleys which were not overridden by the main-valley glaciers during the Pinedale. Deposit 044 is perched in a high hanging valley and shielded from the South Boulder trunk valley. The deposit has very little soil development with only a few vegetated areas. Given the lack of soil, it seems unlikely that this deposit was present during the Pinedale. Also, since the component scores for 044 are not as extreme as those from 014 or 115, it is possible that deposit 044 also formed as an ice-cored rock glacier during the Late Pinedale. However, since 044 is in a hanging valley, it may have been shielded from much of the loess generated by the main valley glaciers compared to deposit 080, explaining the relative lack of soil. Another possibility is that the deposit is actually Early Neoglacial in age and simply has anomalously large lichen diameters because of microclimatic differences. Nevertheless, extreme values for other variables makes Late Pinedale seem like the more appropriate assignment.

An inspection of deposit 014 reveals that the deposit is densely tree-covered over the majority of its surface (see **Figure R-10**). The areas without trees are generally still vegetated, such as the large grassy meadow near the middle of the deposit. The cirque and collapsed footwall offer the only two areas with a significant number of exposed boulders. However,

boulders with diameters up to 3 m can be seen across the deposit, especially along ridges and furrows (see **Figure 22**). Although these features were not analyzed, their general appearance seems consistent with deposits from the Early Neoglacial, suggesting there may have been some reactivation during this period. The boulders exposed in the cirque and on the collapsed footwall of the deposit are heavily covered with lichens. Over half of the visible lichens are brown or black in color, which Birkeland (1973) reports is a good indicator of an older surface. Although this suggests that 014 could possibly predate the Pinedale, more evidence is needed to make a final age assignment.

The Pinedale “snow line” calculated by Jacobs (1969) is about 2,590 m. This is much higher than the cirque floor of deposit 014. The soil pit excavated on 014 revealed the presence of loess to a depth of nearly 1 m and an A-horizon over 0.1 m thick. According to Birkeland (1973), Early Neoglacial deposits typically do not have any loess, Pinedale deposits can have loess depths up to 0.83 m, and Bull Lake deposits can have even thicker sequences of loess. As the total depth of loess could not be determined at the excavation site, it is ultimately unclear whether 014 is Pinedale or older in age. More soil excavations and other methods of dating would improve any age estimates for this deposit; however, a minimum age would be about 25,000 YBP as defined by Hall and Martin (1986).

The three rock-glacier deposits hypothesized to be late Pinedale or older have an average minimum elevation of 2,337 m and a typical length of about 1,050 m. These values clearly define the larger range and size of Pinedale deposits relative to Early Neoglacial or more recent deposits.

Headwall-Retreat Rate

The “headwall-retreat rate” is defined as the average backwearing of the rockshed (estimated by dividing the volume of deposit debris by the area of the contributing headwall) divided by the age of the deposit. Comparing calculated retreat rates above deposits to more

directly measured rockwall-retreat rates (Olyphant, 1983) provided additional tests of the validity of assigned ages.

The data presented in **Table 13** imply that the majority of dated deposits in this study originated in the Early Neoglacial, a period estimated at approximately 3,600 YBP. There are four deposits that are suspected to predate the Early Neoglacial, with 044 and 080 hypothesized to have been active in the late Pinedale around 9,200 YBP, whereas 115 and 014 are speculated to have originated at least 15,000 YBP. Deposits 116, 026_2, and 003 appear to be younger than the Early Neoglacial, making them likely either Late Early Neoglacial (2,600 YBP) or Audubon (1,500 YBP), whereas 036 is the only deposit speculated to be from the Gannett Peak period (300 YBP). Using these assigned ages, the average rates of rockwall retreat range from as little as 0.12 mm/yr to 9.82 mm/yr, with an average rate of 2.06 mm/yr (**Table 19**). Retreat rates are generally within the range of values reported by Olyphant (1983) of 0.5-3 mm/yr, and other studies summarized by Olyphant in which retreat rates have varied from 0.1 mm/yr to 10 mm/yr.

All but four of the headwall-retreat rates calculated for rocksheds above deposits in the Tobacco Root Mountains are within the more refined range of Olyphant (1983). Note that there are two deposits with estimated retreat rates below the refined range; these are 014 (0.12 mm/yr) and 044 (0.28 mm/yr). Deposit 014 has the largest headwall area and one of the largest volumes of rock of the priority deposits. This combination produces the lowest calculated headwall-retreat distance (1.76 m). Because the deposit is speculated to be Pinedale in age, the extreme amount of time for the headwall erosion to occur yields an anomalously low retreat rate. Similarly with 044, the calculated headwall-retreat distance is small (2.61 m) and the deposit is dated as Late Pinedale, resulting in a low calculated retreat rate. These findings cast doubt on the hypothesized Pinedale age, as a younger age of Early Neoglacial would have put them within the range of previously reported retreat rates; however, it seems unlikely that deposit 014 could have originated in the Early Neoglacial and still have the degree of soil development observed.

Table 19: Headwall retreat and retreat rate calculations for dated priority sites. Vol=Volume, HW=Headwall, HWRT=Headwall Retreat

Deposit #	Rock Vol (m^3)	HW Area (m^2)	HWRT (m)	Interpreted Age	Rate (mm/yr)
004	371,931	73,042	5.09	3,600	1.41
008	28,661	12,301	2.33	3,600	0.65
014	1,146,377	650,657	1.76	15,000	0.12
025	212,267	41,029	5.17	3,600	1.44
026	198,098	22,004	9.00	3,600	2.50
028	74,001	20,629	3.59	3,600	1.00
029	46,861	7,717	6.07	3,600	1.69
040	2,557,409	72,355	35.35	3,600	9.82
044	886,126	339,387	2.61	9,200	0.28
080	11,873,797	358,946	33.08	9,200	3.60
094	272,994	30,638	8.91	3,600	2.48
115	6,604,670	365,211	18.08	15,000	1.21
116	108,330	32,319	3.35	1,500	2.23
117	34,903	8,099	4.31	3,600	1.20
172	60,905	13,447	4.53	3,600	1.26
Min	28,661	7,717	1.76	1,500	0.12
Mean	1,631,822	136,519	9.55	5,727	2.06
Max	11,873,797	650,657	35.35	15,000	9.82

Two of the study deposits produced calculated retreat rates that are larger than the more refined range of published results. Deposit 080 has a calculated rate of 3.6 mm/yr, which is nearly within the range. Given that this deposit has by far the largest volume of any priority site, that it exists in a favorable topoclimatic setting known to have produced glaciers, and that there are multiple lobes of flow, the retreat rate seems plausible. Deposit 040 has the largest retreat rate of any deposit at 9.8 mm/yr. It appears to be Early Neoglacial in age based on the PCA, but has an enormous headwall-retreat distance (35.3 m) related to its extreme rock volume. A reexamination of this site revealed the possible presence of a moraine ‘step’ underneath the lower part of the deposit. The thickness estimation included this as part of the rock-glacier deposit, which greatly increased the overall thickness. Without inclusion of this step, the headwall-retreat rates would be more reasonable. Alternatively, if the age of the deposit is assumed to be Late Pinedale rather

than Early Neoglacial, the headwall-retreat rate becomes a much more believable 3.8 mm/yr. However, the lack of soil development and results from the PCA suggest that Early Neoglacial is a more reasonable age.

Future Work

In order to better understand the history of periglacial processes and their underlying controls in the Tobacco Root Mountains, additional work could be done in several areas. First, collecting relative-age data and headwall-fracture measurements on unvisited deposits would assist with recognizing trends and establishing a more complete chronology and topoclimatic signature. The headwall-fracture-density analysis could be augmented through photogrammetry, reducing the need to physically visit every headwall. However, information on fracture orientation (which seems to be an important factor explaining headwall erosion) would likely require more extensive field investigations.

The assessment of additional relative-age indicators such as hornblende etching and weathering profile characteristics could provide more objective criteria for differentiating older deposits within the range. In addition, geophysical methods such as ground penetrating radar, seismic reflection, and core drilling could be employed to validate thickness estimations, better constrain deposit volumes, and confirm whether or not certain deposits are still seasonally active. For deposits determined to be seasonally active, the rate of rock-glacier advance and headwall retreat could be physically measured and compared with estimated headwall-retreat rates.

Finally, as higher resolution aerial photography, multi-spectral imagery, digital elevation models, and LIDAR elevation data become available, they could be used to facilitate improvements in the quality of remotely sensed data. With these improved products, all remote sensing methods described in this paper could be refined and improved (especially volume estimation and radiation reduction). Furthermore, remotely sensed attributes that were only defined for the priority dataset (contributing-headwall area, footprint area, SC thickness) could be

determined for all deposits. The increased sample size would help to more deeply explore the relationship between a rock glacier and its contributing headwall and may yield more statistically significant results.

VI. Conclusions

An analysis of high-resolution aerial photographs revealed a total of 248 rock glaciers and protalus ramparts in the headwater drainages of the Tobacco Root Mountains in southwest Montana. Estimates of deposit volumes indicate that more than 116 million cubic meters of rock rubble has been eroded from contributing headwalls to develop these deposits, most of which has occurred since Pinedale deglaciation. Of the deposits examined, there were 60 protalus ramparts and 188 rock glaciers, 90 of which were tongue-shaped in morphology and 98 that were lobate. Tongue-shaped rock glaciers have statistically larger average areas and lengths than lobate rock glaciers (125,978 m^2; 538.2 m and 56,851 m^2; 220.3 m, respectively), which are statistically larger than protalus ramparts (34,276 m^2; 148.3 m). In general, lobate rock glaciers~are more similar to protalus ramparts than either are to tongue-shaped rock glaciers. All three types of deposits tend to emanate from north-facing topoclimatic niches, and all have statistically different radiation-reduction values on the winter solstice with insolation lowest on tongue-shaped rock glaciers and highest on protalus ramparts. The same increasing trend was also found for average deposit slope (tongue-shaped=~25°, lobate=~27°, protalus rampart=~30°), indicating that the process of post-depositional flow in rock glaciers tends to reduce the overall slope of the deposit. Finally, tongue-shaped rock glaciers have higher average maximum elevations (~2907 m) than the other two morphologies, which have similar averages (lobate=2843 m, protalus rampart=2852 m).

The subset of 21 deposits that were selected for more intensive investigations (including a principle components analysis of relative age data) reveals that most of the deposits probably originated during the Early Neoglacial period (5,000-3,000 YBP), and that there is little evidence

of rock-glacier development during the Little Ice Age (Gannett Peak period). An analysis of the functional relationships between deposit volume and its linear dimensions indicate that as deposits increase in size, they do so primarily by lengthening, although widths and thicknesses also increase with increasing volume. Headwall-retreat values, derived from deposit volumes and source-headwall areas, range from as little as 1 m to more than 35 m. When headwall-retreat rates were computed using inferred ages from relative-age data, the rates fall within a conservative range (0.5-3.5 mm/yr) that is well within the range of headwall-retreat rates reported by other researchers. Headwall-fracture measurements above some of the largest deposits suggest that fracture orientations corresponding with dip slope and compositional banding enhance the rate at which headwalls erode and deposits receive debris. Overall, this study has shown that the Tobacco Root Mountains, which only reach elevations of 3,200 m, tend to have more older (Pinedale) than recent (Gannett Peak) deposits. However, regardless of deposit age, the same topoclimatic controls related to snow and ice preservation are critically important for rock-glacier development. This highlights the importance of continued periglacial research and endorses the use of rock glaciers as indicators of past and future climate shifts.

References

Alden, W. C. (1953). *Physiography and Glacial Geology of Western Montana and Adjacent Areas: A Study of Glacial Features in the Intermontane Valleys and the Drainage Area of the Upper Missouri and Columbia Rivers*. US Government Printing Office.

Benedict, J. B. (1965). Photo-interpretation of two types of rock glaciers in the Colorado Front Range, USA. *Journal of Glaciology*, *5*, 849-856.

Benedict, J. B. (1967). Recent glacial history of an alpine area in the Colorado Front Range, USA. I. Establishing a lichen-growth curve. *Journal of glaciology*,*6*(48), 817-832.

Benedict, J. B. (1973). Chronology of cirque glaciation, Colorado Front Range.*Quaternary Research*, *3*(4), 584-599.

Benedict, J. B. (1990). Experiments on lichen growth. I. Seasonal patterns and environmental controls. *Arctic and Alpine Research*, 244-254.

Benedict, J. B. (1991). Experiments on lichen growth II. Effects of a seasonal snow cover. *Arctic and Alpine Research*, 189-199.

Benedict, J. B. (1993). A 2000-year lichen-snowkill chronology for the Colorado Front Range, USA. *The Holocene*, *3*(1), 27-33.

Birkeland, P. W. (1973). Use of relative age-dating methods in a stratigraphic study of rock glacier deposits, Mt. Sopris, Colorado. *Arctic and Alpine Research*, 401-416.

Birkeland, P. W., Colman, S. M., Burke, R. M., Shroba, R. R., and Meierding, T. C. (1979). Nomenclature of alpine glacial deposits, or, What's in a name?.*Geology*, *7*(11), 532-536.

Brenning, A. (2005). Spatial prediction models for landslide hazards: review, comparison and evaluation. *Natural Hazards and Earth System Science*, *5*(6), 853-862.

Brenning, A., Grasser, M., and Friend, D. A. (2007). Statistical estimation and generalized additive modeling of rock glacier distribution in the San Juan Mountains, Colorado, United States. *Journal of Geophysical Research: Earth Surface (2003–2012)*, *112*(F2).

Capps, S. R. (1910). Rock glaciers in Alaska. *The Journal of Geology*, *18*(4), 359-375.

Dowdeswell, J. A. (1982). Relative dating of late Quaternary deposits using cluster and discriminant analysis, Audubon Cirque, Mt. Audubon, Colorado Front Range. *Boreas*, *11*(2), 151-161.

Fu, P., and Rich, P. M. (1999). Design and implementation of the Solar Analyst: an ArcView extension for modeling solar radiation at landscape scales. In *Proceedings of the 19th annual ESRI user conference, San Diego, USA*.

Gesch, D., Oimoen, M., Greenlee, S., Nelson, C., Steuck, M., and Tyler, D. (2002), The national elevation dataset. *Photogrammetric Engineering and Remote Sensing, 68*(1), 5-11

Gibbons, A. B., Megeath, J. D., and Pierce, K. L. (1984). Probability of moraine survival in a succession of glacial advances. *Geology*, *12*(6), 327-330.

Graf, W. L. (1970). The geomorphology of the glacial valley cross section. *Arctic and Alpine Research*, 303-312.

Haeberli, W., Hoelzle, M., Kääb, A., Keller, F., Vonder Mühll, D., and Wagner, S. (1998). Ten years after drilling through the permafrost of the active rock glacier Murtèl, Eastern Swiss Alps: answered questions and new perspectives. In *Proceedings of the Seventh International Conference on Permafrost* (pp. 403-410).

Hall, R. D. (1977). Preliminary investigation of the glacial history of the Tobacco Root Range, southwestern Montana: Geol. *Soc. of America Abstract with Program*, *9*(6), 728-729.

Hall, R. D. (1984). Late Quaternary history of the Tobacco Root Range, southwestern Montana, as interpreted from radiocarbon dates: *Geological Society of America Abstracts with Programs*, 16, 223.

Hall, R. D. (1990). Quaternary Geology of the Tobacco Root Range. *In* Hall, R. D. (ed.) *Quaternary Geology of the Western Madison Range, Madison Valley, Tobacco Root Range, and Jefferson Valley,* Indiana University, Indianapolis. 183-193.

Hall, Robert D., and Heiny, J.S., (1983). Glacial and postglacial physical stratigraphy and chronology, North Willow Creek and Cataract Creek drainage basins, eastern Tobacco Root Range, southwestern Montana, USA. *Arctic and Alpine Research:* 19-52.

Hall, R. D., and Martin, R. E. (1986). The etching of hornblende grains in the matrix of alpine tills and periglacial deposits. *Rates of Chemical Weathering of Rocks and Minerals: Orlando, Florida, Academic Press, Inc.*, 101-128.

Hall, R. D., and Horn, L. L. (1993). Rates of hornblende etching in soils in glacial deposits of the northern Rocky Mountains (Wyoming-Montana, USA): Influence of climate and characteristics of the parent material. *Chemical geology*, *105*(1), 17-29.

Hall, R. D., and Michaud, D. (1988). The use of hornblende etching, clast weathering, and soils to date alpine glacial and periglacial deposits: A study from southwestern Montana. *Geological Society of America Bulletin*, *100*(3), 458-467.

Hall, R. D., Ward, P., Heiny, J. S., and Kodidek, K. (1980). Glacial geology of the Cataract Creek and North Willow Creek Valleys, Tobacco Root Range, Montana (abs.) Geological *Society of America Abstracts*, *12*(6), 274.

Humlum, O. (1998). The climatic significance of rock glaciers. *Permafrost and Periglacial Processes*, *9*(4), 375-395.

Jacobs, A. M. (1967). Pleistocene proto-cirque hollows in the Cataract Creek Valley, Tobacco Root Mountains, Montana (Doctoral dissertation, Indiana University).

Jacobs, A. M. (1969). Pleistocene Niche Glaciers and Proto-Cirques, Cataract Creek Valley, Tobacco Root Mountains, Montana. *Geological Society of America Special Papers*, *123*, 103-114.

Janke, J. R. (2007). Colorado Front Range rock glaciers: distribution and topographic characteristics. *Arctic, Antarctic, and Alpine Research*, *39*(1), 74-83.

Janke, J., and Frauenfelder, R. (2008). The relationship between rock glacier and contributing area parameters in the Front Range of Colorado. *Journal of Quaternary Science*, *23*(2), 153-163.

Konrad, S. K., Humphrey, N. F., Steig, E. J., Clark, D. H., Potter, N., and Pfeffer, W. T. (1999). Rock glacier dynamics and paleoclimatic implications. *Geology*, *27*(12), 1131-1134.

Madole, R. F. (1972). Neoglacial facies in the Colorado Front Range. *Arctic and Alpine Research*, 119-130.

Miller, C. D. (1973). Chronology of Neoglacial deposits in the northern Sawatch Range, Colorado. *Arctic and Alpine Research*, 385-400.

Morris, S. E. (1981). Topoclimatic factors and the development of rock glacier facies, Sangre de Cristo Mountains, southern Colorado. *Arctic and Alpine Research*, 329-338.

Morris, S. E., and Olyphant, G. A. (1990). Alpine lithofacies variation: working toward a physically-based model. *Geomorphology*, *3*(1), 73-90.

Mueller, P. A., and Cordua, W. S. (1976). Rb-Sr whole rock age of gneisses from the Horse Creek area. *Tobacco Root Mountains, Montana: Isochron/West*, *16*, 33-36.

Olyphant, G. A. (1981). Allometry and cirque evolution. *Geological Society of America Bulletin*, *92*(9), 679-685.

Olyphant, G. A. (1983). Computer simulation of rock-glacier development under viscous and pseudoplastic flow. *Geological Society of America Bulletin*, *94*(4), 499-505.

Pearson, K. (1901). Principal components analysis. *The London, Edinburgh, and Dublin Philosophical Magazine and Journal of Science*, *6*(2), 559.

Porter, S. C. (1975). Equilibrium-line altitudes of late Quaternary glaciers in the Southern Alps, New Zealand. *Quaternary research*, *5*(1), 27-47.

Refsnider, K. A., and Brugger, K. A. (2007). Rock glaciers in central Colorado, USA, as indicators of Holocene climate change. *Arctic, Antarctic, and Alpine Research*, *39*(1), 127-136.

Reshkin, M. (1963). *Geomorphic History of the Jefferson Basin, Jefferson, Madison and Silverbow Counties, Montana* (Doctoral dissertation, Indiana University).

Roy, W. R. (1980). *Glacial chronology of the South Boulder Valley, Tobacco Root Range, Montana* (Doctoral dissertation, Indiana University).

Roy, W. R., and Hall, R. D. (1980). Glacial geology of the South Boulder Valley, Tobacco Root Range, Montana. Montana Geol. Soc. Field Conf., Southwest Montana, 125-132.

Sarkar, A., Brophy, J. G., Ripley, E. M., Li, C., and Kamo, S. L. (2009). Geochemical and isotopic studies of the Lady of the Lake Intrusion and associated tobacco root Batholith: Constraints on the genetic relation between Cretaceous mafic and silicic magmatism in Southwestern Montana. *Lithos*,*113*(3), 555-569.

Schmidt, C. J., Smedes, H. W., and O'Neill, M.J. (1990). Syncompressional Emplacement of the Boulder and Tobacco Root Batholiths (Montana-USA) by Pull-apart along Old Fault Zones. *Geological Journal*, *25*(3-4), 305-318.

Tansley, W., Schafer, P. A., and Hart, L. H., Montana Bureau of Mines and Geology, (1933). *A Geological Reconnaissance of the Tobacco Root Mountains, Madison County, Montana*. Montana School of Mines.

USDA-FSA Aerial Photography Field Office, Tobacco Root Mountains [air photo]. 1:10,000. Photo # 2533, 2534, 2535, 2633, 2634, and 2635. Montana Base Map Service Center, Helena, MT. 2009.

Vitaliano, C.J., and Cordua, W.S. (1979). Geologic map of southern Tobacco Root Mountains, Madison County, Montana*. Geological Society of America.*

Wahrhaftig, C., and Cox, A. (1959). Rock glaciers in the Alaska Range.*Geological Society of America Bulletin*, *70*(4), 383-436.

Ward, P. N., and Hall, R. D. (1982). Rock glaciers of the Tobacco Root Range, southwestem Montana. In *Geological Society of America Abstracts with Programs,* 14, 353).

White, S. E. (1971). Rock glacier studies in the Colorado Front Range, 1961 to 1968. *Arctic and Alpine Research*, 43-64.

Winchell, A. N. (1914). *Mining districts of the Dillon quadrangle, Montana, and adjacent areas*. US Government Printing Office.

Wold, S., Esbensen, K., and Geladi, P. (1987). Principal component analysis.*Chemometrics and intelligent laboratory systems*, *2*(1), 37-52.

Appendix R

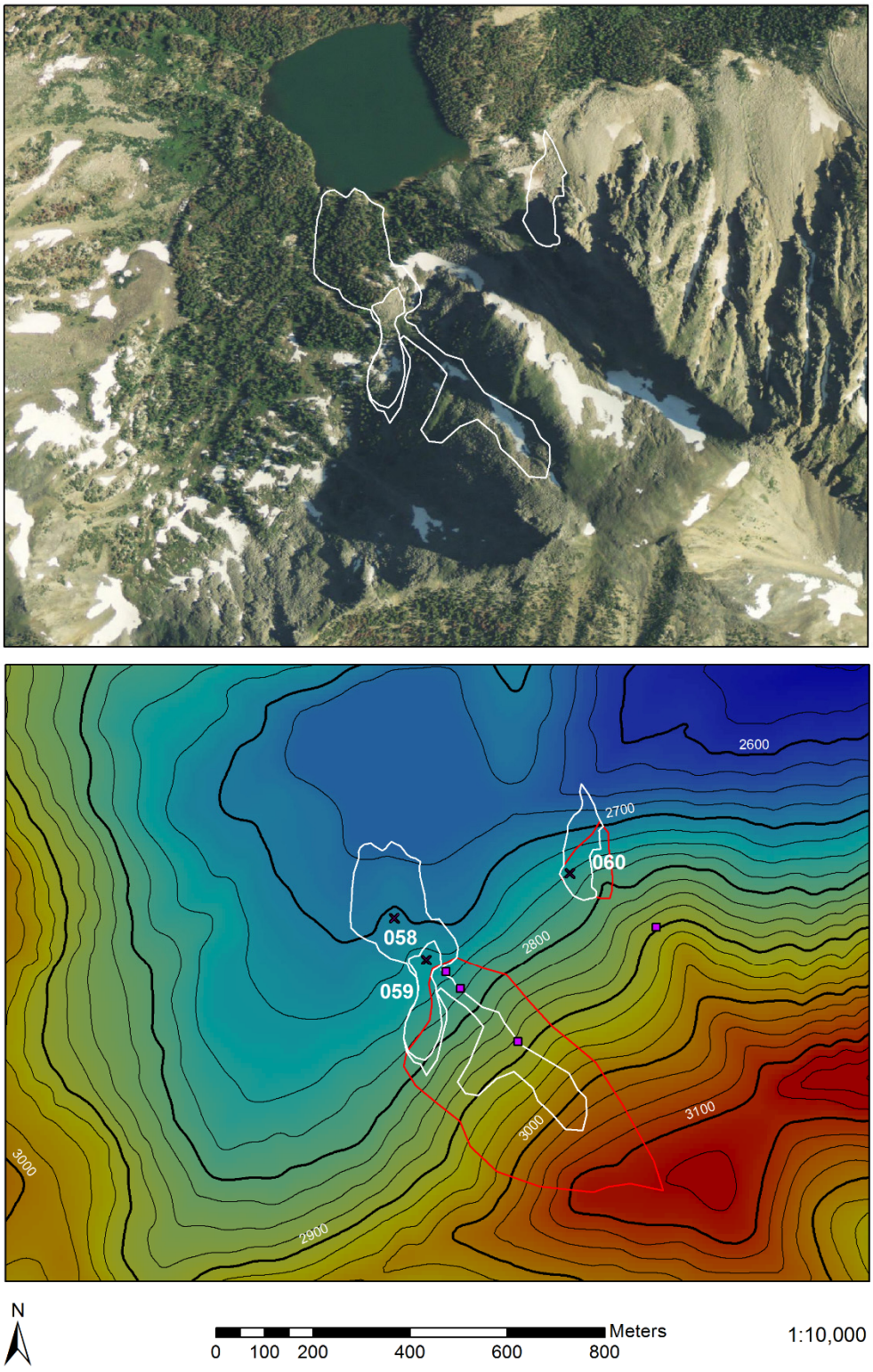

Figure R-1: Natural color 1 m aerial photograph from 2009 (top) and DEM with 25 m contours (bottom), showing deposit (white), rockshed (red), relative age sites (X), and headwall sites (square)

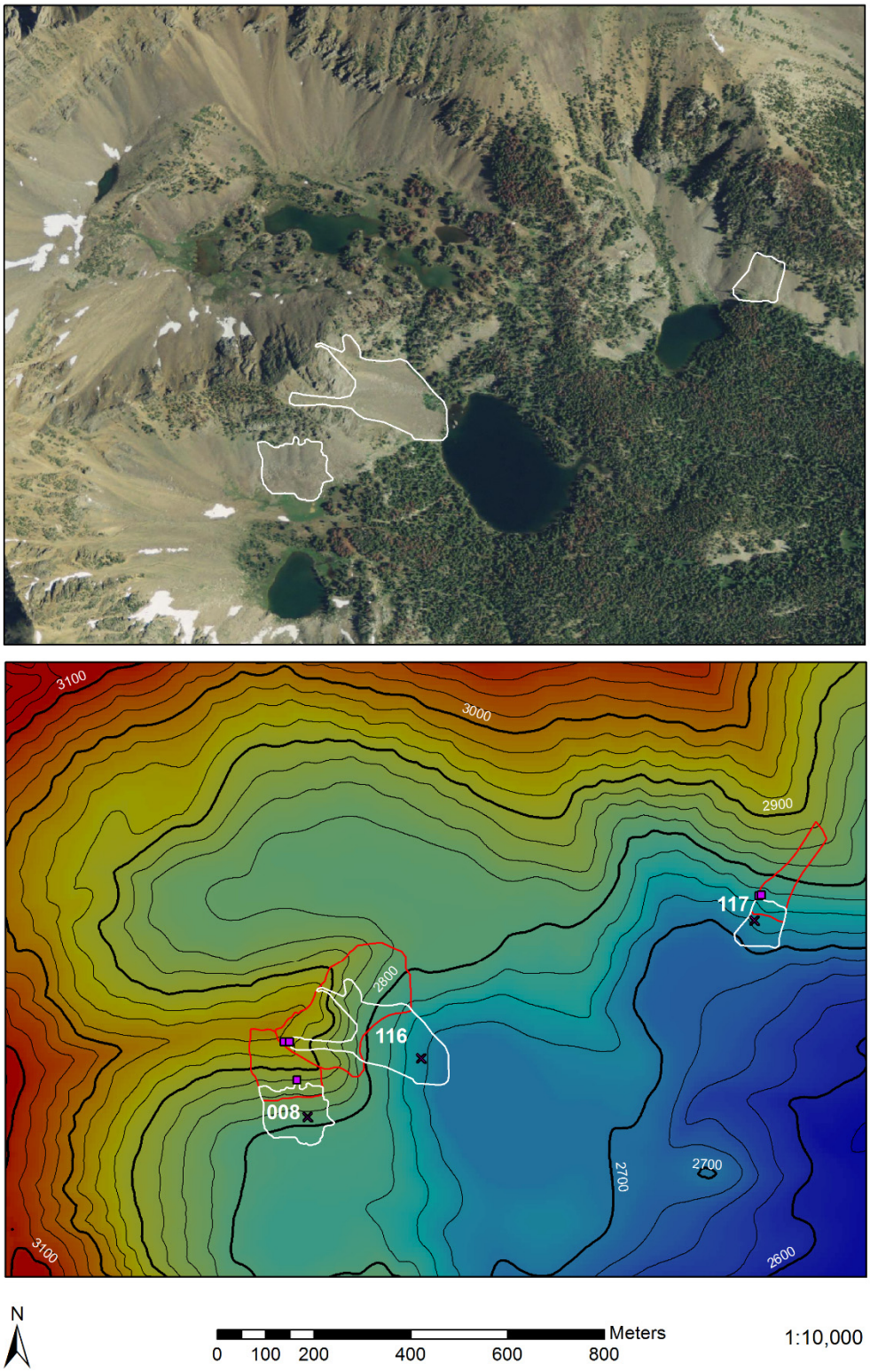

Figure R-2: Natural color 1 m aerial photograph from 2009 (top) and DEM with 25 m contours (bottom), showing deposit (white), rockshed (red), relative age sites (X), and headwall sites (square).

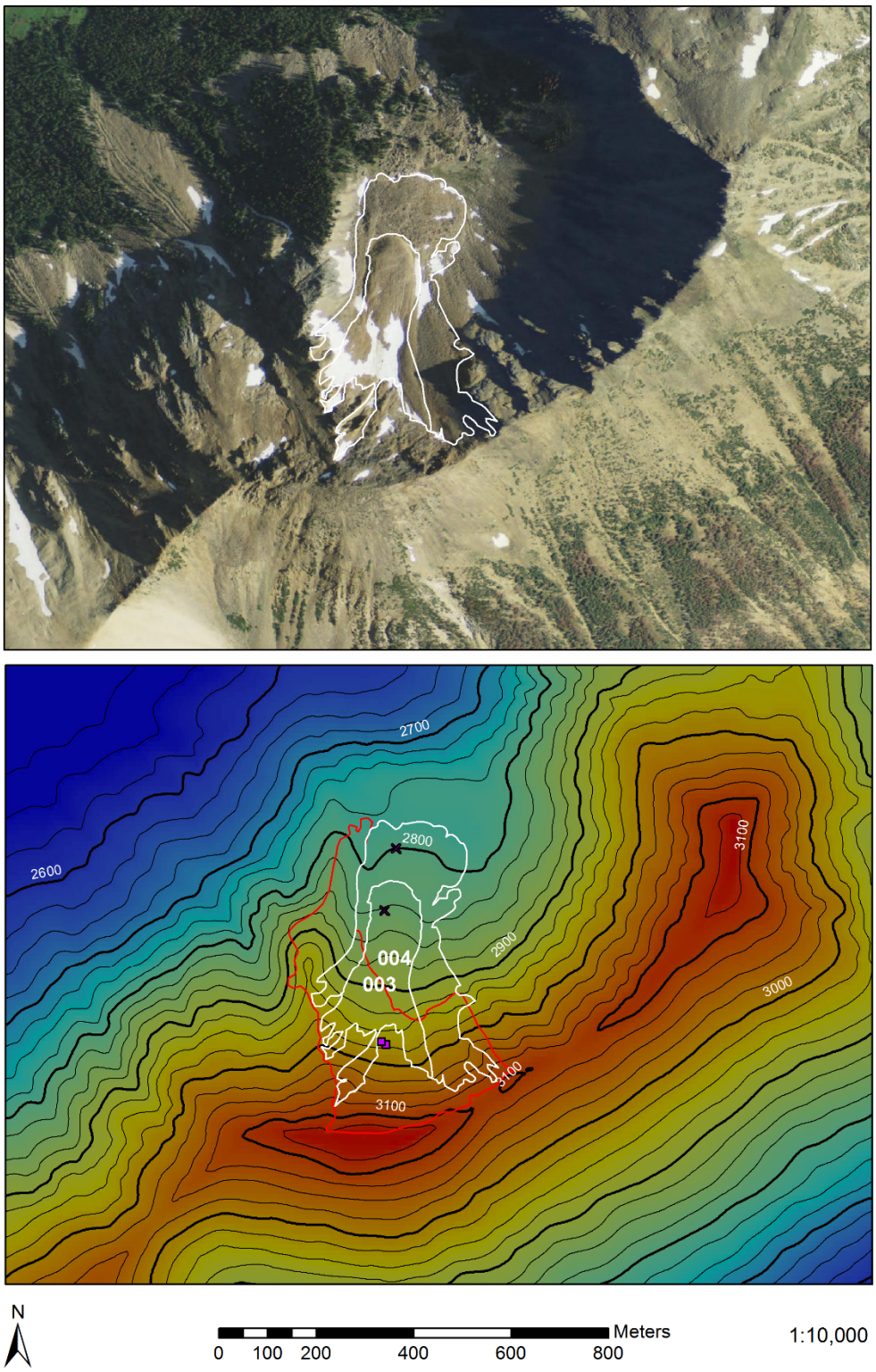

Figure R-3: Natural color 1 m aerial photograph from 2009 (top) and DEM with 25 m contours (bottom), showing deposit (white), rockshed (red), relative age sites (X), and headwall sites (square)

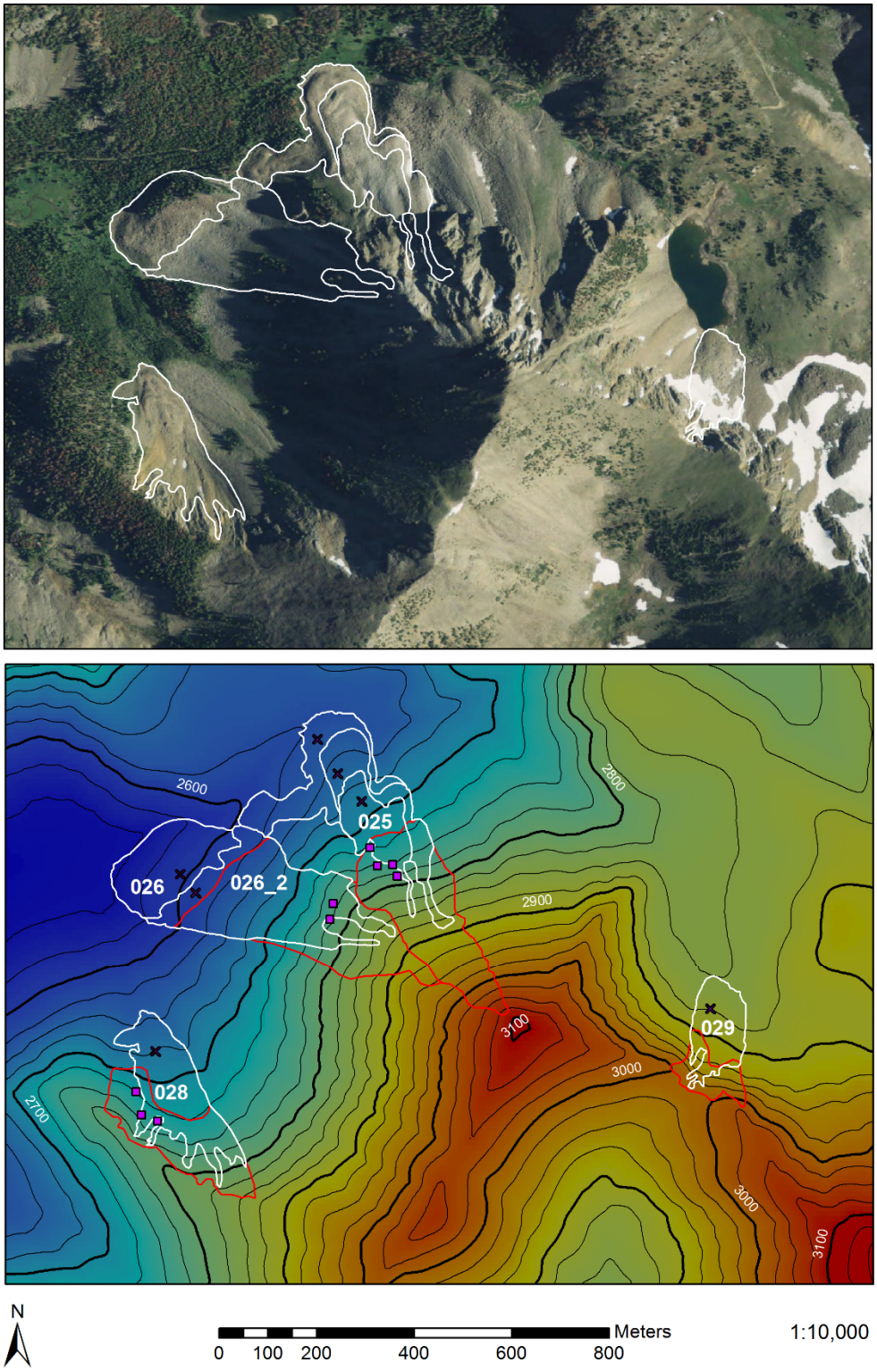

Figure R-4: Natural color 1 m aerial photograph from 2009 (top) and DEM with 25 m contours (bottom), showing deposit (white), rockshed (red), relative age sites (X), and headwall sites (square)

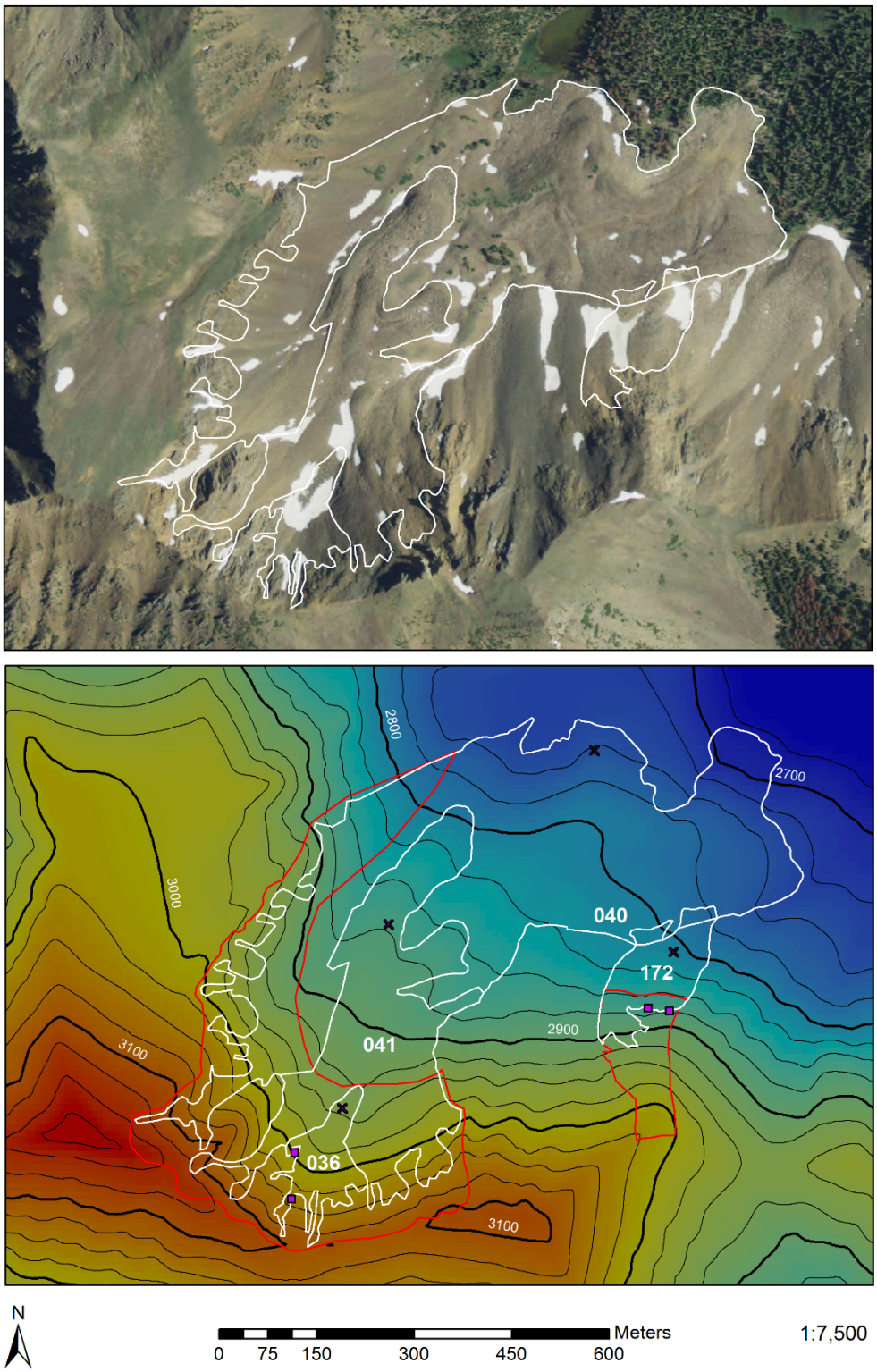

Figure R-5: Natural color 1 m aerial photograph from 2009 (top) and DEM with 25 m contours (bottom), showing deposit (white), rockshed (red), relative age sites (X), and headwall sites (square)

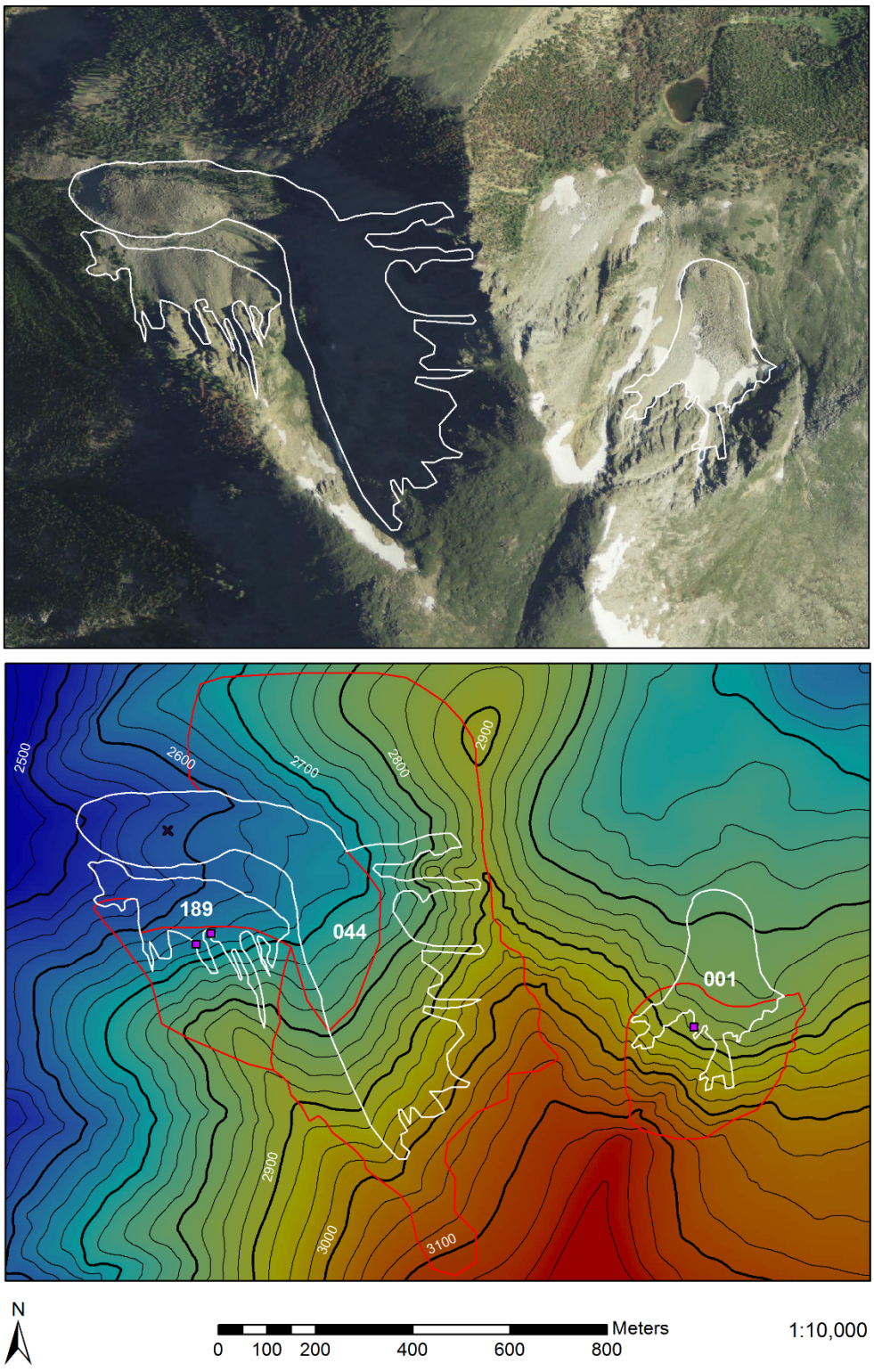

Figure R-6: Natural color 1 m aerial photograph from 2009 (top) and DEM with 25 m contours (bottom), showing deposit (white), rockshed (red), relative age sites (X), and headwall sites (square)

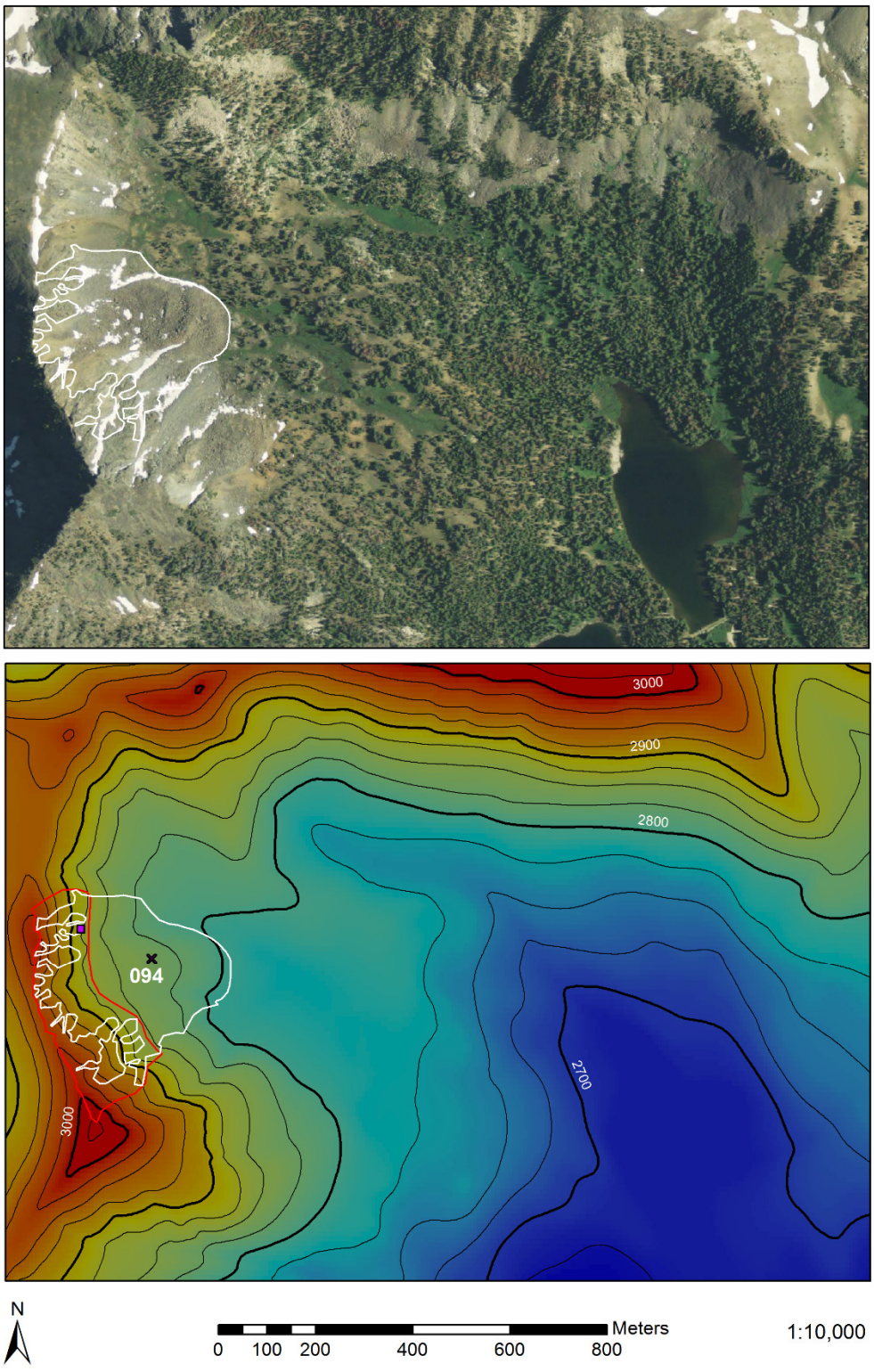

Figure R-7: Natural color 1 m aerial photograph from 2009 (top) and DEM with 25 m contours (bottom) showing deposit (white), rockshed (red), relative age sites (X), and headwall sites (square)

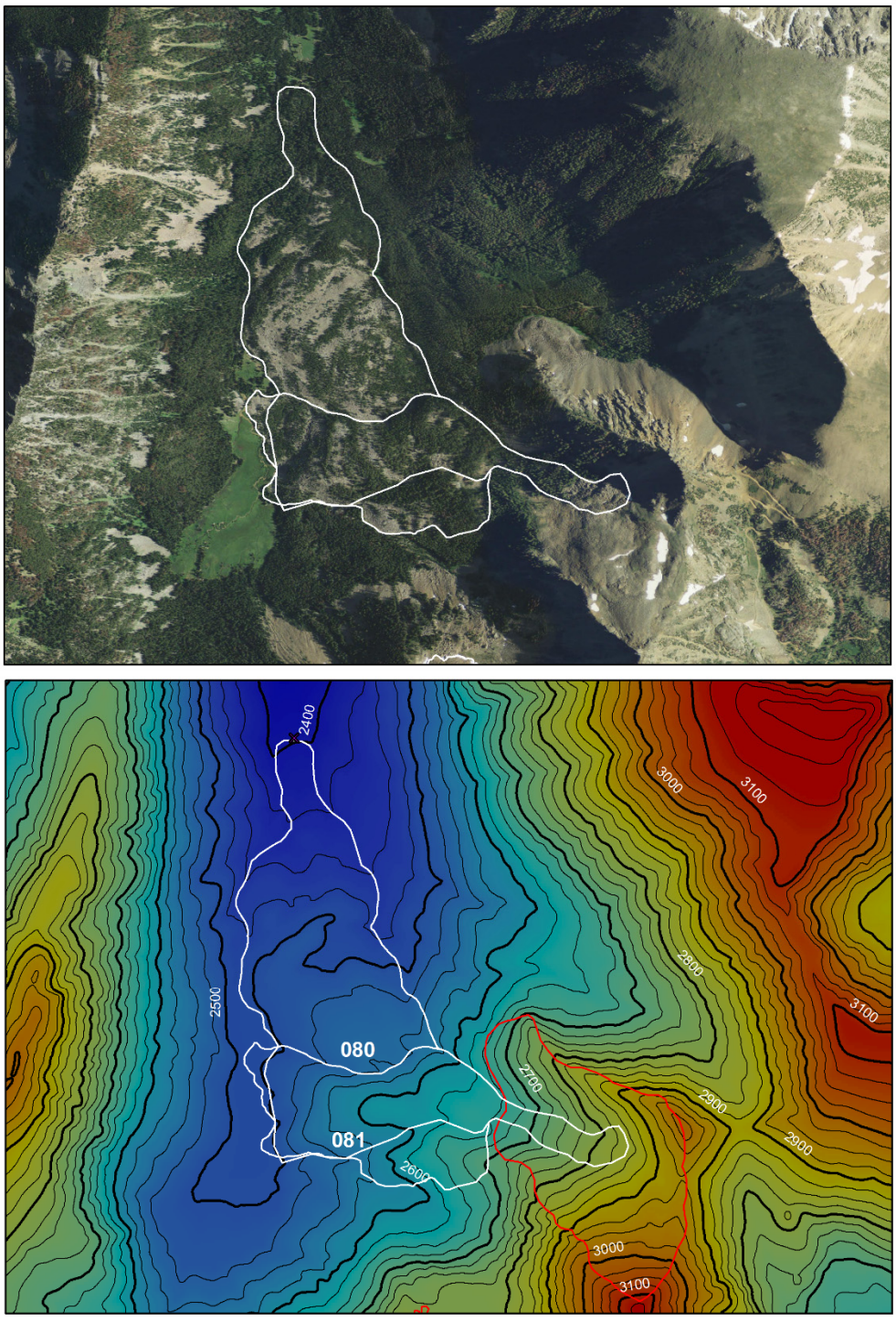

Figure R-8: Natural color 1 m aerial photograph from 2009 (top) and DEM with 25m contours (bottom) showing deposit (white), rockshed red), and relative age sites (X)

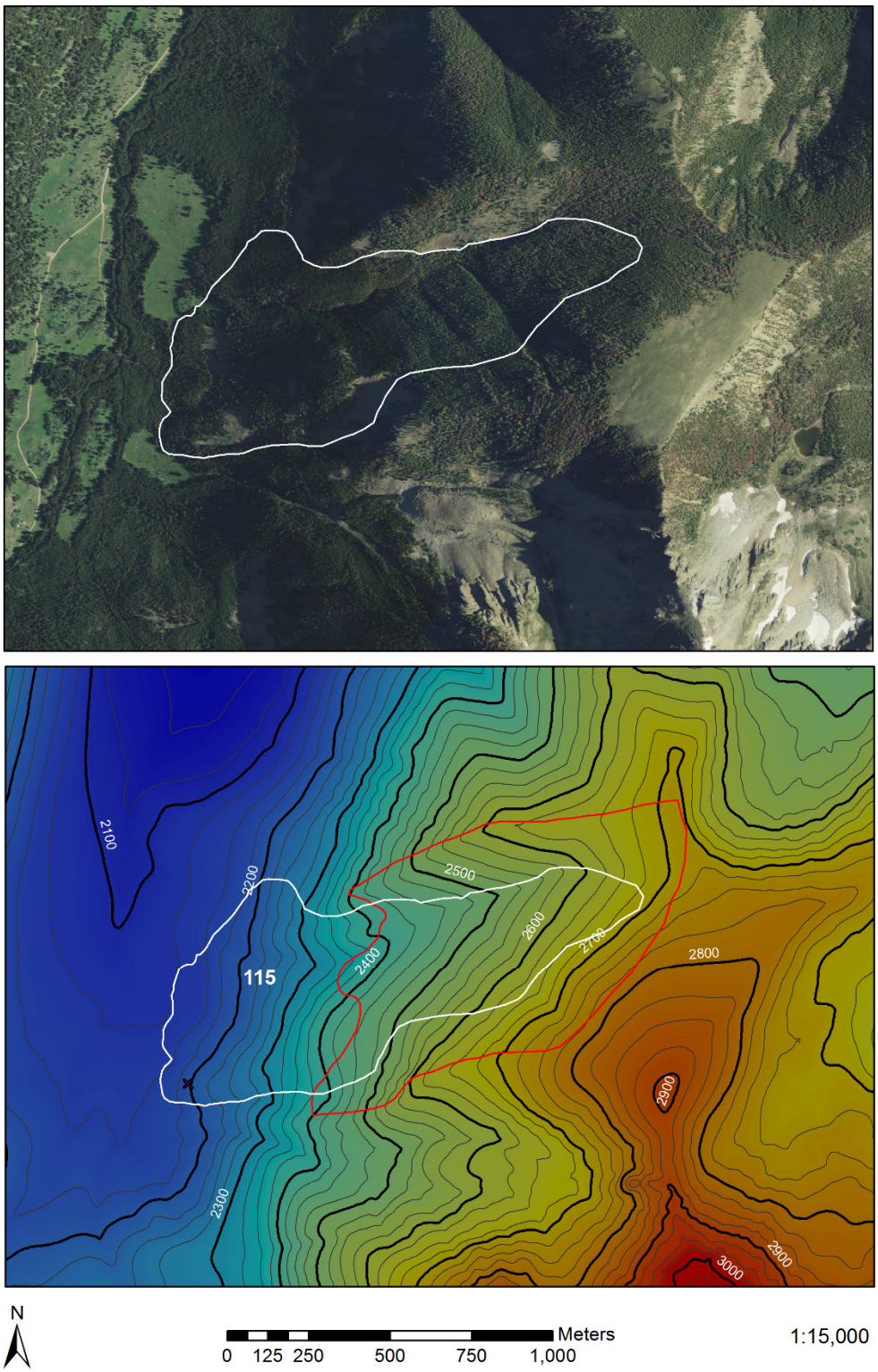

Figure R-9: Natural color 1 m aerial photograph from 2009 (top) and DEM with 25 m contours (bottom) showing deposit (white), rockshed (red), and relative age site (X)

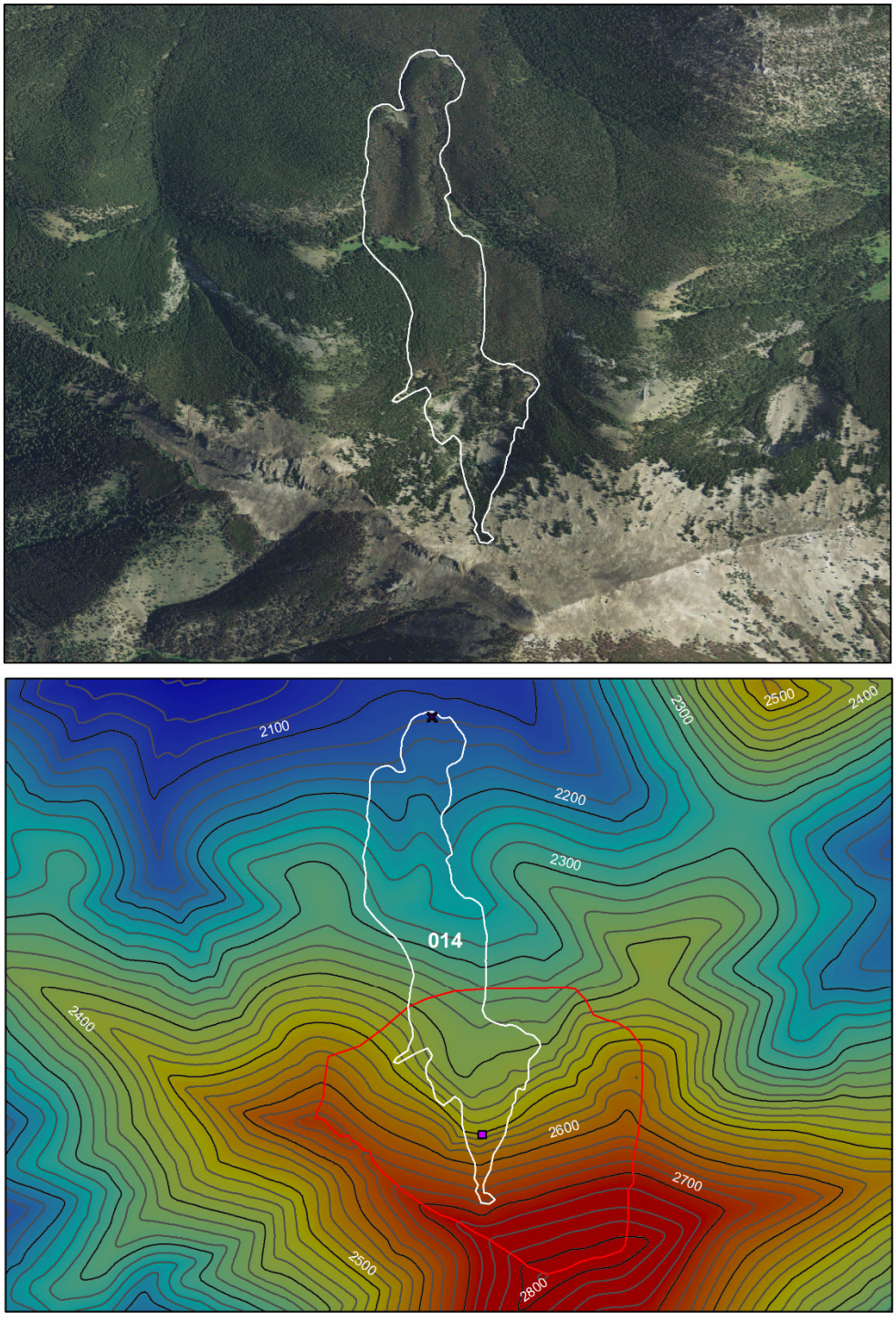

Figure R-10: Natural color 1 m aerial photograph from 2009 (top) and DEM with 25 m contours (bottom), showing deposit (white), rockshed (red), relative age site (X), and headwall site (square)

Appendix S

Figure S-1: Bell Lake

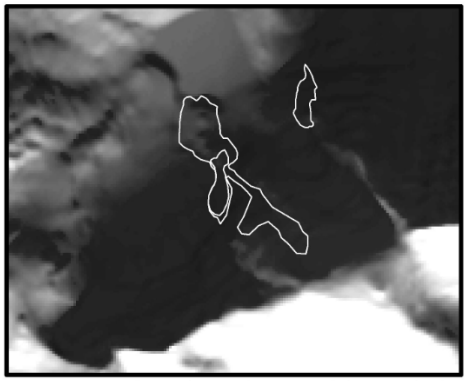

Figure S-1a: Winter Solstice Radiation Reduction (%) with deposits outlined

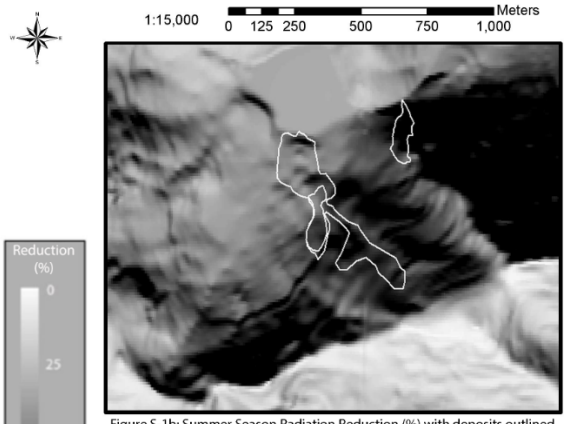

Figure S-1b: Summer Season Radiation Reduction (%) with deposits outlined

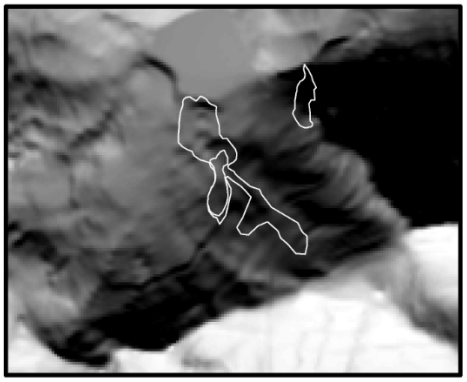

Figure S-1c: Vernal Equinox Radiation Reduction (%) with deposits outlined

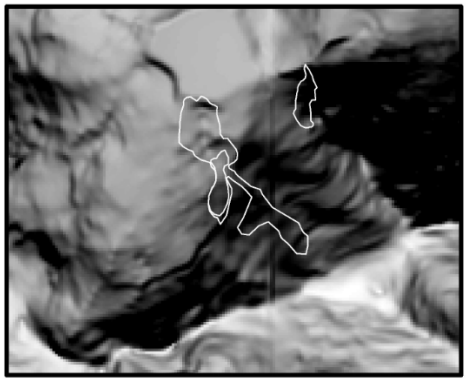

Figure S-1d: Summer Solstice Radiation Reduction (%) with deposits outlined

Figure S-2: Sailor Lake

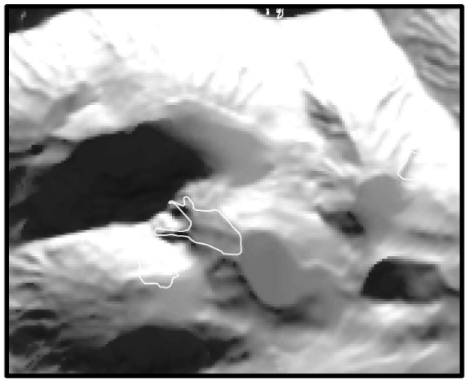

Figure S-2a: Winter Solstice Radiation Reduction (%) with deposits outlined

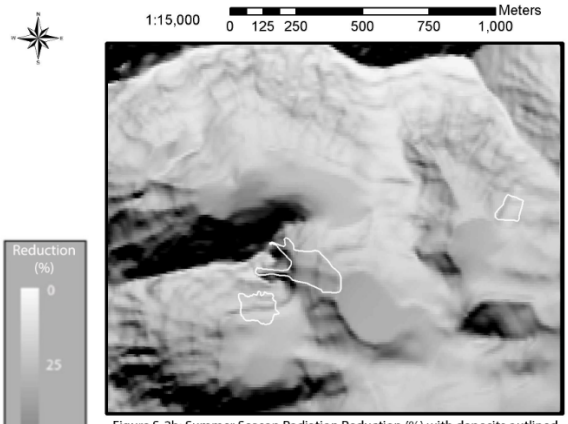

Figure S-2b: Summer Season Radiation Reduction (%) with deposits outlined

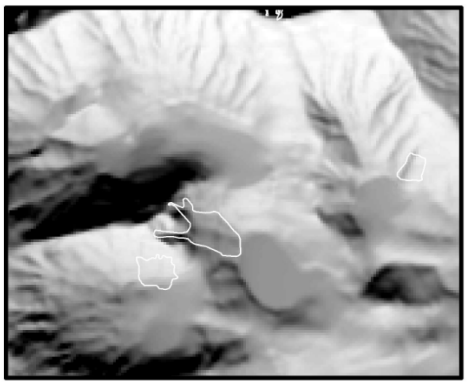

Figure S-2c: Vernal Equinox Radiation Reduction (%) with deposits outlined

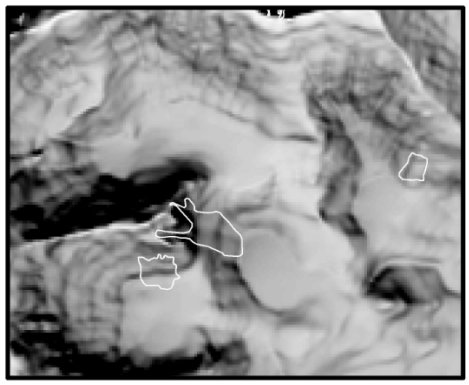

Figure S-2d: Summer Solstice Radiation Reduction (%) with deposits outlined

Figure S-3: Little Granite Peak

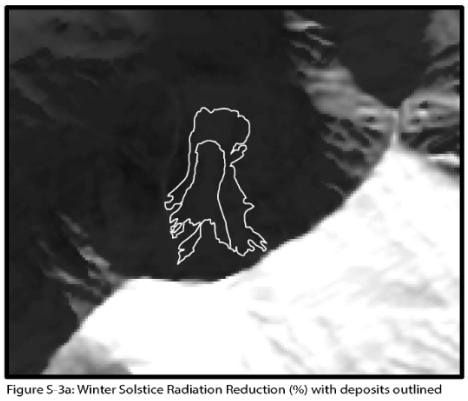

Figure S-3a: Winter Solstice Radiation Reduction (%) with deposits outlined

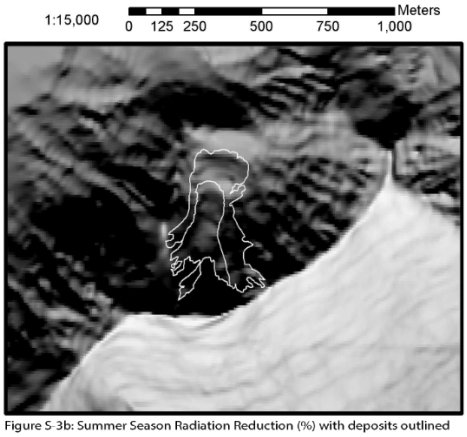

Figure S-3b: Summer Season Radiation Reduction (%) with deposits outlined

Figure S-3c: Vernal Equinox Radiation Reduction (%) with deposits outlined

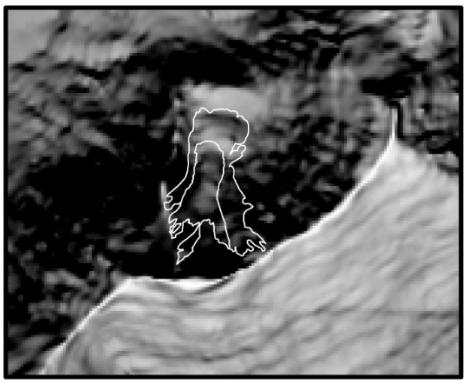

Figure S-3d: Summer Solstice Radiation Reduction (%) with deposits outlined

Figure S-4: Sunrise Peak

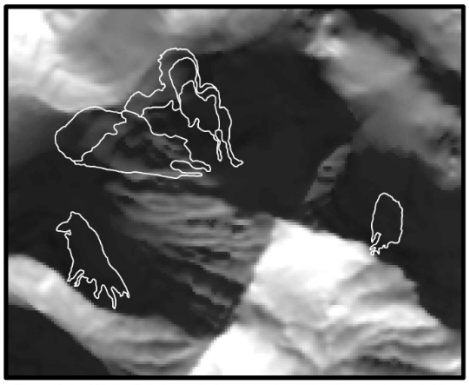

Figure S-4a: Winter Solstice Radiation Reduction (%) with deposits outlined

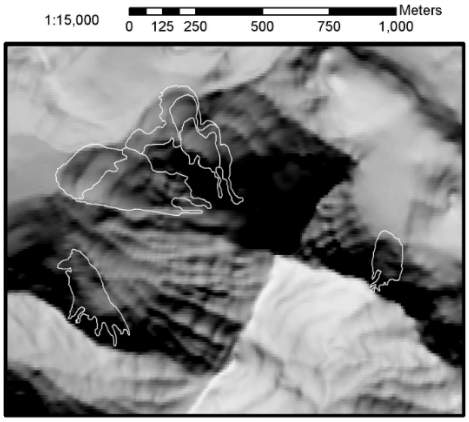

Figure S-4b: Summer Season Radiation Reduction (%) with deposits outlined

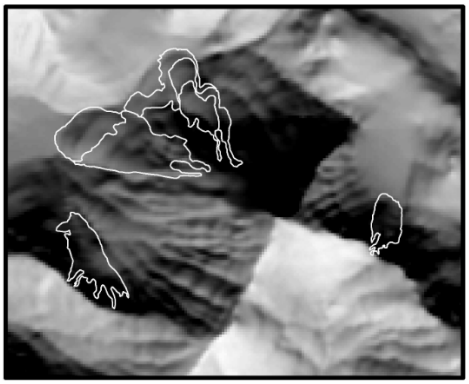

Figure S-4c: Vernal Equinox Radiation Reduction (%) with deposits outlined

Figure S-4d: Summer Solstice Radiation Reduction (%) with deposits outlined

Figure S-5: Curly Lake

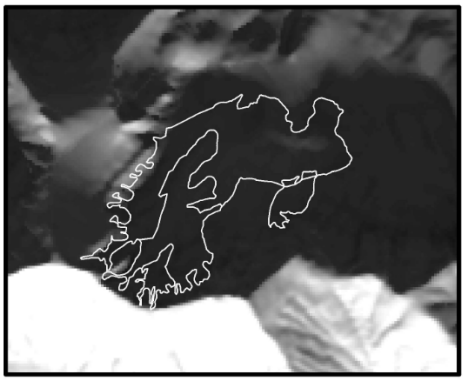

Figure S-5a: Winter Solstice Radiation Reduction (%) with deposits outlined

Figure S-5b: Summer Season Radiation Reduction (%) with deposits outlined

Figure S-5c: Vernal Equinox Radiation Reduction (%) with deposits outlined

Figure S-5d: Summer Solstice Radiation Reduction (%) with deposits outlined

Figure S-6: Hollowtop Mountain

Figure S-6a: Winter Solstice Radiation Reduction (%) with deposits outlined

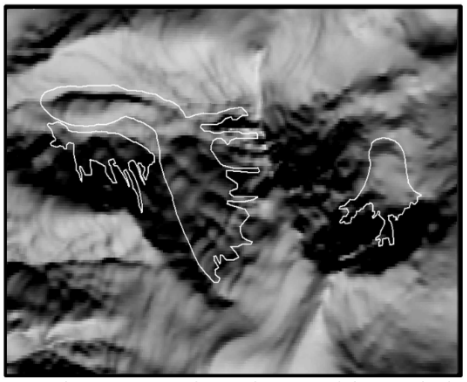

Figure S-6b: Summer Season Radiation Reduction (%) with deposits outlined

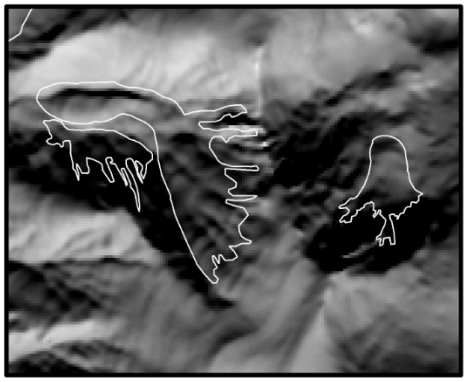

Figure S-6c: Vernal Equinox Radiation Reduction (%) with deposits outlined

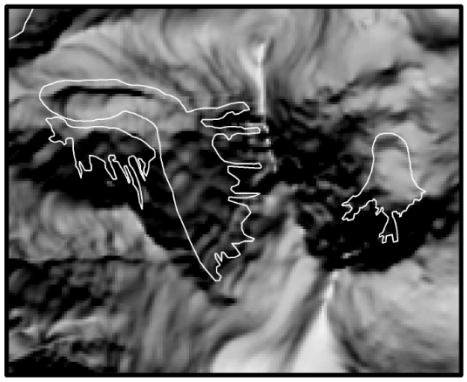

Figure S-6d: Summer Solstice Radiation Reduction (%) with deposits outlined

Figure S-7: Branham Lakes

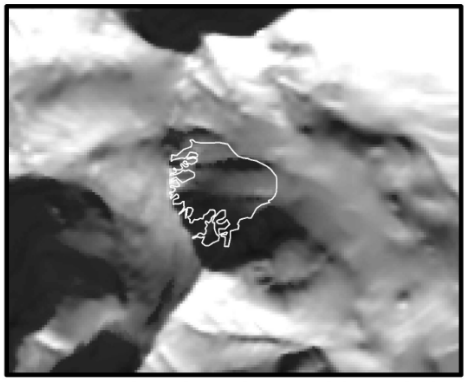

Figure S-7a: Winter Solstice Radiation Reduction (%) with deposit outlined

Figure S-7b: Summer Season Radiation Reduction (%) with deposit outlined

Figure S-7c: Vernal Equinox Radiation Reduction (%) with deposits outlined

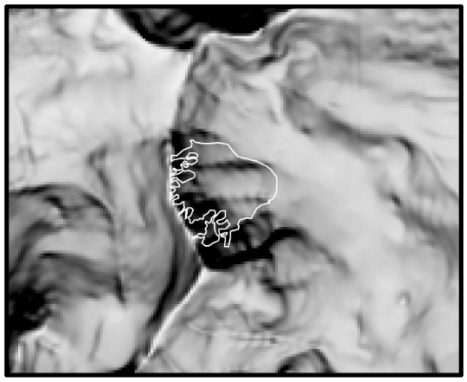

Figure S-7d: Summer Solstice Radiation Reduction (%) with deposits outlined

Figure S-8: Deposits 080 & 081

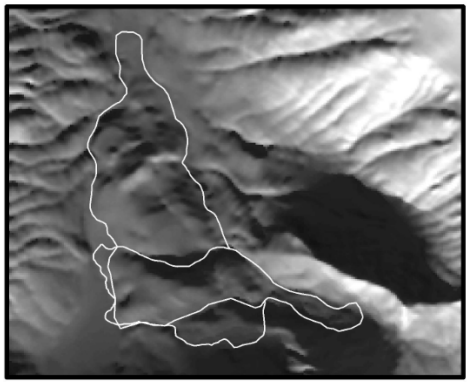

Figure S-8a: Winter Solstice Radiation Reduction (%) with deposits outlined

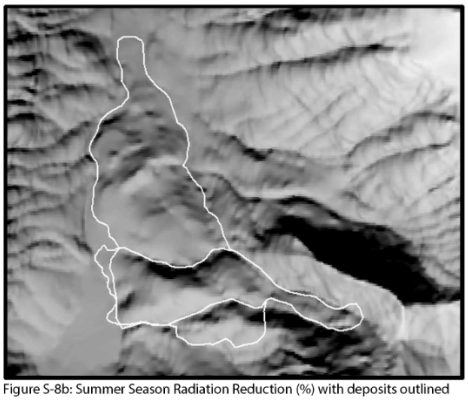

Figure S-8b: Summer Season Radiation Reduction (%) with deposits outlined

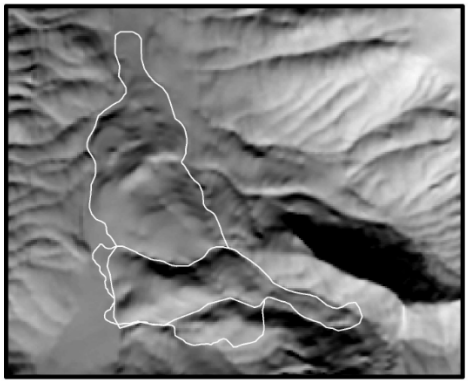

Figure S-8c: Vernal Equinox Radiation Reduction (%) with deposits outlined

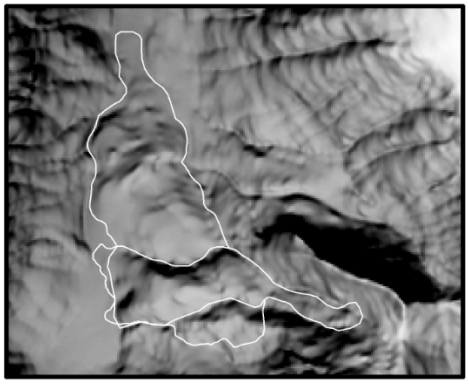

Figure S-8d: Summer Solstice Radiation Reduction (%) with deposits outlined

Figure S-9: Deposit 115

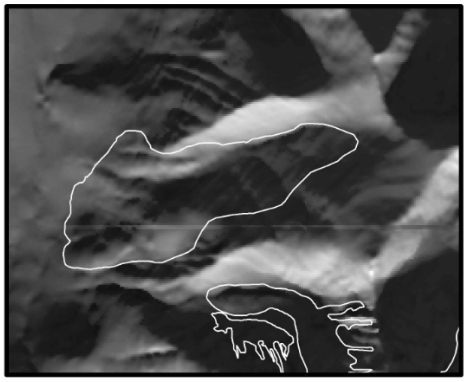

Figure S-9a: Winter Solstice Radiation Reduction (%) with deposits outlined

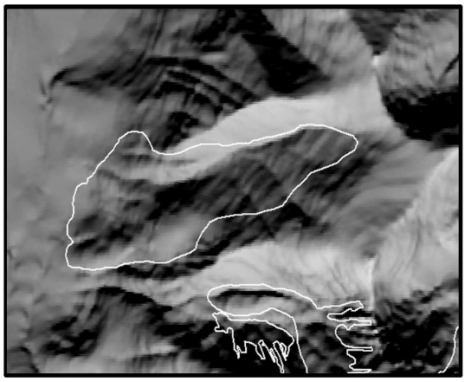

Figure S-9b: Summer Season Radiation Reduction (%) with deposits outlined

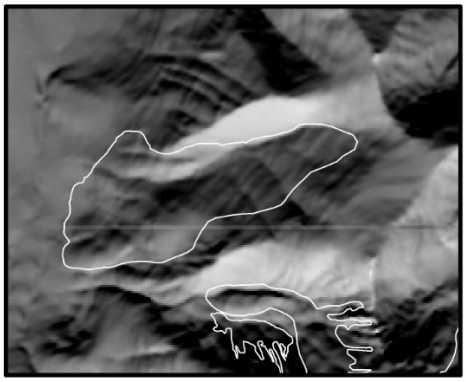

Figure S-9c: Vernal Equinox Radiation Reduction (%) with deposits outlined

Figure S-9d: Summer Solstice Radiation Reduction (%) with deposits outlined

Figure S-10: Brownback Mountain

Figure S-10a: Winter Solstice Radiation Reduction (%) with deposit outlined

Figure S-10b: Summer Season Radiation Reduction (%) with deposit outlined

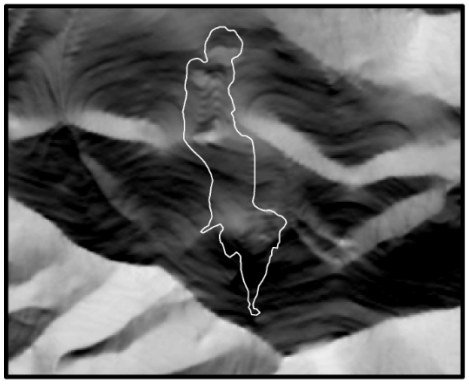

Figure S-10c: Vernal Equinox Radiation Reduction (%) with deposit outlined

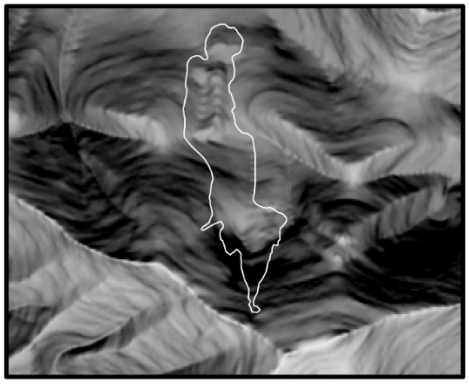

Figure S-10d: Summer Solstice Radiation Reduction (%) with deposit outlined

Appendix T

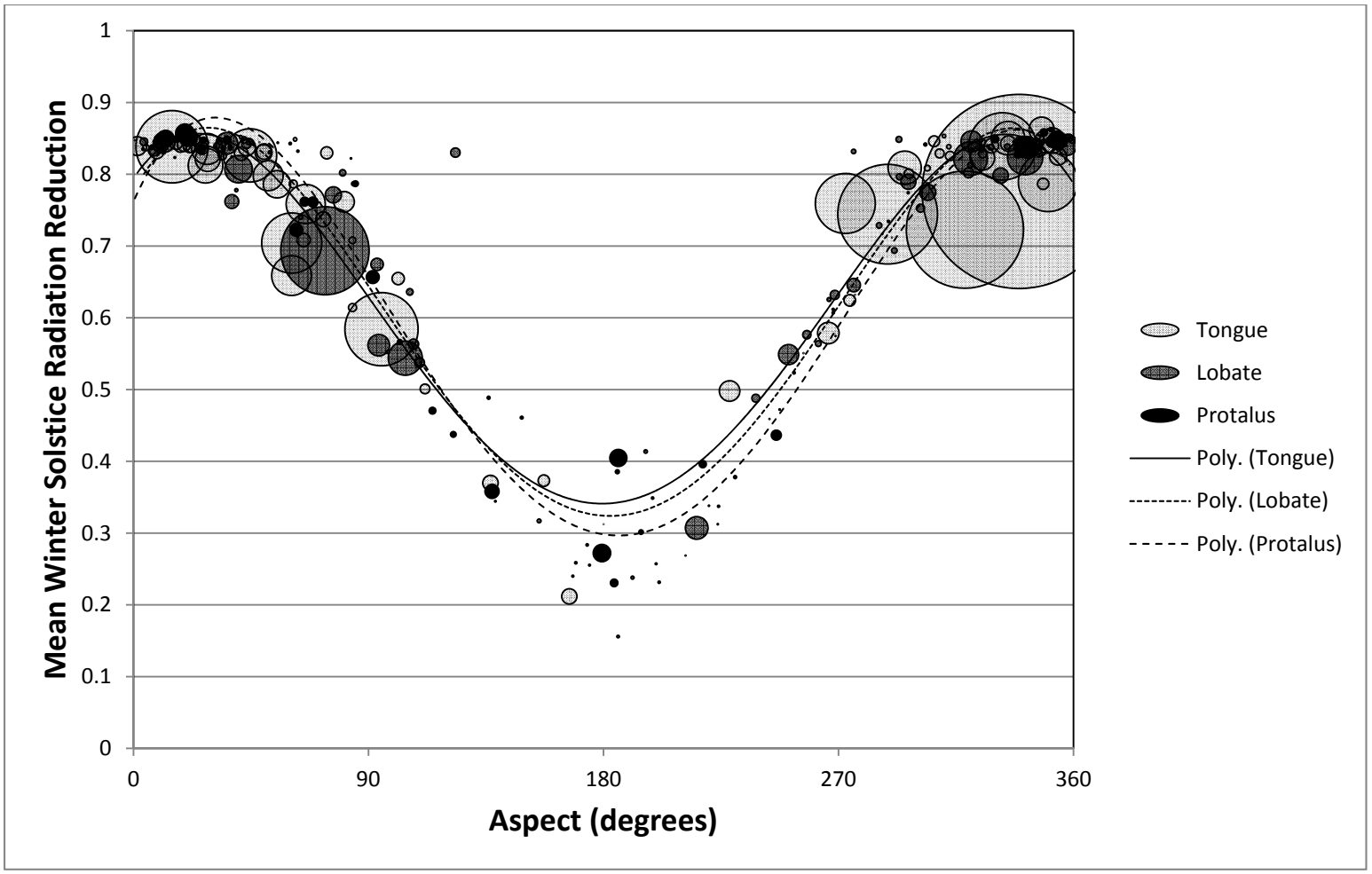

Figure T-1 – Average deposit aspect and winter solstice radiation reduction, divided by morphological class. The size of data points represents the relative area of the deposit.

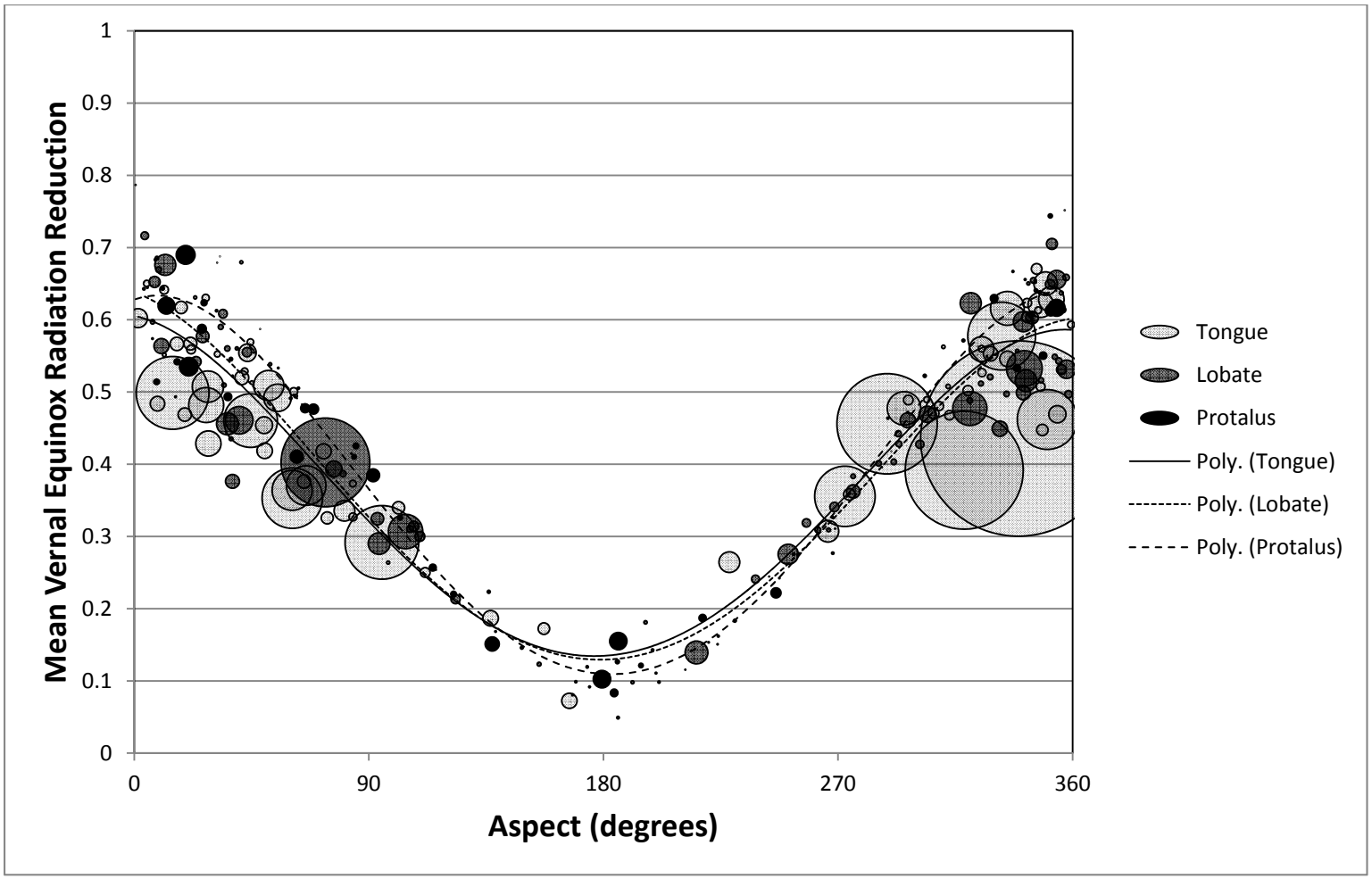

Figure T-2 – Average deposit aspect and vernal equinox radiation reduction, divided by morphological class. The size of data points represents the relative area of the deposit.

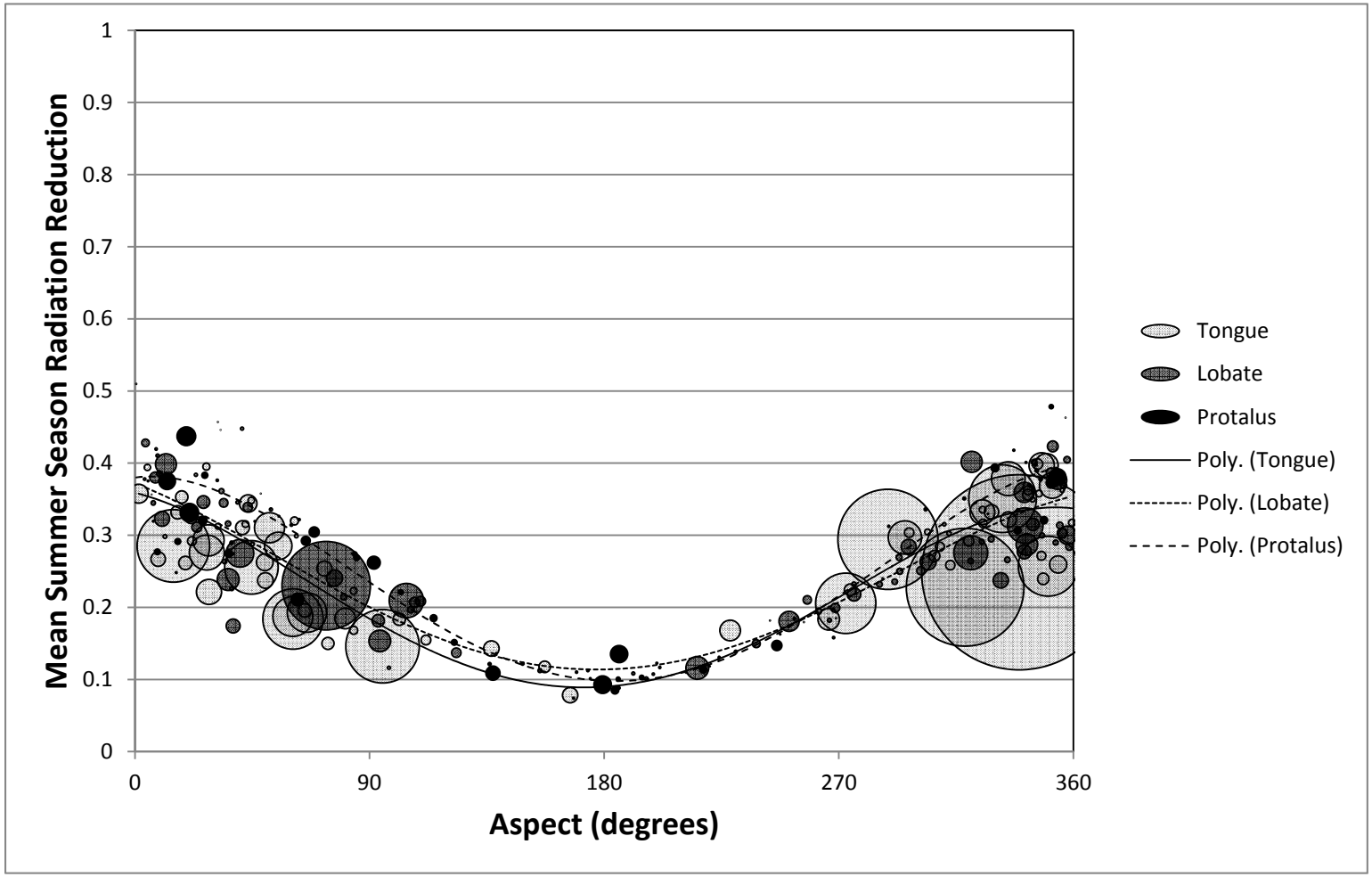

Figure T-3 – Average deposit aspect and summer season radiation reduction, divided by morphological class. The size of data points represents the relative area of the deposit.

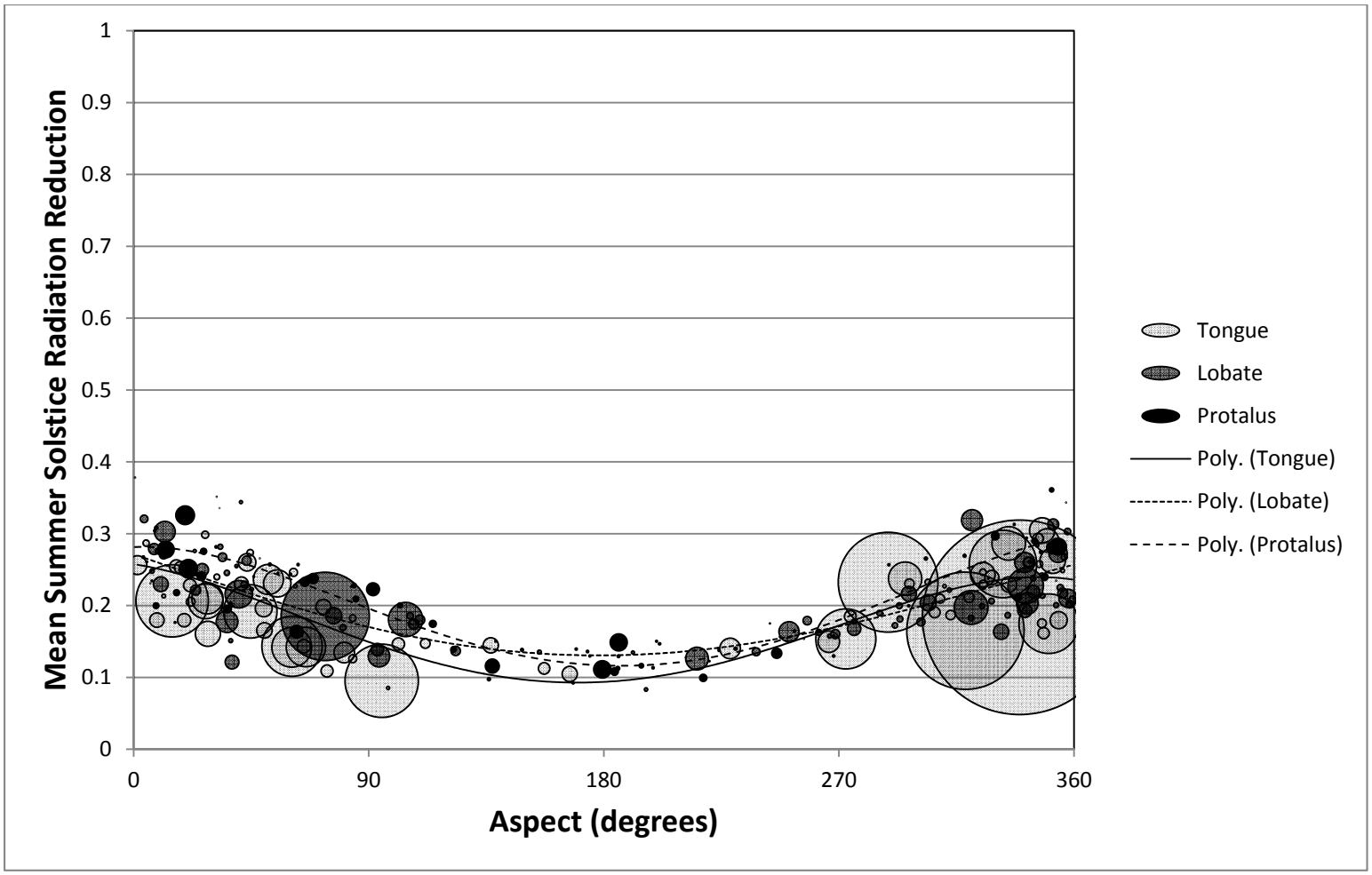

Figure T-4 – Average deposit aspect and summer solstice radiation reduction, divided by morphological class. The size of data points represents the relative area of the deposit.

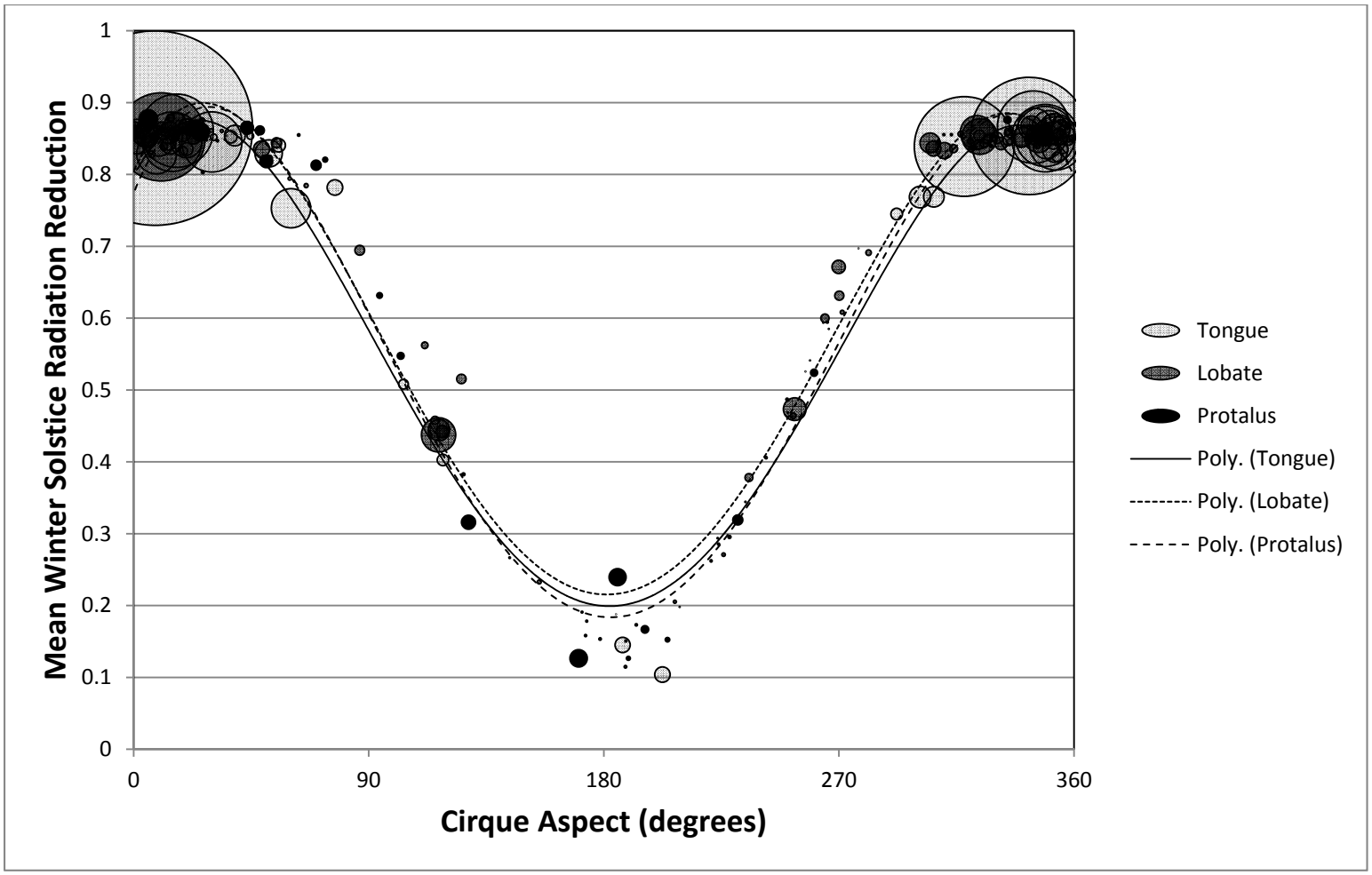

Figure T-5 – Average cirque aspect and winter solstice radiation reduction, divided by morphological class. The size of data points represents the relative area of the deposit.

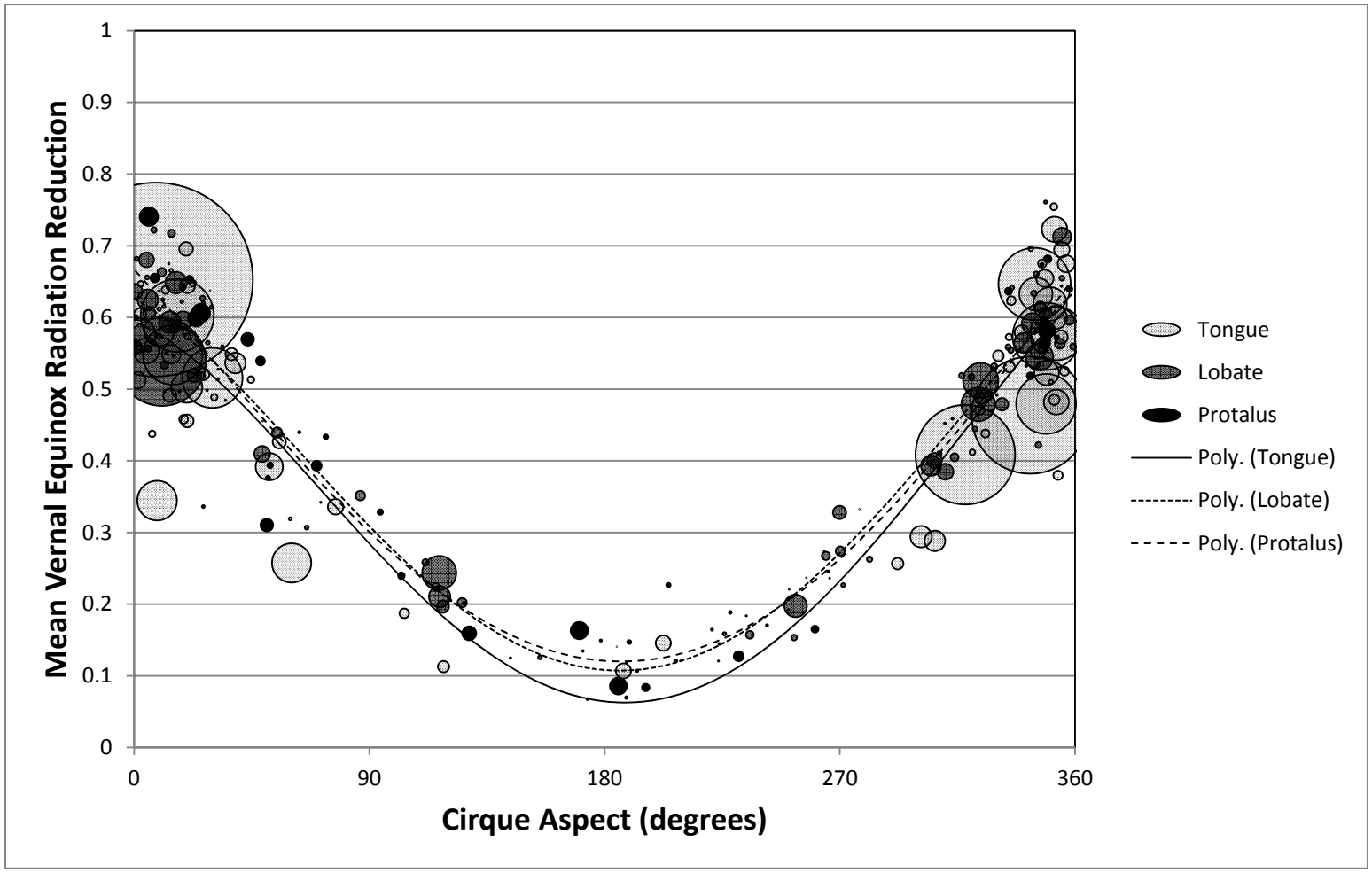

Figure T-6 – Average cirque aspect and vernal equinox radiation reduction, divided by morphological class. The size of data points represents the relative area of the deposit.

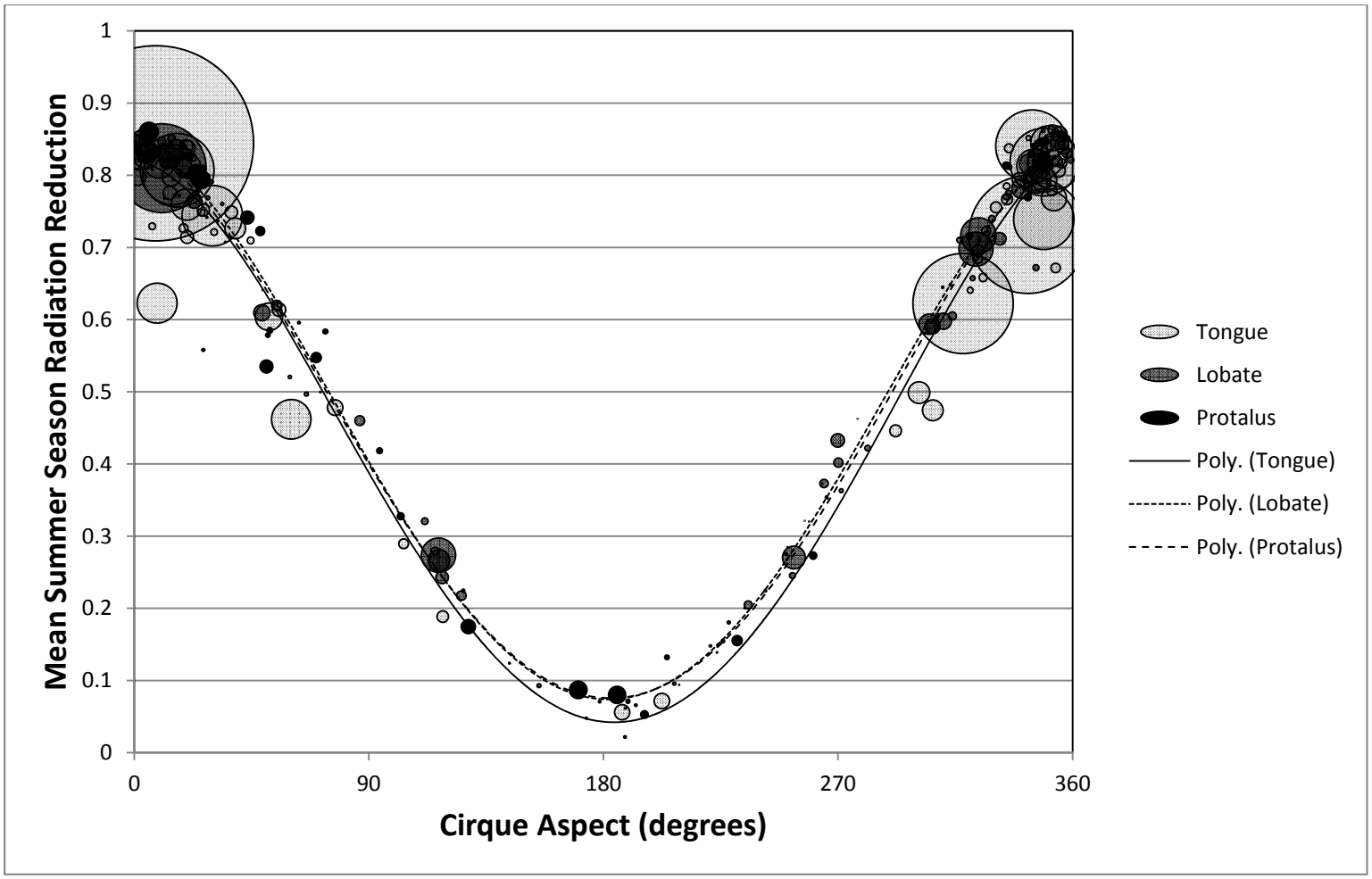

Figure T-7 – Average cirque aspect and summer season radiation reduction, divided by morphological class. The size of data points represents the relative area of the deposit.

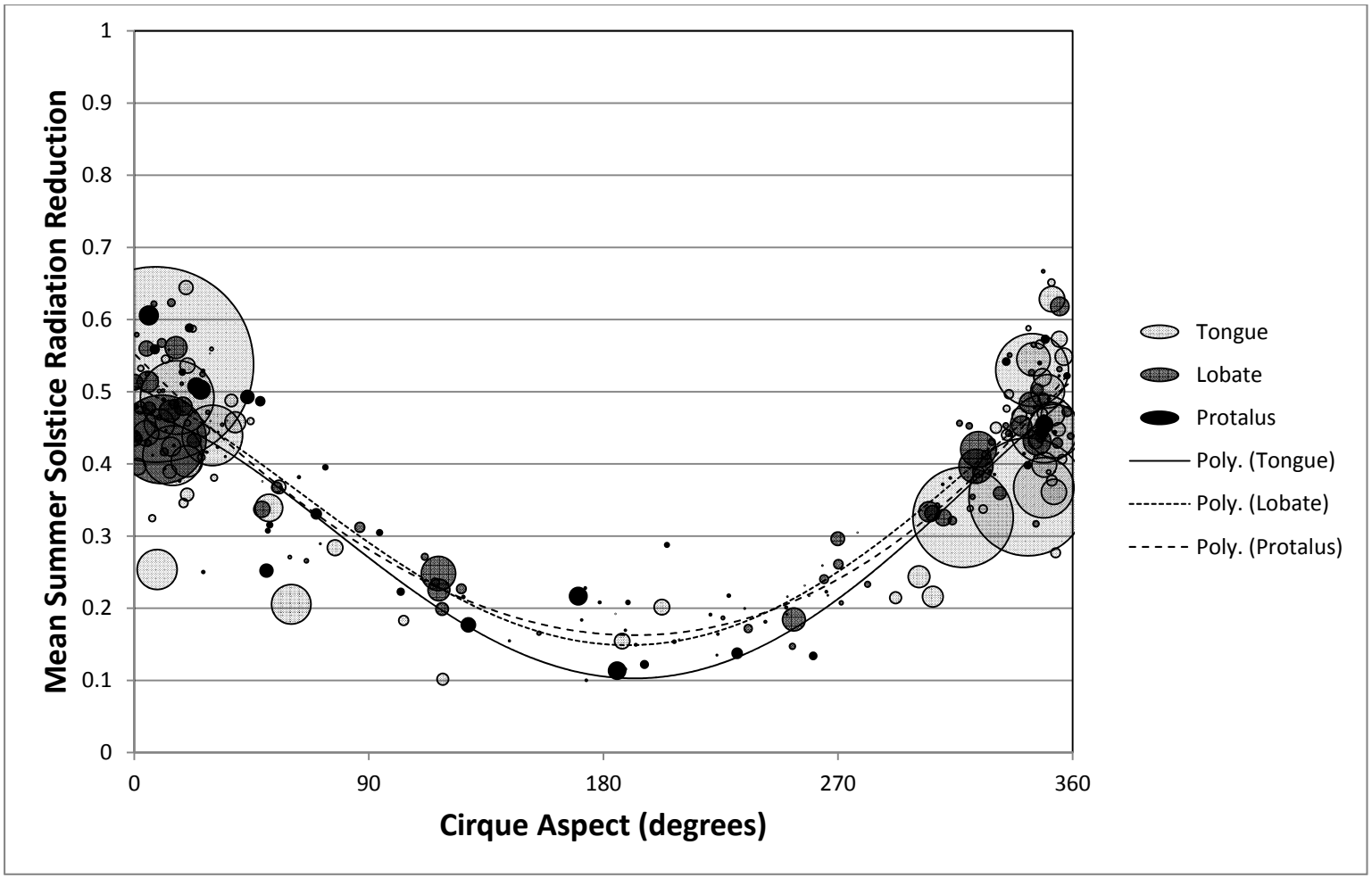

Figure T-8 – Average cirque aspect and summer solstice radiation reduction, divided by morphological class. The size of data points represents the relative area of the deposit.

Appendix U

Table U-1: Summary of priority data

Table U-2: Summary of all data

Table U-1: Summary of priority data with non-visited deposits shaded in the first column. Dep.=Deposit, Morph.=Morphology, MBR=Minimum Bounding Rectangle, Int.=Interpolated, Thick.=Thickness, FP=Footprint, Ele.=Elevation, HW=Headwall, Ht.=Height

Dep. #	Morph.	Dep. Slope (°)	Dep. Aspect (°)	Deposit Area (m^2)	FP Length (m)	FP Width (m)	MBR Length (m)	MBR Width (m)	SC Thick (m)	Int. Thick (m)	SC Volume (m^3)	Int. Volume (m^3)	Min. Dep. Ele. (m)	Max. HW Ele. (m)	HW Ht. (m)
1	T	14.8	21	53,104	236	94	382	262	11.4	14.4	253,918	320,019	2,777	3,128	299
2	T	21.1	11	50,779	155	103	438	218	8.5	19.2	136,297	308,262	2,644	2,950	212
4	T	21.2	0	112,655	275	138	572	357	16.4	34.2	619,884	1,295,626	2,778	3,143	364
6	P	26.2	19	111,394	201	226	329	588	6.7	40.1	306,786	1,825,474	2,266	2,716	340
8	L	36.5	173	14,048	79	63	135	145	9.5	20.6	47,769	103,966	2,791	2,963	107
9	T	13.0	11	209,774	305	234	663	591	17.8	12.6	1,267,169	900,262	2,731	3,089	306
14	T	15.6	15	435,586	704	163	1,730	514	16.7	32.7	1,910,628	3,738,284	2,117	2,825	493
16	T	18.5	342	152,944	262	211	676	380	19.2	18.8	1,060,960	1,041,948	2,551	2,930	284
18	T	15.9	344	93,343	372	139	635	302	27.4	41.1	1,422,015	2,128,363	2,658	2,947	183
25	T	21.5	339	60,494	288	115	489	310	10.6	21.2	353,778	704,144	2,604	3,084	360
26	L	20.9	339	90,223	165	193	230	592	10.4	16.3	330,163	516,870	2,549	2,954	268
28	T	20.6	339	36,030	209	78	393	180	7.5	16.6	123,334	271,987	2,646	2,860	161
29	T	27.8	24	18,255	117	92	232	115	7.3	15.5	78,102	165,846	2,850	3,021	106
32	T	25.1	335	56,095	158	137	419	212	10.4	34.0	224,808	731,989	2,917	3,116	56
40	T	21.8	40	321,036	688	188	1,123	545	33.0	48.7	4,262,348	6,287,435	2,680	3,163	404
44	T	28.3	332	200,634	591	108	985	546	23.2	32.7	1,476,877	2,080,125	2,496	3,118	525
48	T	17.9	60	164,311	352	186	766	409	34.5	13.7	2,267,412	900,439	2,622	3,055	292
57	T	28.4	15	73,615	126	115	419	330	7.0	9.7	101,826	140,525	2,816	3,090	169
58	T	20.1	340	67,995	258	129	741	249	11.4	10.0	379,956	331,426	2,670	3,124	387
60	P	18.2	342	11,709	52	84	79	237	5.4	8.3	23,771	36,452	2,644	2,810	101
61	T	20.0	340	14,005	123	56	200	133	5.5	6.3	37,329	43,002	2,790	2,975	132
62	T	14.0	346	86,338	193	176	455	364	10.9	20.5	370,949	697,457	2,713	3,029	233
66	L	30.8	329	108,904	117	584	323	458	20.5	15.3	1,397,134	1,042,043	2,563	2,973	359
72	T	16.7	46	100,622	284	164	586	267	11.5	15.1	535,798	701,102	2,766	3,086	217
80	T	17.5	342	706,876	1,047	524	1,889	997	36.1	33.0	19,789,661	18,124,509	2,398	3,113	472
86	T	24.8	335	56,742	191	127	450	186	8.6	16.1	207,591	391,292	2,767	3,077	228
89	L	30.1	330	91,705	181	431	264	500	14.2	7.9	1,110,559	618,367	2,647	2,913	269
94	T	30.9	72	89,968	233	132	393	391	14.8	40.1	454,991	1,230,481	2,791	3,020	160
114	T	26.9	333	202,329	274	241	706	437	9.6	15.7	636,374	1,037,669	2,329	2,786	344
115	T	27.8	332	600,955	533	479	1,533	676	43.1	51.0	11,007,784	13,021,639	2,125	2,788	407
116	P	35.3	99	28,894	167	101	169	334	10.7	19.1	180,550	322,623	2,702	2,959	185
117	L	24.8	335	13,808	83	111	97	178	6.3	9.5	58,172	88,633	2,673	2,876	124
172	P	15.9	15	20,493	91	111	128	265	10.1	13.6	101,509	136,784	2,775	3,026	164
189	P	23.5	337	45,784	103	247	231	475	6.4	12.5	163,324	317,752	2,521	2,871	309

Table U-2: Results from the analysis of all identified deposits. Morph=Morphology, MBR=Minimum Bounding Rectangle, Int.=Interpolated, Thick.=Thickness, FP=Footprint, Dep.=Deposit, WS=Winter Solstice, RR=Radiation Reduction. Deposit UTM coordinates are in NAD83 Z12.

Deposit Name	Morph.	Dep. Slope (°)	Dep. Aspect (°)	Deposit Area (m^2)	MBR Length (m)	MBR Width (m)	Int. Thick. (m)	FP Area (m^2)	Int. Volume (m^3)	Min. Dep. Elevation (m)	Deposit WS RR (%)	Deposit UTM (X)	Deposit UTM (Y)
001	T	23.0	22	53,104	382	262	14.4	24,860	358,177	2,777	0.837	421482	5052197
002	T	28.1	11	50,779	438	218	19.2	23,884	459,619	2,644	0.848	415393	5049076
002b	L	27.8	343	18,966	107	343	12.8	10,349	132,818	2,704	0.845	415524	5049007
004	T	27.7	1	112,655	572	357	34.2	46,324	1,585,450	2,778	0.839	420120	5048042
005	L	20.2	348	30,615	142	322	11.4	12,609	143,179	2,609	0.844	420501	5049426
005a	L	24.9	339	19,159	106	405	8.8	11,866	103,978	2,666	0.850	420831	5049322
006	P	32.8	20	111,394	329	588	40.1	44,146	1,769,762	2,267	0.857	419079	5051744
007	T	32.0	43	104,204	584	345	11.2	45,672	513,578	2,734	0.838	418027	5049099
007a	P	35.9	84	25,780	103	349	8.8	10,203	89,831	2,748	0.787	417993	5049293
008	L	33.1	174	14,048	135	145	20.6	6,015	124,101	2,792	0.284	414096	5050470
009	T	23.7	28	209,774	663	591	12.6	81,682	1,033,174	2,730	0.812	422633	5049156
010	L	19.7	16	10,442	85	162	4.5	4,442	19,942	2,786	0.823	422336	5049628
011	L	20.7	64	24,339	163	196	7.6	9,232	70,072	2,716	0.740	422564	5049532
012	T	11.3	74	72,266	363	260	7.6	23,604	179,085	2,830	0.830	421770	5049738
013	T	18.3	61	362,443	915	601	39.1	109,617	4,287,585	2,681	0.704	422194	5049963
014	T	20.1	15	435,586	1,730	514	32.7	166,542	5,437,607	2,116	0.838	418198	5064067
014a	T	15.4	339	1,171,393	2,668	929	48.6	406,481	19,748,663	1,945	0.776	418062	5064629
015	T	23.4	45	21,033	209	147	6.4	8,894	57,332	2,639	0.843	416506	5057977
016	T	27.6	352	152,944	676	380	18.8	56,517	1,064,847	2,550	0.847	416996	5057802
017	L	25.4	342	213,586	550	723	27.5	82,623	2,270,049	2,545	0.824	415980	5052523
018	T	24.2	335	93,343	635	302	41.1	43,812	1,798,625	2,659	0.843	415620	5051894

Deposit Name	Morph.	Dep. Slope (°)	Dep. Aspect (°)	Deposit Area (m^2)	MBR Length (m)	MBR Width (m)	Int. Thick. (m)	FP Area (m^2)	Int. Volume (m^3)	Min. Dep. Elevation (m)	Deposit WS RR (%)	Deposit UTM (X)	Deposit UTM (Y)
019	L	29.1	26	75,216	283	485	31.6	32,702	1,032,131	2,712	0.836	415302	5051772
020	T	18.1	354	102,773	430	319	22.0	32,779	721,073	2,636	0.825	416530	5047736
021	T	16.9	81	123,567	592	358	13.3	47,723	633,889	2,634	0.762	416155	5047978
022	T	19.4	307	65,541	535	205	16.1	26,973	433,048	2,766	0.846	417167	5046810
023	L	24.1	9	33,289	182	301	9.4	14,747	139,093	2,792	0.848	417066	5046586
024	T	22.6	310	20,733	236	130	11.0	8,880	97,541	2,754	0.853	415142	5048745
025	T	23.0	320	60,494	489	310	21.2	35,648	754,193	2,599	0.802	414331	5047791
026	L	27.1	297	90,223	230	592	16.3	32,546	528,905	2,549	0.790	414088	5047613
028	T	26.0	356	36,030	393	180	16.6	18,390	304,964	2,642	0.849	413969	5047190
029	T	28.5	23	18,255	232	115	15.5	7,853	121,558	2,850	0.842	415079	5047323
030	T	24.4	344	28,823	286	143	10.5	11,420	119,859	2,745	0.844	412869	5049876
031	L	24.8	344	74,838	244	403	17.0	24,483	416,379	2,760	0.837	413465	5051805
032	T	25.7	313	56,095	419	212	34.0	22,448	762,331	2,918	0.825	415634	5047209
033	L	30.8	266	22,904	153	313	25.5	13,096	333,312	2,915	0.625	415672	5047429
034	T	28.2	348	151,959	614	376	22.8	51,457	1,174,240	2,242	0.862	418336	5054133
035	P	15.3	136	17,713	128	228	11.4	8,494	97,242	2,538	0.489	415909	5050767
038	L	31.7	345	33,723	171	367	31.9	16,606	529,818	2,859	0.838	414698	5051639
039	L	38.0	357	4,028	51	142	13.4	2,543	33,948	2,869	0.839	414798	5051717
040	T	23.8	45	321,036	1,123	545	48.7	120,373	5,863,501	2,682	0.826	414795	5051902
042	P	34.2	115	40,380	201	362	32.2	18,840	606,223	2,682	0.471	414778	5050858
043	L	17.1	36	130,786	267	743	15.0	45,118	675,954	2,407	0.843	417768	5055711
044	T	30.6	295	200,634	985	546	32.7	107,406	3,512,804	2,494	0.809	420673	5052296
045	T	26.2	32	34,834	331	171	10.8	15,113	163,043	2,713	0.839	421219	5052456
046	L	33.2	12	124,963	281	626	12.3	40,606	498,066	2,887	0.845	421507	5050678

Deposit Name	Morph.	Dep. Slope (°)	Dep. Aspect (°)	Deposit Area (m^2)	MBR Length (m)	MBR Width (m)	Int. Thick. (m)	FP Area (m^2)	Int. Volume (m^3)	Min. Dep. Elevation (m)	Deposit WS RR (%)	Deposit UTM (X)	Deposit UTM (Y)
047	L	28.8	341	120,628	334	581	16.4	44,274	724,852	2,634	0.838	423558	5049508
048	T	31.0	55	164,311	766	409	13.7	67,166	920,962	2,623	0.786	424700	5048691
049	T	18.7	28	150,563	598	367	24.8	49,172	1,221,188	2,692	0.821	424242	5049205
050	T	25.0	12	22,477	210	178	10.9	10,542	114,429	2,718	0.831	424439	5049051
051	L	24.1	325	29,035	187	239	9.7	12,354	119,315	2,777	0.834	423207	5049116
052	T	29.0	45	38,509	284	205	12.5	15,496	193,753	2,670	0.845	422232	5052117
053	T	17.0	19	79,552	543	256	17.5	33,109	579,650	2,528	0.841	417862	5050119
054	L	22.3	356	58,961	219	356	9.3	20,039	185,558	2,539	0.845	417499	5056526
054a	L	26.6	36	31,681	118	367	16.4	12,048	197,835	2,645	0.850	416500	5056354
054b	P	20.6	16	34,872	135	330	6.5	12,278	79,552	2,606	0.849	416833	5056420
054c	P	19.1	9	33,171	148	352	8.6	14,078	121,043	2,564	0.845	417189	5056472
055	T	18.1	66	236,976	827	364	25.1	64,905	1,629,168	2,603	0.759	422053	5045790
056	T	20.1	61	239,786	603	577	23.6	73,618	1,740,899	2,703	0.659	421729	5045731
057	T	28.5	18	73,615	419	330	9.7	32,988	320,367	2,817	0.839	421131	5043970
058	T	14.0	348	67,995	741	249	10.0	42,397	423,260	2,666	0.787	421714	5042620
058a	T	15.0	65	80,033	486	227	12.8	27,031	345,367	2,666	0.708	421349	5042855
060	P	34.6	337	11,709	79	237	8.3	5,786	48,283	2,641	0.845	421995	5042899
060a	L	30.1	351	57,731	198	749	12.5	35,047	438,117	2,549	0.846	422684	5043053
060b	L	31.5	358	38,424	197	403	10.2	20,313	208,100	2,596	0.851	422101	5043004
060c	L	32.0	9	19,097	133	210	9.6	8,183	78,256	2,591	0.851	422252	5043045
060d	L	34.4	4	45,595	203	733	10.3	35,128	360,112	2,566	0.845	422357	5042887
060e	L	33.5	352	64,787	220	574	10.5	30,521	320,990	2,571	0.847	422492	5042972
060f	L	29.6	346	19,861	97	480	6.8	12,830	87,403	2,534	0.849	422793	5043162
061	T	31.2	346	14,005	200	133	6.3	7,816	49,157	2,788	0.840	423875	5041733

Deposit Name	Morph.	Dep. Slope (°)	Dep. Aspect (°)	Deposit Area (m^2)	MBR Length (m)	MBR Width (m)	Int. Thick. (m)	FP Area (m^2)	Int. Volume (m^3)	Min. Dep. Elevation (m)	Deposit WS RR (%)	Deposit UTM (X)	Deposit UTM (Y)
062	T	26.6	329	86,338	455	364	20.5	38,608	791,577	2,712	0.840	424904	5041952
063	L	30.7	60	14,781	133	193	9.1	7,594	69,432	2,670	0.843	423676	5042238
064	L	23.4	276	79,809	215	512	12.0	27,093	325,821	2,539	0.646	424543	5043206
064	L	30.7	258	50,218	112	573	13.1	16,873	220,579	2,655	0.576	424798	5042740
065	T	19.9	350	358,208	776	597	30.0	94,423	2,828,010	2,765	0.789	420290	5045077
066	L	22.2	358	108,904	323	458	15.3	34,981	534,761	2,662	0.839	415671	5044911
066a	L	22.7	328	34,033	155	490	7.6	19,550	148,942	2,564	0.838	414768	5044904
066b	L	21.7	342	129,710	379	502	16.4	43,518	713,095	2,701	0.838	416091	5044810
066c	L	20.8	341	84,833	258	467	12.1	29,256	352,993	2,629	0.837	415252	5044970
067	T	25.0	22	76,660	349	295	17.8	25,446	451,706	2,792	0.839	416513	5044648
069	T	27.0	266	129,367	192	104	11.7	6,103	71,251	2,770	0.579	416534	5044619
070	T	30.6	274	69,602	686	241	27.8	38,551	1,072,642	2,831	0.624	414991	5046598
071	L	21.1	291	32,965	476	190	17.2	22,784	392,950	2,668	0.694	415093	5046712
072	T	24.0	50	100,622	184	230	12.0	11,766	141,592	2,766	0.830	414298	5046039
073	T	20.0	9	86,863	586	267	15.1	36,719	554,886	2,731	0.832	417144	5044780
074	L	32.8	289	12,920	371	334	19.9	29,916	595,923	2,751	0.734	417690	5044841
075	T	18.1	359	41,788	95	160	11.4	4,830	54,940	2,768	0.848	416374	5045924
076	T	24.3	42	39,324	266	209	23.9	14,930	357,308	2,767	0.848	419690	5042402
077	T	38.8	41	18,037	280	175	18.6	13,331	248,593	2,813	0.852	419515	5042479
078	L	22.0	355	38,303	195	124	25.5	7,233	184,307	2,448	0.850	419536	5042281
079	L	18.5	358	44,205	187	261	14.8	13,320	196,599	2,461	0.851	423219	5037274
080	T	14.0	318	706,876	184	305	13.4	15,029	201,090	2,398	0.723	423479	5037236
081	T	18.6	273	361,445	1,889	997	33.0	320,002	10,573,870	2,492	0.759	419793	5049392
082	L	31.1	104	206,127	1,356	500	20.1	131,492	2,646,414	2,610	0.544	419971	5048992

Deposit Name	Morph.	Dep. Slope (°)	Dep. Aspect (°)	Deposit Area (m^2)	MBR Length (m)	MBR Width (m)	Int. Thick. (m)	FP Area (m^2)	Int. Volume (m^3)	Min. Dep. Elevation (m)	Deposit WS RR (%)	Deposit UTM (X)	Deposit UTM (Y)
083	T	22.1	228	123,430	388	802	38.1	66,698	2,538,755	2,608	0.498	416114	5048405
084	L	26.8	110	58,535	758	305	20.0	51,511	1,030,373	2,600	0.538	413048	5048746
085	L	14.4	37	23,006	186	368	14.6	17,861	260,089	2,619	0.837	412656	5048280
086	T	31.6	297	56,742	195	212	7.4	11,538	85,702	2,766	0.801	411183	5046773
087	L	19.1	321	204,093	450	186	16.1	21,326	344,154	2,299	0.822	417329	5047003
088	L	35.4	321	125,939	426	712	27.9	65,254	1,821,514	2,354	0.846	415908	5041098
089	L	18.3	332	91,705	386	447	36.5	39,975	1,458,216	2,647	0.798	415822	5040700
089a	L	21.3	353	30,329	264	500	7.9	31,632	250,408	2,755	0.839	423506	5038234
089b	L	19.5	335	32,869	122	373	7.0	12,547	87,519	2,698	0.839	424197	5038114
090	T	12.1	95	440,909	129	331	6.2	11,878	73,082	2,681	0.584	423866	5038171
091	L	30.0	34	51,286	179	508	12.7	22,895	289,900	2,420	0.826	427665	5039248
091a	L	19.6	321	33,197	139	387	8.9	14,542	129,808	2,551	0.813	427211	5039146
091b	L	30.3	106	39,209	199	273	12.3	14,627	180,307	2,439	0.636	427753	5038997
092	P	22.1	297	12,208	107	155	5.1	5,183	26,643	2,427	0.774	414657	5054297
093	L	26.6	7	26,170	152	292	8.9	12,214	108,872	2,926	0.838	420756	5040562
094	T	26.9	73	89,968	393	391	40.1	36,133	1,450,565	2,792	0.737	421353	5041381
094a	L	32.5	52	17,792	101	317	12.4	9,217	113,888	2,793	0.831	421461	5041207
094b	L	30.4	39	19,177	135	209	23.2	8,295	192,830	2,801	0.778	421562	5041152
095	L	27.0	304	96,859	241	573	19.4	32,910	637,780	2,693	0.775	425252	5034452
096	L	17.6	196	20,224	139	215	7.5	8,667	65,349	2,835	0.414	425177	5035430
097	P	27.8	122	33,359	151	380	10.9	15,273	166,090	2,683	0.438	425682	5033589
098	P	19.6	349	43,252	170	371	9.2	16,645	153,140	2,110	0.858	431612	5033739
099	P	29.0	194	26,554	139	307	13.3	11,803	156,920	2,676	0.301	427957	5034423
100	P	17.7	36	45,356	181	467	6.5	21,425	138,324	2,726	0.847	425635	5038134

Deposit Name	Morph.	Dep. Slope (°)	Dep. Aspect (°)	Deposit Area (m^2)	MBR Length (m)	MBR Width (m)	Int. Thick. (m)	FP Area (m^2)	Int. Volume (m^3)	Min. Dep. Elevation (m)	Deposit WS RR (%)	Deposit UTM (X)	Deposit UTM (Y)
101	L	10.5	38	82,895	298	528	13.9	36,941	513,443	2,499	0.762	427512	5042390
102	L	18.2	94	129,747	214	840	18.4	41,479	764,232	2,498	0.562	426283	5043433
103	P	28.7	66	53,253	227	490	10.9	27,303	296,645	2,683	0.762	424841	5040711
104	T	29.0	333	406,368	1,038	597	28.7	121,609	3,495,624	2,317	0.839	428629	5038588
105	T	27.8	16	79,834	318	310	29.9	24,594	735,500	2,730	0.844	427967	5036154
106	L	25.8	73	531,191	835	919	70.1	146,320	10,253,339	2,441	0.693	429545	5035878
107	T	23.9	157	68,772	353	269	25.5	23,766	606,148	2,750	0.373	428328	5034952
108	L	23.0	107	61,678	218	413	16.4	22,656	371,522	2,728	0.563	428336	5034595
109	L	21.4	301	48,437	189	418	11.0	20,233	222,711	2,619	0.753	427522	5037243
110	T	24.0	356	23,283	251	135	10.3	9,683	99,967	2,659	0.846	426798	5036473
111	T	27.0	62	20,987	275	101	16.1	8,168	131,479	2,612	0.849	426509	5036776
112	T	17.6	84	48,338	375	184	9.1	17,988	164,234	2,607	0.614	426786	5037725
113	L	22.4	34	25,988	165	230	9.8	10,725	105,632	2,680	0.837	428637	5036129
114	T	30.1	335	202,329	706	437	15.7	66,247	1,037,833	2,329	0.850	422340	5037280
115	T	28.7	289	600,955	1,533	676	51.0	190,068	9,691,601	2,125	0.744	420064	5053050
116	P	34.8	102	28,894	169	334	19.1	15,117	288,208	2,703	0.566	414285	5050623
117	L	27.1	199	13,808	97	178	9.5	5,415	51,671	2,675	0.349	415050	5050822
117a	L	35.7	200	10,931	93	243	19.6	6,819	133,492	2,684	0.257	415015	5050909
117b	P	34.7	169	13,061	154	183	7.9	8,276	65,525	2,613	0.259	415310	5050767
117c	P	27.4	180	2,537	43	85	2.9	1,379	4,045	2,628	0.312	415245	5050742
117d	P	34.1	175	11,032	88	224	11.7	6,074	70,948	2,629	0.255	415162	5050802
117e	L	34.3	191	18,123	118	438	26.9	13,965	375,916	2,705	0.238	414935	5051083
117f	L	36.9	201	13,557	83	347	23.4	8,419	196,840	2,700	0.231	414977	5051020
117g	L	38.1	186	15,250	95	358	33.0	9,721	320,809	2,777	0.156	414880	5051218

Deposit Name	Morph.	Dep. Slope (°)	Dep. Aspect (°)	Deposit Area (m^2)	MBR Length (m)	MBR Width (m)	Int. Thick. (m)	FP Area (m^2)	Int. Volume (m^3)	Min. Dep. Elevation (m)	Deposit WS RR (%)	Deposit UTM (X)	Deposit UTM (Y)
118	P	30.5	179	103,730	295	674	19.1	45,144	861,542	2,825	0.272	414181	5051194
118a	P	31.6	137	83,695	225	684	16.1	36,142	581,725	2,925	0.358	413704	5051164
119	T	29.8	84	40,340	378	168	29.2	16,754	489,276	2,848	0.708	413609	5050893
120	L	30.8	43	55,898	242	306	19.4	19,152	371,799	2,829	0.842	413750	5050761
121	P	35.9	351	24,651	145	332	16.4	13,175	215,893	2,833	0.862	414029	5050778
122	P	34.2	149	16,644	100	255	13.8	7,602	104,957	2,828	0.461	413878	5051000
123	T	22.5	101	73,778	750	215	30.2	37,690	1,138,839	2,781	0.655	413906	5050295
124	T	20.2	28	187,302	972	352	27.3	72,610	1,984,101	2,630	0.835	414249	5052702
124a	L	25.2	77	96,650	269	584	22.7	36,812	835,012	2,632	0.771	414119	5052927
125	L	29.3	354	109,682	316	550	23.4	40,253	940,786	2,623	0.847	413044	5052013
125a	L	23.3	10	89,371	192	682	16.1	31,363	504,123	2,562	0.840	412335	5052388
125b	L	22.5	24	60,846	251	301	21.0	19,473	409,648	2,612	0.849	412694	5052200
126	P	27.8	21	109,803	310	548	37.3	39,393	1,469,133	2,644	0.852	411976	5050496
127	L	30.8	251	120,351	275	741	12.1	46,105	556,903	2,697	0.549	412809	5050831
127a	L	24.8	238	46,979	239	279	16.7	17,462	290,779	2,612	0.488	412441	5051285
127b	L	23.7	269	54,907	277	289	14.2	20,471	290,581	2,620	0.632	412548	5051103
128	P	28.6	69	60,337	155	571	21.7	22,400	485,795	2,501	0.761	411570	5051815
129	P	28.7	186	102,090	229	644	20.3	34,871	707,883	2,210	0.405	409954	5052390
130	T	32.7	346	63,134	500	174	16.7	22,058	368,344	2,532	0.841	411275	5051426
131	T	33.8	27	42,664	450	127	15.2	15,328	232,989	2,550	0.844	411084	5051438
132	L	26.6	40	165,610	447	675	35.6	65,024	2,316,882	2,764	0.807	413961	5049675
133	L	25.4	80	36,958	206	256	10.4	14,212	148,178	2,799	0.802	414507	5048952
134	P	34.3	92	76,621	226	644	17.2	34,485	593,367	2,546	0.657	416101	5049294
135	P	31.6	354	100,465	291	594	35.1	39,988	1,402,043	2,551	0.847	415830	5049421

Deposit Name	Morph.	Dep. Slope (°)	Dep. Aspect (°)	Deposit Area (m^2)	MBR Length (m)	MBR Width (m)	Int. Thick. (m)	FP Area (m^2)	Int. Volume (m^3)	Min. Dep. Elevation (m)	Deposit WS RR (%)	Deposit UTM (X)	Deposit UTM (Y)
136	L	25.4	293	35,460	133	327	10.7	12,056	129,115	2,630	0.849	415500	5049285
137	T	29.9	61	47,316	350	230	13.1	20,574	269,327	2,597	0.786	416155	5048786
138	T	31.1	52	180,639	601	519	34.4	66,945	2,304,554	2,799	0.798	417908	5046744
139	P	29.0	12	99,284	315	471	10.4	34,967	364,115	2,510	0.850	421610	5046566
140	T	31.7	350	140,671	656	363	25.8	52,835	1,362,220	2,579	0.846	421134	5046264
140a	P	23.2	339	41,958	162	484	11.9	20,155	239,586	2,670	0.828	420801	5046152
141	L	32.0	216	136,293	314	794	16.8	55,074	925,481	2,815	0.307	422986	5041901
141a	T	33.8	137	91,976	394	338	38.4	31,861	1,223,679	2,907	0.370	422507	5042181
142	T	24.9	41	82,409	707	180	18.1	30,671	556,429	2,599	0.829	423605	5042348
143	P	27.7	185	23,223	101	366	10.5	10,487	109,687	2,804	0.386	424736	5041336
144	P	27.9	26	52,457	200	512	14.5	25,307	367,090	2,860	0.836	424317	5040818
145	P	30.6	352	64,055	240	622	17.1	35,267	603,408	2,655	0.845	425737	5039375
146	T	11.0	97	18,634	241	109	7.1	7,797	55,375	2,718	0.552	426074	5039047
147	L	27.5	46	9,238	95	124	6.8	3,856	26,349	2,682	0.841	426256	5038103
148	L	23.5	38	10,682	91	149	5.1	4,372	22,242	2,698	0.824	426138	5038171
149	L	24.5	7	9,700	110	127	9.1	4,489	40,948	2,705	0.838	425992	5038215
150	T	26.8	312	25,742	346	142	9.9	13,379	132,397	2,695	0.838	423812	5039164
152	P	32.3	342	11,164	75	273	22.6	6,260	141,424	2,815	0.841	420243	5048049
153	P	32.9	318	16,893	90	435	34.9	10,991	384,040	2,799	0.835	420341	5048043
154	P	26.4	327	7,857	77	226	16.9	5,424	91,553	2,787	0.840	420304	5048175
155	P	34.9	303	18,210	119	391	32.7	12,753	416,798	2,782	0.842	420395	5048173
156	L	24.2	276	26,993	222	302	27.5	17,561	482,159	2,780	0.832	420360	5048320
157	L	34.8	155	22,794	126	321	24.6	11,352	279,111	2,800	0.317	413925	5050501
158	T	32.5	112	58,260	553	247	27.9	32,596	908,505	2,797	0.501	413744	5050450

Deposit Name	Morph.	Dep. Slope (°)	Dep. Aspect (°)	Deposit Area (m^2)	MBR Length (m)	MBR Width (m)	Int. Thick. (m)	FP Area (m^2)	Int. Volume (m^3)	Min. Dep. Elevation (m)	Deposit WS RR (%)	Deposit UTM (X)	Deposit UTM (Y)
159	L	30.4	33	29,969	144	481	16.3	18,068	293,771	2,779	0.845	414010	5050137
160	T	24.8	309	54,514	447	229	20.2	25,346	512,234	2,621	0.829	414086	5047249
161	T	28.9	304	34,627	579	149	10.6	21,931	232,210	2,573	0.809	414073	5047451
162	T	27.6	325	39,219	503	147	17.5	19,128	335,325	2,647	0.845	414527	5047771
163	T	28.7	343	65,210	588	232	12.6	32,625	411,878	2,677	0.842	414682	5047730
164	L	30.7	347	16,911	144	194	5.5	8,181	45,015	2,765	0.843	414856	5047709
165	P	35.3	139	9,478	106	165	11.1	5,451	60,396	2,762	0.344	414211	5050499
166	P	33.6	83	7,302	79	166	16.4	4,271	69,922	2,851	0.822	414947	5047547
167	P	34.5	63	12,971	91	360	18.4	9,445	173,531	2,850	0.832	414900	5047441
168	P	29.2	55	8,575	80	186	10.0	4,728	47,323	2,850	0.844	414973	5047405
169	P	30.5	48	3,415	32	151	8.6	1,775	15,275	2,851	0.845	415004	5047377
170	P	36.8	33	2,613	50	114	10.6	2,064	21,792	2,865	0.845	415010	5047334
171	L	31.9	8	65,703	239	447	19.4	26,356	511,840	2,813	0.833	414915	5051713
172	P	31.6	11	20,493	128	265	13.6	9,684	132,048	2,779	0.835	415085	5051837
173	L	27.9	5	9,435	76	250	11.3	5,825	65,878	2,858	0.841	415162	5047278
174	L	25.6	6	3,164	59	103	4.3	2,171	9,294	2,881	0.837	415209	5047245
175	T	31.0	4	14,638	363	120	19.8	12,080	238,975	2,895	0.835	415279	5047103
176	T	26.0	353	4,032	155	47	11.7	2,523	29,531	2,882	0.839	415237	5047236
177	P	40.7	32	3,984	61	166	13.9	3,389	46,955	2,924	0.844	415239	5047135
178	T	19.1	348	53,167	426	211	19.5	22,670	441,217	2,884	0.832	415292	5047191
179	T	31.3	343	54,633	459	222	17.2	25,320	436,678	2,889	0.830	415406	5047106
180	T	31.3	347	40,037	361	145	28.2	14,102	398,351	2,909	0.829	415536	5047109
182	L	32.3	286	32,981	218	223	27.6	13,285	366,086	2,968	0.729	415756	5047260
183	P	39.8	1	4,501	56	133	17.1	2,601	44,353	2,751	0.847	415376	5051762

Deposit Name	Morph.	Dep. Slope (°)	Dep. Aspect (°)	Deposit Area (m^2)	MBR Length (m)	MBR Width (m)	Int. Thick. (m)	FP Area (m^2)	Int. Volume (m^3)	Min. Dep. Elevation (m)	Deposit WS RR (%)	Deposit UTM (X)	Deposit UTM (Y)
184	T	33.3	8	14,376	294	83	15.3	7,259	111,363	2,738	0.840	415436	5051761
185	T	31.9	5	37,349	409	188	26.6	19,757	524,728	2,731	0.837	415513	5051674
186	L	24.7	293	35,840	270	289	12.3	20,055	247,064	2,690	0.797	415724	5052112
187	L	32.7	32	13,958	98	304	13.0	8,665	112,859	2,731	0.838	415192	5051846
189	P	31.7	330	45,784	231	475	12.5	26,921	337,676	2,519	0.849	420409	5052328
190	T	30.2	325	148,223	809	355	24.9	62,293	1,551,446	2,653	0.823	422064	5042594
191	T	26.6	325	49,192	623	230	9.2	34,020	312,503	2,692	0.828	421746	5042576
194	T	33.4	167	91,116	654	329	29.3	48,416	1,418,404	2,683	0.212	414712	5051240
195	P	27.4	62	76,287	302	439	19.5	31,743	619,906	3,054	0.722	421393	5051670
196	T	16.7	50	93,169	469	301	17.6	33,507	588,924	2,461	0.832	421367	5053916
197	T	21.9	268	13,893	175	131	17.1	6,889	117,933	2,903	0.607	415565	5047515
198	P	26.6	269	5,379	86	109	7.3	3,152	23,060	2,890	0.575	415484	5047688
199	P	32.8	247	7,521	91	125	12.2	3,742	45,483	2,901	0.472	415532	5047605
200	L	32.4	224	12,289	101	185	13.9	5,776	80,298	2,807	0.337	415172	5048281
201	T	24.7	268	12,597	147	115	9.6	5,290	51,042	2,830	0.612	415397	5047904
202	L	32.6	276	3,735	48	106	5.5	1,852	10,168	2,879	0.632	415470	5047740
203	L	30.8	290	3,318	42	90	3.0	1,454	4,315	2,863	0.712	415444	5047774
204	L	27.5	287	5,737	82	95	6.8	2,704	18,442	2,839	0.717	415419	5047818
205	L	27.9	257	4,566	48	145	10.5	2,428	25,583	2,822	0.551	415348	5048078
206	L	31.0	253	14,791	139	141	8.6	6,013	51,587	2,831	0.523	415395	5048012
207	P	36.2	244	4,694	48	153	12.3	2,556	31,504	2,833	0.459	415368	5048122
208	P	33.0	230	17,513	113	195	11.7	6,635	77,675	2,819	0.378	415322	5048178
209	P	35.8	224	6,933	81	123	10.3	3,364	34,800	2,827	0.312	415259	5048244
210	P	29.2	220	7,596	60	158	12.4	3,200	39,617	2,804	0.338	415103	5048312

Deposit Name	Morph.	Dep. Slope (°)	Dep. Aspect (°)	Deposit Area (m^2)	MBR Length (m)	MBR Width (m)	Int. Thick. (m)	FP Area (m^2)	Int. Volume (m^3)	Min. Dep. Elevation (m)	Deposit WS RR (%)	Deposit UTM (X)	Deposit UTM (Y)
211	P	29.9	168	11,827	147	197	8.8	8,424	73,906	2,810	0.240	414819	5048415
212	P	33.6	211	5,159	63	143	9.3	3,060	28,435	2,803	0.269	415078	5048355
213	P	32.0	184	44,725	229	274	26.5	16,574	438,828	2,803	0.231	414952	5048429
214	P	31.4	246	60,224	228	363	23.6	21,140	498,388	2,865	0.436	415079	5046979
215	P	24.1	218	42,726	194	346	11.3	17,601	198,831	2,867	0.396	414958	5047097
216	L	29.6	262	34,292	142	431	14.8	16,227	240,919	2,841	0.564	415069	5046847
301	P	30.5	85	33,511	144	320	6.6	12,637	83,136	2,711	0.787	418139	5049532
302	P	22.1	37	20,320	99	304	4.4	8,718	38,603	2,705	0.839	416648	5057790
303	P	27.2	27	35,361	197	282	12.0	14,874	178,883	2,754	0.848	414955	5048788
304	L	26.9	123	56,116	163	503	8.6	20,925	180,776	2,865	0.830	421418	5050939
305	L	20.7	93	74,437	265	471	6.0	30,113	181,187	2,632	0.674	410976	5046915

VITA

Andrew R. Gustin

Birth 8/18/1984 – Evansville, Indiana

Education

Bachelor of Science in Geology; minor in Physics

Indiana University, Bloomington, IN 5/2006

Master of Science in Geology

Indiana University, Bloomington, IN 9/2013

Professional Experience

Research

Research Environmental Geologist 1/2012 – 12/2013

Indiana Geological Survey (IGS), Bloomington, IN

GIS Analyst, Field Technician 9/2007 – 12/2011

IGS, Center for Geospatial Data Analysis, Bloomington, IN

Geologic Sample Preparer 5/2005 – 6/2007

IGS, Subsurface Section, Bloomington, IN

Teaching

Associate Instructor (introductory geology, earth materials) 8/2008 – 5/2010

Department of Geological Sciences, Indiana University

Associate Instructor (structural geology, mapping)

IU Geological Field Station, Cardwell, MT Summers of 2006, 2007, 2010

Publications

Gustin, A. R. (2013). The Distribution, Morphology, and Temporal Signature of Rock Glaciers in the Tobacco Root Mountains, Montana. In *Geological Society of America Abstracts with Programs* (Vol. 45, No. 7).

Gustin, A. R., Ellett, K. M., Naylor, S. C., and Waldoch, C. (2013). Heat Transfer Controls in Soil: Recommendations for Improved Ground Source Heat Pump System Design. In *Geological Society of America Abstracts with Programs* (Vol. 45, No. 7).